Cold polar molecules in bilayers

Von der Fakultät für Mathematik und Physik der
Gottfried Wilhelm Leibniz Universität Hannover

zur Erlangung des Grades
Doktor der Naturwissenschaften
Dr. rer. nat

genehmigte Dissertation von

Dipl.-Phys. Alexander Pikovski

geboren am 3. August 1980 in Gorki, Russland

2012

Referent:	Prof. Dr. Luis Santos
Korreferent:	Dr. A. Recati
Tag der Promotion:	12. Juli 2012

Abstract

Experiments with ultracold gases study quantum-mechanical many-particle systems in different regimes; it is possible to control the interactions and to tailor the confinement geometry. Dipolar gases, i.e. gases where the atoms or molecules have a dipole moment, are a promising new direction in this field. In particular, they allow for the observation of new states which arise from the dipole interaction, which is fundamentally different from the interaction of atomic gases. Here we investigate theoretically the physics of a dipolar gas in a bilayer geometry at very low temperatures.

We study the two-body physics of a gas interacting by the dipole–dipole interaction in the quantum regime. Some general methods, analytical and numerical, are presented for the calculation of binding energies and scattering states close to the threshold of a two-dimensional system. This is used to calculate the weakly bound states and scattering properties due to the interaction of dipolar particles in different layers. Approximate analytical results are compared with exact numerical calculations. The special properties of the dipole–dipole interaction regarding scattering and bound states are discussed.

Next we consider the many-body physics of the dipolar gas of fermions in a bilayer geometry. The interaction between dipoles in different layers may lead to a Cooper pairing of particles, such that molecules in different layers form one pair. This results in a BCS-like interlayer superfluid. For stronger dipole moments, the particles form pairs in real space (dimers). The system can be tuned between the BCS state and the condensate of dimers by an external electric field, thus showing a peculiar BCS–BEC crossover. The crossover is described here by the Eagles–Leggett model. The critical temperature for the superfluid transition is determined, using Kosterlitz–Thouless theory. Insights from the investigation of the two-body physics are used to compare analytical and numerical results.

Finally, we consider the non-equilibrium dynamics of a polar gas for small external electric fields. Here the particles populate the lowest rotational states. The dipole–dipole interaction leads to state exchange collisions, which are similar to spin-changing collisions. The rate of these collisions is calculated. It is shown that the state-changing collisions can be observed, if a certain initial state is prepared, for chemically reactive molecules (such as KRb) at temperatures far above the Fermi temperature.

Keywords: ultracold gases; dipole interaction; two-dimensional scattering

Zusammenfassung

Experimente mit ultrakalten Gasen können quantenmechanische Vielteilchensysteme in verschiedenen Regimes untersuchen, die Wechselwirkungen können kontrolliert und die Fallengeometrie kann gewählt werden. Polare Gase, d.h. Gase aus Atomen oder Molekülen mit einem Dipolmoment, sind eine vielversprechende neue Forschungsrichtung. Sie ermöglichen insbesondere die Beobachtung von Effekten der Dipolwechselwirkung, die sich von der Wechselwirkung atomarer Gase wesentlich unterscheidet. In der vorliegenden Arbeit wird die Physik polarer Gase in einer Doppelschicht bei sehr tiefen Temperaturen theoretisch untersucht.

Zuerst betrachten wir die Physik zweier Teilchen in einem Gas mit Dipol–Dipol-Wechselwirkung im Quantenregime. Allgemeine analytische und numerische Methoden für die Berechnung von Bindungsenergien und Streuzuständen für ein zweidimensionales System werden dargestellt. Dieses wird angewandt, um schwach gebundene Zustände und Streuung bei kleinen Energien beim Potential zweier wechselwirkender Dipole, die sich in verschiedenen Schichten befinden, zu bestimmen. Näherungsweise analytische Formeln werden mit exakten numerischen Berechnungen verglichen. Die besonderen Eigenschaften der Dipol–Dipol-Wechselwirkung werden diskutiert.

Als nächstes betrachten wir die Vielteilchenphysik eines polaren Gases von Fermionen in einer Doppelschicht. Die Wechselwirkung zwischen Dipolen in verschiedenen Schichten kann zu einer Cooper-Paarung führen, bei der Teilchen in verschiedenen Schichten ein Paar bilden. Dies führt, bei genügend niedriger Temperatur, zu einem BCS-ähnlichem superfluiden Zustand. Für höhere Dipolmomente bilden die Teilchen Paare im Ortraum (Dimere). Das System kann zwischen dem BCS-Zustand und einem Kondensat von Dimeren durch Änderung des äußeren elektrischen Feldes durchgefahren werden. Der Übergang zwischen diesen Zuständen wird durch das Eagles–Legget Modell beschrieben. Die kritische Temperatur für den superfluiden Übergang wird mit Hilfe der Kosterlitz–Thouless Theorie bestimmt. Ergebnisse aus der Untersuchung der Zweiteilchenphysik werden dazu benutzt, analytische und numerische Resultate zu vergleichen.

Schließlich untersuchen wir die Nichtgleichgewichts-Dynamik eines polaren Gases bei schwachem elektischen Feld. Hier besetzen die Teilchen die untersten Rotationsniveaus. Die Dipol–Dipol-Wechselwirkung führt zu einer Streuung mit Austausch von Zuständen, die einer Spin-Austausch-Streuung ähnlich ist. Die Rate dieser Streuung wird berechnet. Die Austauschstreuung ist besonders dann relevant, wenn das System in einem bestimmten Anfangszustand präpariert ist. Dies ist bei chemisch reaktiven Molekülen, z.B. KRb, beobachtar für Temperaturen, die viel höher als die Fermitemperatur sind.

Schlagworte: ultrakalte Gase; Dipol-Wechselwirkung; zweidimensionale Streuung

Contents

CHAPTER 1

Introduction

In the past three decades, the creation of ultracold atomic gases opened the door for the direct experimental study of quantum-mechanical many-particle systems. The highly controllable interactions and the design of the confinement geometry allows investigations which were not possible before. Ultracold gases are also used in atom interferometry, high precision measurements, and as a tool in quantum information.

Gases of dipolar atoms or molecules, which have recently begun to be studied, enrich the field of ultracold gases. In particular, they allow for the observation of new states which arise from the dipole interaction, which is fundamentally different from the interaction of atomic gases.

In this thesis, we explore theoretically the physics of a gas consisting of ultracold polar fermionic molecules in a bilayer geometry. We consider collisions of dipolar particles, developing methods to study two-body scattering and shallow two-body bound states in two dimensions. Next, the many-body physics of fermions interacting by the dipole–dipole force is studied. It is shown that the interaction causes the formation of pairs, which can condense to a peculiar BCS-like superfluid or to a superfluid of dimers. The system can be continuously tuned between these two states by changing the external electric field, showing a novel type of BCS–BEC crossover. Finally, we study the non-equilibrium physics which results from state-changing collisions due to the dipole–dipole interaction. It is shown that signatures of the dipole–dipole interactions can be observed for temperatures well above the Fermi temperature.

1.1 Many-body physics with cold gases

Understanding many-body systems in the quantum regime is a challenge for experimental and theoretical physics. Although quantum many-body systems have been studied in solid-state and nuclear physics for a long time, experiments with ultracold gases give a different and better view on known phenomena and allow for the observation of new ones. The possibility to control the interactions using Feshbach resonances, to change the confinement geometry (cf. Sec. 1.2), and to perform direct measurements allows investigations which were not possible before. From a theoretical perspective, experiments with ultracold gases allow for the experimental tests of many-body theories and, sometimes, motivate a fresh approach to some old many-body problems.

Some landmarks in the experimental study of many-body systems with cold gases are the Bose–Einstein consensate in 1995 [5, 23], the preparation of a Fermi degenerate gases in 1999 [28], the Mott insulator phase in an optical lattice in 2002 [37], and the observation of BCS–BEC crossover in 2004 (cf. Sec. 1.3). Examples of interesting novel many-body systems created with ultracold gases are the one-dimensional hard-core gas [44, 70], the unitary Fermi gas [95], and spinor condensates [87]. Ultracold gases have been used to study a wide range phenomena [13, 20, 21, 39], such as quantized vortices, disorder and localization, nonlinear phenomena in Bose-Einstein-Condensates, the Kosterlitz–Thouless transition, and the Efimov effect.

Cooling gases of molecules, instead of atoms, to low temperatures is the next frontier. Gases of ultra-cold molecules are quantum many-body systems, in the same way as ultra-cold atomic gases. In addition, the rich structure of internal states (rotational, vibrational, electronic), which is already present in the simplest diatomic molecules, opens new possibilities for control and manipulation of these objects in the quantum regime. Some new directions [17] are: tests for fundamental laws like symmetry and parity, precise spectroscopy of molecular structure, and the control of chemical reactions. Most relevant for our topic are the opportunities for the study of novel many-body systems.

Polar molecules, i.e. molecules with an electric dipole moment, provide yet more new possibilities to study many-body systems. The anisotropic and long-range interactions between such molecules differ significantly from the interaction between atoms (cf. Sec. 1.5). In addition, the dipole moment of a polar molecules can easily be tuned with an external electric field, thus giving rise to a controllable interaction. Systems with dipolar interactions are predicted to show a variety of new phenomena [7, 47].

1.2 Cooling and trapping atoms

The creation of cold atomic and molecular gases, beginning in the 1980s, has been made possible by the invention of a variety cooling and trapping techniques.

Laser cooling transfers momentum from a laser beam to a moving atom in such a way that the atom is slowed down. Doppler cooling uses the Doppler effect to reduce the velocity of atoms. Consider a light beam directed at a moving atom. The atom sees the laser frequency Doppler-shifted to the blue/red if it moves towards/away from the direction of propagation of the light beam. Therefore, if the frequency of the laser beam is slightly below a transition frequency of the atom at rest ω_0, this compensates the Doppler shift. Then, only atoms which move towards the light beam are resonant and can absorb photons. The change of momentum associated with the absorption, also taking into account subsequent spontaneous emission, leads to a decrease in the kinetic energy of the atoms. Doppler cooling is used in an arrangement of six laser beams, the so-called optical molasses, to cool atoms which are located in a central region.

Another cooling method is sympathetic cooling. Here one species of atoms, which has been cooled by some other method, is used to cool another species. Two gases are brought into contact, i.e. they exchange momentum and energy. Later one species is discarded, and the remaining gas cloud has a lower temperature than before.

In evaporative cooling, the fastest atoms are selectively removed from the cloud. Starting from a gas in thermal equilibrium, the confinement is reduced and the atoms with the highest kinetic energy escape from the trap. In this way the average energy of the cloud is reduced, and after subsequent re-thermalization the temperature is lower.

It is also possible to use the magneto-optical trap, which is described below, both for cooling and trapping.

Atoms and molecules can be trapped in a well-defined region in space by external electromagnetic fields. Electrically charged particles can be trapped using time-dependent electric fields. For neutral particles, a confinement is much more difficult. One can make use of the induced electric dipole in an external electric field or the magnetic moment in a magnetic field. In an inhomogeneous electric (or magnetic) field, a force acts on the dipole (or magnetic moment), which can be used to trap the particles. The forces are very small, however, and the confinement only works for particles with very small kinetic energy, i.e. for very cold gases. Trapping techniques are reviewed in [38, 94].

The magnetic trap uses external magnetic fields to provide confinement. The magnetic field splits the energy levels of the atom, and in an inhomogeneous field a restoring force acts to trap the particles. Only certain hyperfine states are trapped.

The magneto-optical trap (MOT) consists of a magnetic field together with laser fields. An inhomogeneous magnetic field produces a spatially varying Zee-

man splitting. A configuration of lasers, with a frequency close to a resonant transition, provides a restoring force towards the center of the trap. The confined atoms dissipate energy during the process, thus the MOT, in contrast to other trap types, is used to both hold the atoms and to cool them.

The optical dipole trap uses laser fields only to exert a force on the atoms. If the laser frequency ω is close to a frequency of an atomic transition ω_0, the atom experiences a conservative force proportional to the field intensity $I = |E|^2$, with the potential

$$V_{\text{opt}}(\mathbf{r}) \propto I(\mathbf{r})/\Delta \tag{1.1}$$

where $\Delta = \omega - \omega_0$ is the detuning ($|\Delta| \ll \omega_0$). There is also an additional dissipative force, but it scales as I/Δ^2 and can be made small by going to large detunings. In the photon picture, the conservative dipole force arises from stimulated emission while the dissipative part is due to spontaneous emission.

The principle of the optical dipole trap can be used to create optical lattices. Standing waves of light of different shapes are created using an arrangement of lasers. In this way one can produce a confining potential in the form of one-, two-, or three-dimensional lattices where the geometry and the depth of the lattice can be controlled [12].

All schemes requiring a laser field need the laser frequency to be close to an optical transition of the atom which is to be cooled or trapped. Thus the possibility of cooling or trapping atoms depends on their level structure, and each atomic species needs a specialized trap. Traps have been designed and used for certain elements, mostly for the alkali and alkaline earth metals.

1.3 Ultra-cold Fermi gases

Experiments with ultra-cold gases can directly observe quantum coherence. This requires the gas to be quantum degenerate. A system is in the quantum degenerate regime if the phase-space density is of the order of one or smaller,

$$n\Lambda_T^3 \lesssim 1, \tag{1.2}$$

where n is the number density and

$$\Lambda_T = \frac{h}{\sqrt{2\pi m T}} \tag{1.3}$$

is the thermal de Broglie wavelength (m is the mass and T is the temperature in energy units). Equivalently, for fermions one can say that the temperature should be lower than the Fermi energy (here for spin 1/2 fermions)

$$T \lesssim E_F = \frac{\hbar^2}{2m}(3\pi^2 n)^{2/3} \tag{1.4}$$

The relations (1.2) and (1.4) differ only by a numerical factor.

The atoms of an ultra-cold gas are bosons or fermions, depending on the total spin. Ultra-cold bosonic gases, already in the absence of any interactions, form a Bose-Einstein condensate for sufficiently high phase-space density. In a noninteracting gas of fermions, in contrast, nothing spectacular happens: the degenerate Fermi gas fills all states up to the Fermi level. An interacting Fermi gas, however, can show the remarkable phenomenon of Cooper pairing and BCS superfluidity. Here, if there is a weak attractive interaction between the particles, the fermions can form Cooper pairs. These are not two-body bound states in the usual sense, but pairs of fermions which exist only in a many-body setting, namely in the presence of the filled Fermi sea. These pairs, in turn, can form a condensate[1], similar to a Bose-Einstein condensate, and show superfluidity. (Cold gases consist of electrically neutral atoms, thus one does not observe superconductivity.) The interesting point about experiments with ultra-cold Fermi gases is that the effective interaction between the atoms can be tuned experimentally.

At very low temperatures, the interatomic collisions can be approximated by scattering in the s-wave channel only (however, not for identical fermions). The interaction may be modelled, considering only binary collisions, by a contact interaction, whose strength is proportional to the s-wave scattering length a. Most importantly, the value of the scattering length can be tuned experimentally by an external magnetic field at a Feshbach resonance [20, 34, 52, 88]. This phenomenon occurs if two atoms scatter with an energy which is close to the energy of a bound state in a different hyperfine state. The energy of the bound state depends on the applied magnetic field, in this way changing the magnetic field by a small amount around the resonance value one can change the *magnitude and sign* of the scattering length experimentally. The effective scattering length a at a Feshbach resonance, as a function of the magnetic field B, has the form

$$a = a_{\mathrm{bg}} \left(1 - \frac{\Delta_B}{B - B_0} \right), \tag{1.5}$$

where B_0 is the resonance point, a_{bg} is the background scattering length (i.e. the value of the scattering length away from resonance), and Δ_B is a constant which gives the width. The parameters B_0 and Δ_B depend on the atomic species and are usually determined experimentally [20].

The interacting Fermi gas can be studied in different regimes by tuning the scattering length a with a Feshbach resonance. Experiments have been perfomed by many groups, see the references in [13, 34]. Changing a from negative to positive values through a pole using a Feshbach resonance [cf. Eq. (1.5)], one can observe the so-called BCS–BEC crossover[2] [13, 19, 34, 95]. It is characterized by

[1] The condensate of Cooper pairs is not exactly the same as a Bose-Einstein condensate, since the Cooper pairs are not ordinary bosons; but often this picture is sufficient, see e.g. the discussion in [52].

[2] Note that there is, in fact, a smooth crossover between the BCS and BEC regimes and no phase transition. The mathematical singularity of a, where it becomes infinite, is not a physical singularity.

the following regimes:

$a < 0$: attractive gas

Here the phenomenon of Cooper pairing and BCS superfluidity takes place, for sufficiently low temperatures.

$a = \pm\infty$ (pole) : unitarity

This is the so-called unitary Fermi gas, or Fermi gas with a resonant interaction. Experiments with ultra-cold gases provide the first direct realization of this state. Experiments and theory are beginning to explore this interesting regime, see [95].

$a > 0$: repulsive gas / BEC of dimers

The system can be in two states here:

a) repulsive interaction

b) dimers

For large a, the fermions form two-body bound pairs. These so-called Feshbach molecules [20] are very shallow (delocalized) bound states with binding energy $E_b = -\hbar^2/(ma^2)$. If the temperature is low enough, these pairs condense to form a Bose-Einstein condensate.

In Chapter 3, we will study a different kind of BCS–BEC crossover, which is controlled not by the scattering length (experimentally, the magnetic field), but by the dipole moment (experimentally, the electric field).

Additionaly, we remark that interesting phenomena occur in an ultra-cold Fermi gas with a population imbalance, that is, if fermions of different types (or in internal states) are present which have different densities [34, 95]. Furthermore, experiments with a two-species mixture of gases can explore the physics of Bose–Fermi mixtures, see e.g. [68].

1.4 Dipolar gases

Gases of polar molecules are already encountered in classical physics. A molecule is called polar if its charge distribution has a permanent electrical dipole moment; this moment is to be measured relative to the axes of the molecule. The electric susceptibility χ, i.e. the response to an applied external electric field E, of a gas of N polar molecules obeys the classical Langevin-Debye law [92] (weak fields, $dE \ll T$)

$$\chi/N = \alpha + \frac{d^2}{3T} \tag{1.6}$$

where d is the permanent dipole moment and T is the temperature in energy units. The constant α arises from induced polarization of the molecule by the field. The temperature-dependent term is the orientational polarization first studied by Debye. In the absence of an external electric field, the permanent dipole

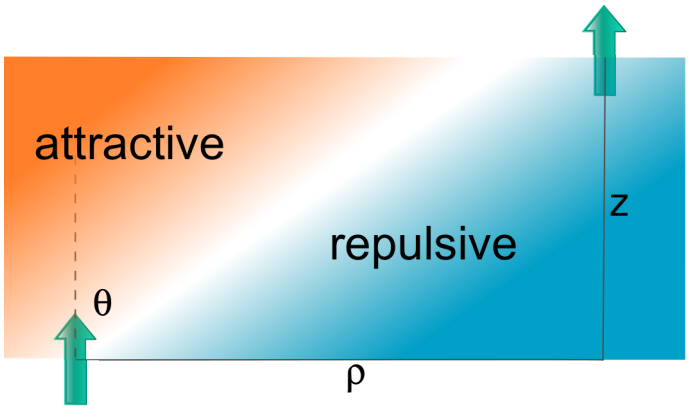

Figure 1.1: Dipole–dipole interaction: attractive and repulsive regions. The boundary between the attractive and repulsive region is at $\theta = 54.7°$, or equivalently at $\rho = \sqrt{2}z$.

moments point in random directions, and thus average to zero. In an applied field E, the dipole moments tend to align along the field, but temperature prevents a perfect alignment. The $1/T$ dependence is valid only for high temperatures, at lower temperatures or high fields the orientational susceptibility slowly saturates to d/E. A quantum-mechanical discussion and calculation of orientational polarization will be given in Sec. 4.2.

The susceptibility of a gas consisting of polar molecules measures the interaction of the dipoles with the *external* electric field. On the other hand, a new range of phenomena results from the interactions *between* polar particles. Since the dipole–dipole forces are weak, however, low temperatures are usually required to see the influence of this interaction.

1.5 Interaction between two dipoles

The interaction between particles posessing an electric or magnetic dipole moment has two novel features compared to interactions of van der Waals type. First, it is anisotropic, as its strength and its sign depend on the mutual orientation of the dipole moments. Second, it decays as $1/r^3$ for large distances, and is, therefore, felt at long distances. Here we consider the interaction of two electric dipoles.

The potential of the field of an electrical dipole with dipole moment $\mathbf{d}$ is

$$\varphi_d(\mathbf{r}) = \frac{1}{4\pi\epsilon_0}\frac{\mathbf{d}\cdot\mathbf{r}}{r^3} \tag{1.7}$$

and the field is

$$\mathbf{E}(\mathbf{r}) = -\nabla\varphi_d = -\frac{1}{4\pi\epsilon_0}\frac{\mathbf{d} - 3\hat{\mathbf{r}}\,(\mathbf{d}\cdot\hat{\mathbf{r}})}{r^3} \tag{1.8}$$

where $\hat{\mathbf{r}} = \mathbf{r}/r$ is the unit vector. If, on the other hand, a dipole is placed in an

external electric field, its potential energy is [42]

$$U = -\mathbf{d} \cdot \mathbf{E}. \tag{1.9}$$

Two dipoles with dipole moments $\mathbf{d}_1$, $\mathbf{d}_2$ interact when one dipole creates an electric field which affects the other dipole. The potential energy is, from (1.8) and (1.9):

$$U_{\mathrm{dd}} = \frac{1}{4\pi\epsilon_0}\left[\frac{\mathbf{d}_1 \cdot \mathbf{d}_2 - 3(\mathbf{d}_1 \cdot \hat{\mathbf{r}})(\mathbf{d_2} \cdot \hat{\mathbf{r}})}{r^3}\right] \tag{1.10}$$

where $\mathbf{r} = \mathbf{r}_2 - \mathbf{r}_1$.

For two dipoles oriented in the z direction, $\mathbf{d}_1 = d_1\hat{\mathbf{z}}$ and $\mathbf{d}_2 = d_2\hat{\mathbf{z}}$, the interaction energy (1.10) becomes

$$U_{\mathrm{dd}} = d_1 d_2 \, \frac{1}{4\pi\epsilon_0}\left[\frac{1}{r^3} - \frac{3r_z^2}{r^5}\right] \tag{1.11}$$

$$= d_1 d_2 \, \frac{1}{4\pi\epsilon_0} \, \frac{1 - 3\cos^2\theta}{r^3} \tag{1.12}$$

$$= d_1 d_2 \, \frac{1}{4\pi\epsilon_0} \, \frac{\rho^2 - 2z^2}{(\rho^2 + z^2)^{5/2}} \tag{1.13}$$

where θ is the azimuthal angle in spherical coordinates (the angle with the vertical direction) and $\rho = \sqrt{r_x^2 + r_y^2}$, $z = r_z$ are cylindrical coordinates. This interaction is attractive for $\cos^2\theta > 1/3$ (this is $\theta < 54.7°$) or $\rho < \sqrt{2}z$ and repulsive otherwise, see Fig. 1.1. The interaction is cylindrically symmetric.

We will often consider the interaction between two dipoles, each of them located in a layer, the layers separated by distance λ. The interaction potential for this inter-layer dipole–dipole interaction is, from (1.13),

$$V_{\mathrm{dd}}(r) = D^2 \frac{\rho^2 - 2\lambda^2}{(\rho^2 + \lambda^2)^{5/2}}. \tag{1.14}$$

Here $D^2 = d^2/(4\pi\epsilon_0)$ is the dipole moment.

It will be convenient to use the following units:

$$\begin{aligned} &\lambda && \text{as the unit of length,} \\ &E_0 = \frac{\hbar^2}{m\lambda^2} && \text{as the unit of energy,} \\ &U_0 = \frac{mD^2}{\hbar^2\lambda} && \text{as dimensionless coupling.} \end{aligned} \tag{1.15}$$

Then the potential (1.14) becomes

$$V_{\mathrm{dd}}(r)/E_0 = U_0 \frac{r^2 - 2}{(r^2 + 1)^{5/2}}. \tag{1.16}$$

with $r = \rho/\lambda$. One may also define the dipole–dipole interaction length $r_d = mD^2/\hbar^2$, so $U_0 = r_d/\lambda$. In SI units, an electric dipole moment d gives $U_0 =$

$d^2m/(4\pi\epsilon_0\hbar^2\lambda)$. For $\lambda = 530\,\mathrm{nm}$ and $k_F^2 = 4\pi n_{2d}$ this gives:

$$\begin{aligned} U_0 &= 0.0282\,\mathrm{Debye}^{-2}\,\mathrm{amu}^{-1}\cdot d^2m \\ \lambda k_F &= 1.88\cdot 10^{-4}\,\mathrm{cm}\cdot\sqrt{n_{2d}} \end{aligned} \tag{1.17}$$

For a mass of $m = 127\,\mathrm{amu}$ (KRb-molecule), $U_0 = 1.0$ is equivalent to a dipole moment of $0.53\,\mathrm{Debye}$.

1.6 Cold polar atomic gases

The properties of gases at ultra-low temperatures are governed by interparticle interactions. Usually, at very low temperatures, the interaction between atoms can be modelled by a point interaction. The rich variety of phenomena observed in ultra-cold quantum gases can all be described by a contact interaction.

New and interesting phenomena are expected if a different type of atom–atom interaction can be produced, namely, the dipole–dipole interaction. The effects of this interaction have been studied theoretically, see [7, 47] for a review. In the last years, experiments started to explore dipolar effects in ultra-cold atomic gases.

Experiments with a Bose-Einstein condensate of ^{52}Cr atoms (which have a permanent magnetic dipole moment of $6\mu_B$) have observed the effect of the dipole–dipole interactions during the expansion of the atomic cloud [46]. Interestingly, in these experiments a Feshbach resonance was used to reduce the effective scattering length for the non-dipolar interactions, thereby enchancing the relative strength of the dipolar forces. Effects of dipolar interactions on the stability of the condensate were studied as well [47].

The anisotropic character of the dipole–dipole interaction was observed in experiments with a BEC of potassium [31] and on lithium atoms [78]. Experiments on a spinor condensate of rubidium atoms (in which the atoms have several internal states), have shown the dipolar character of the condensate [93].

Recently, experiments started to focus on rare earth elements with large permanent magnetic moments. Using atoms of dysprosium (magnetic moment of $10\mu_B$), a BEC with dipolar effects was created [59]. Using a different, fermionic isotope of dysprosium, a degenerate Fermi gas with magnetic dipole interactions was produced [58]. Recently, a dipolar BEC of erbium atoms (magnetic moment $7\mu_B$) was produced [4].

It is challenging, however, to observe quantum many-body physics where the dipolar interactions are crucial [7, 47]. Polar molecules open opportunities in this direction, since their electric dipole moment can be made quite large. In addition, electric dipole–dipole forces are much stronger than magnetic dipole–dipole forces, cf. [47]. This is the topic of the following section.

1.7 Cold polar molecules

While atoms can be cooled to ultra-low temperatures, cooling molecules is more difficult. Two different paths have been pursued to produce cold and ultra-cold[3] molecules. One path is direct cooling, which attempts to cool ground-state molecules. This is done, for example, by bringing the molecules into contact with a cold atomic gas or by slowing down a molecular beam using external electric or magnetic fields. Another path are indirect cooling methods, which start with an ultra-cold gas of atoms and assemble molecules from the atoms. Here it is crucial that no heating occurs while the molecules are formed.

Using laser-association of ultra-cold atoms, cold molecules LiCs [27], Rb_2 [49], KRb [66], and Cs_2 [22] have been produced. Here we focus on the KRb molecules.

In experiments at the Joint Institute for Laboratory Astrophysics (JILA), ultra-cold $^{40}K^{87}Rb$ molecules have been created [66, 65]. The experiments started with an ultra-cold gas of K and Rb atoms, trapped in an optical trap. Using a Feshbach resonance, weakly bound states of K and Rb (Feshbach molecules) were produced first. Then, using a laser, the molecules were transferred coherently into the molecular ground state, bridging an energy gap of about 6000 K. The coherent transition prevented heating, and a gas of KRb molecules with a temperature of several hundred nK and density $\sim 10^{12}\,\mathrm{cm}^{-3}$ was produced. This corresponds, see Eq. (1.2) and (1.4), to the phase-space density $n\Lambda_T^3 = 0.01$ or temperature $T = 27E_F$, for $T = 500\,\mathrm{nK}$.

Collisions between cold molecules are cruial in determining the properties of the molecular gas. It was observed that, not surprisingly, at ultra-low temperatures the collisions are determined by quantum statistics. The $^{40}K^{87}Rb$ molecules are fermions. If the fermionic molecules are in the same internal state, collision rates are strongly reduced because of the Pauli principle. To be more precise, non-identical particles collide in the s-wave channel (and higher odd channels), but identical fermions scatter in p-wave (and higher even channels). Furthermore, it was observed that when KRb molecules collide, they undergo the chemical reaction [69]

$$\mathrm{KRb} + \mathrm{KRb} \rightarrow \mathrm{K_2} + \mathrm{Rb_2}. \tag{1.18}$$

This reaction is exothermic and realeases $\sim 1.2\,\mathrm{meV} = 14\,\mathrm{K}$ of kinetic energy; the products K_2 and Rb_2 thus leave the trap immediately.

Polar molecules are particularly interesting because the dipole moment, and therefore the dipolar interactions, can be tuned by applying an external electric field. The common unit for molecular dipole moments is

$$1\,\mathrm{Debye} = 3.33564 \times 10^{-30}\,\mathrm{C\ m}, \tag{1.19}$$

and the typical dipole moment of polar molecules is of the order of magnitude $\sim 1\,\mathrm{Debye}$. The properties of the KRb molecule will be discussed in Sec. 4.1.

[3] It is common [17] to call temperatures below 1 Kelvin cold and below 1 mK ultra-cold.

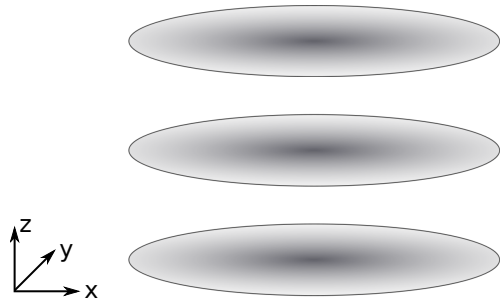

Figure 1.2: Pancake-shaped trap geometry, produced by an optical lattice in the z direction.

It has been observed that the rate of collisions for KRb molecules, which are polar, is strongly dependent on the electric field [26]. The dipolar interaction *increases* the rate of collisions and, therefore, the rate of chemical reactions (1.18). This makes a gas of oriented KRb molecules highly unstable and prevents cooling to lower temperatures. Thus, the fact that chemical reactions take place is an obstacle for the observation of ultra-cold gases of oriented KRb molecules in the quantum degenerate regime.

In order to circumvent this problem, the JILA experiments confined the gas in a pancake-shaped geometry [26]. By applying an additional optical potential in the z direction, the geometry of the trap consists of several flat layers, stacked on top of each other (see Fig. 1.2). In this way, the dipolar interaction is mostly repulsive and the rate of chemical reactions is *reduced*.

1.8 Overview of the thesis

This thesis contains theoretical investigations of the physics of a dipolar gas in a bilayer system at very low temperatures.

In Chapter 2 we study the two-body physics of a gas interacting by the dipole–dipole interaction. Some general methods, analytical and numerical, are presented for the calculation of binding energies and scattering states close to the threshold of a two-dimensional system. The results are used to calculate the weakly bound states and scattering properties which arise from the interaction of dipolar particles in different layers. It is pointed out that this interaction V_{dd} has somewhat special properties regarding bound and scattering states, due to the relation $\int V_{\mathrm{dd}}\, d^2r = 0$.

In Chapter 3 we consider the many-body physics of the dipolar gas of fermions in a bilayer geometry. The interaction between dipoles in different layers may lead to a Cooper pairing of particles, such that molecules in different layers form one pair. This results in a BCS-like interlayer superfluid. For stronger dipole moments, the dipoles form pairs in real space (dimers). The system can be tuned between the BCS state and the condensate of dimers by an external electric field,

thus showing a peculiar BCS–BEC crossover. The crossover is described here based on the Eagles–Leggett model for $T = 0$; and for $T > 0$ the critical temperature for the superfluid transition is determined using Kosterlitz–Thouless theory. Insights from the investigation of the two-body physics are used to compare analytical and numerical results.

In Chapter 4 we consider the non-equilibrium dynamics of a polar gas for small external electric fields. The particles populate rotational states (Stark states), and the dipole–dipole interaction leads to state exchange collisions. The rate of these collisions is calculated. The state-changing collisions can be observed, if a certain initial state is prepared, for chemically reactive molecules (such as KRb) at temperatures far above the Fermi temperature.

The results of Chapter 2, 3 and 4 have been published in [45], [77] and [76], respectively.

CHAPTER 2

Scattering and bound states in two dimensions

Ultracold atomic gases are many-body systems, but many of their fundamental properties originate from the underlying two-body problem. Usually the interaction in the gas can be described by a contact potential, but the situation is completely different in dipolar gases due to the long-range character of the dipole–dipole interaction. A promising route towards quantum degenerate gases of polar molecules is by confining the gas in two-dimensional geometries, see Sec. 1.7.

Two-dimensional scattering at low energies determines the properties of 2D quantum gases [61, 74, 80]; they are particularly sensitive to the existence and properties of weakly bound states. Although low-energy 2D scattering [14, 15, 18, 33, 43] and weakly bound states [72, 73, 86] have been studied, little is known for the case when $\int V(r)\, r dr = 0$. The binding energy for weak bound states in this case was calculated to first order [86], but a detailed investigation of the binding energy and of the low-energy scattering properties is lacking.

Motivation & Summary

- Two-body properties at low energies determine the many-body physics of ultracold gases. We consider scattering and bound states in 2D geometries.
- Weakly bound states are studied and an expression for the binding energy is given which is valid also when $\int V(r)\, r dr = 0$.
- It is shown that the presence of an anomalously weak bound state modifies significantly the scattering amplitude, compared to the usual case. An expression for the low-energy scattering phase shift is given.
- The results are specialized for the dipole–dipole inter-layer potential V_{dd}. The validity of the analytical expressions is checked using exact numerical calculations.

2.1 Introduction

We consider the two-dimensional Schrödinger equation

$$\left(-\frac{\hbar^2}{2m}\nabla^2 + U(\mathbf{r})\right)\Psi(\mathbf{r}) = E\,\Psi(\mathbf{r}). \tag{2.1}$$

For a radially symmetric potential $U = U(|\mathbf{r}|)$, changing to polar coordinates (r, φ) and writing

$$\Psi(\mathbf{r}) = \sum_{\ell=-\infty}^{\infty} \psi_\ell(r) e^{i\ell\varphi} \tag{2.2}$$

leads to the radial equation

$$\left(\frac{d^2}{dr^2} + \frac{1}{r}\frac{d}{dr} - \frac{\ell^2}{r^2} + \frac{2m}{\hbar^2}E\right)\psi(r) = V(r)\psi(r) \tag{2.3}$$

where $V(r) = \frac{2m}{\hbar^2}U(r)$. The solutions of this equation for different ℓ are referred to as partial waves. Since the equation contains ℓ^2, it is sufficient to restrict attention to $\ell = 0, 1, 2\ldots$ which are known as s-wave, p-wave, d-wave etc. It should be kept in mind that for each positive ℓ, there are two wave functions: one with angular dependence $e^{i\ell\varphi}$ and one with $e^{-i\ell\varphi}$.

Our investigations will allow long-range[1] potentials. Only a certain regularity of $V(r)$ at $r = 0$ and at $r = \infty$ needs to be assumed, we take (these are conditions from [64, 86]):

- $\int_0^b r|V(r)|dr$ is finite, i.e. $V(r)$ grows slower than r^{-2} at $r = 0$.
- $\int_c^\infty r|V(r)|dr$ is finite, i.e. $V(r)$ decays faster than $1/r^2$ at infinity.

It will be understood that we consider scattering states with positive energy and bound states with negative energy.

The solutions of the free two-dimensional radial Schrödinger equation are the Bessel functions. We use the following notation: $J_\ell(x)$, $Y_\ell(x)$ are the Bessel functions of the first and second kind, respectively, and $H_\ell(x) = J_\ell(x) + iY_\ell(x)$ is the Hankel function of the first kind, often written $H_\ell^{(1)}(x)$. Also $I_\ell(x)$ and $K_\ell(x)$ are the modified Bessel functions and $\gamma = 0.577\cdots$ is Euler's constant. Identities involving Bessel functions can be found in [1].

[1] It depends very much on the physical problem what type of potential is to be considered "long-range" and what type "short-range". In scattering theory, potentials of finite range (i.e. they vanish for all $r > R_*$) are often considered.

2.2 Two-dimensional scattering

In scattering theory, one writes the wave function as a sum of an incoming wave and a scattered wave. At large r, there is a region where the potential is not effective any more. This means that in this asymptotic region the wave function is that of the free Schrödinger equation. The solutions of the free radial two-dimensional Schrödinger equation are the Bessel functions.

The wave function for the asymptotic region is conventionally written as

$$\Psi^+(r,\varphi) = \sum_{\ell=-\infty}^{\infty} i^\ell \left(J_\ell(kr) + i f_\ell H_\ell(kr)\right) e^{i\ell\varphi}, \tag{2.4}$$

a different form for $kr \gg 1$ is

$$\Psi^+(r,\varphi) = e^{i\mathbf{k}\cdot\mathbf{r}} + f(\varphi;k)\sqrt{\frac{2}{\pi kr}} e^{i\pi/4} e^{i|\mathbf{k}||\mathbf{r}|} \qquad (kr \gg 1) \tag{2.5}$$

where φ is the angle between $\mathbf{k}$ and $\mathbf{r}$. These forms define the scattering amplitude: $f(\varphi)$ is the total scattering amplitude, and the partial scattering amplitudes f_ℓ are

$$f(\varphi;k) = \sum_{l=-\infty}^{\infty} f_\ell(k)\, e^{i\ell\varphi}. \tag{2.6}$$

Yet another way to write the scattering wave function in the asymptotic region for $kr \gg 1$ is

$$\Psi^+(r,\varphi) = \sum_{\ell=-\infty}^{\infty} A_\ell \sqrt{\frac{2}{\pi kr}} \cos\Big(kr - \ell\frac{\pi}{2} - \frac{\pi}{4} + \delta_\ell\Big) e^{i\ell\varphi} \qquad (kr \gg 1) \tag{2.7}$$

which defines the scattering phase shifts $\delta_\ell(k)$.

The relation between Eq. (2.4) and Eq. (2.5) can be seen using the identity

$$e^{ikr\cos\varphi} \;=\; \sum_{\ell=-\infty}^{\infty} i^\ell J_\ell(kr) e^{i\ell\varphi} \tag{2.8}$$

and the asymptotic limit

$$H_\ell(x) = \sqrt{\frac{2}{\pi x}}\, e^{i(x-\pi/4-\ell\pi/2)} \qquad \text{for } x \to \infty. \tag{2.9}$$

Comparing Eq. (2.7) and Eq. (2.4) and using the asymptotic limit

$$J_\ell(x) = \sqrt{\frac{2}{\pi x}}\, \cos\Big(x - \frac{\pi}{4} - \ell\frac{\pi}{2}\Big) \qquad \text{for } x \to \infty \tag{2.10}$$

it is seen that $A_\ell = i^\ell e^{i\delta_\ell}$ and

$$f_\ell = e^{i\delta_l} \sin\delta_\ell. \tag{2.11}$$

Physically, all this describes the situation after an incoming plane wave $e^{i\mathbf{k}\cdot\mathbf{r}}$ has scattered off the potential: the scattered wave Ψ^+ is the sum of the incoming wave and the scattered radial wave. The wave function contains only one free constant (scattering amplitude or phase shift, depending on which form one chooses); the overall normalization of the wave function has been chosen such that the coefficient in front of the incoming wave $e^{i\mathbf{k}\cdot\mathbf{r}}$ is 1.

The conventions for scattering parameters in two dimensions differ sometimes, in particular Refs [3, 48, 64, 75] use different conventions for the scattering amplitude. Our conventions are the same as in [48]. Ref. [75, 77] uses a different scattering amplitude $\bar{f}$, it is related to ours by $f = -\bar{f}/4$.

The scattering amplitude is a complex quantity; the scattering phase shifts are real and can be restricted to lie between 0 and π, as seen from Eq. (2.11). The relations between f_ℓ and δ_ℓ are listed in the following table (the index ℓ is omitted for clarity):

$$f = e^{i\delta}\sin\delta \tag{2.12a}$$

$$f = \frac{\tan\delta}{1+\tan^2\delta} + i\frac{\tan^2\delta}{1+\tan^2\delta} \tag{2.12b}$$

$$f^{-1} = \frac{1}{\tan\delta} - i \tag{2.12c}$$

$$\tan\delta = \frac{\operatorname{Im} f}{\operatorname{Re} f} \tag{2.12d}$$

Integral equation for scattering

The scattering amplitude f has the integral representation

$$f(\theta) = -\frac{m}{2\hbar^2}\int e^{-i\mathbf{k}'\cdot\mathbf{r}}\, V(\mathbf{r})\Psi_k^+(\mathbf{r})\, d^2r, \qquad \theta = \angle(\mathbf{k},\mathbf{k}'), \quad |\mathbf{k}| = |\mathbf{k}'| \tag{2.13}$$

in terms of the scattering wave function Ψ_k^+ for momentum k.

Relaxing the condition $|\mathbf{k}| = |\mathbf{k}'|$ in the integral representation (2.13), one defines the off-shell scattering amplitude

$$f(\mathbf{k},\mathbf{k}') = -\frac{m}{2\hbar^2}\int e^{-i\mathbf{k}'\cdot\mathbf{r}}\, V(\mathbf{r})\Psi_k^+(\mathbf{r})\, d^2r. \tag{2.14}$$

Using Fourier transformed quantities, one can show that the off-shell scattering amplitude satisfies the integral equation

$$f(\mathbf{k},\mathbf{k}') = -\frac{m}{2\hbar^2}\int\frac{d^2q}{(2\pi)^2}\,\frac{V(\mathbf{q}-\mathbf{k}')f(\mathbf{k},\mathbf{q})}{-q^2+k^2+i\epsilon} - \frac{m}{2\hbar^2}\,V(\mathbf{k}-\mathbf{k}'). \tag{2.15}$$

We used the following conventions[2] for the Fourier transform:

$$g(\mathbf{p}) = \int g(\mathbf{r})e^{i\mathbf{p}\cdot\mathbf{r}}\, d^2r, \qquad g(\mathbf{r}) = \int g(\mathbf{p})e^{-i\mathbf{p}\cdot\mathbf{r}}\,\frac{d^2p}{(2\pi)^2}. \tag{2.16}$$

[2] When comparing these formulas to [2, pp. 232–3], it should be kept in mind that A.G.D. has a different convention for Fourier transform: $V(\mathbf{p}) = V_{\text{AGD}}(-\mathbf{p})$.

2.3 Physical interpretation

Let us first give the physical interpretation in the three-dimensional case, following [36]. Consider a stream of incoming particles with number/area=I_{in} scattering with a target containing N_T particles. The counting apparatus observes N_{sc} scattered particles. The scattering cross-section σ is defined by

$$N_{\text{sc}} = N_T I_{\text{in}}\, \sigma, \tag{2.17}$$

or in terms of the velocity v_{in} and the number density $\rho_{\text{in}} = N_{\text{in}}/\text{Vol}$ of incoming particles (since $I = \text{time} \times \text{density} \times v$):

$$\begin{aligned} N_{\text{sc}} \,/\, \text{time} &= N_T \rho_{\text{in}} v_{\text{in}}\, \sigma & (2.18)\\ &= \frac{N_T N_{\text{in}}}{\text{Vol}} v_{\text{in}}\, \sigma. & (2.19) \end{aligned}$$

It is understood that the observation detects particles in a certain range of *final states* (e.g. region of space, internal state). The cross-section defined above is the cross-section for this specific process. As a special case, $\sigma(d\Omega) = \frac{d\sigma}{d\Omega} d\Omega$ is the cross-section for detection of particles in the spherical angle $d\Omega$.

All of the preceding discussion is easily transcribed to two dimensions. In 2D, the dimensions of the quantities are: $[\sigma] = \text{length}$, $[I] = 1/\text{length}$, $[\rho] = 1/\text{area}$ and the solid angle $d\Omega$ is replaced by the plane angle $d\varphi$.

Using the scattering wave function (2.5), it can be shown that the two-dimensional differential scattering cross-section is

$$\frac{d\sigma}{d\varphi} = \frac{2}{\pi k} |f(\varphi)|^2. \tag{2.20}$$

The total scattering cross-section in two dimensions is

$$\begin{aligned} \sigma_{\text{tot}} &= \int_0^{2\pi} \frac{d\sigma}{d\varphi}\, d\varphi = \frac{2}{\pi k} \int_0^{2\pi} |f(\varphi)|^2\, d\varphi & (2.21)\\ &= \frac{4}{k}\Big(|f_0(k)|^2 + 2\sum_{\ell=1}^{\infty} |f_\ell(k)|^2 \Big) = \frac{4}{k}\Big(\sin^2 \delta_0(k) + 2\sum_{\ell=1}^{\infty} \sin^2 \delta_\ell(k) \Big), & (2.22) \end{aligned}$$

where the second line gives the expression in terms of the partial scattering amplitudes (2.6) and scattering phase shifts.

We have considered so far the collision of a particle with a fixed target, i.e. scattering from a fixed scattering center with interaction potential $V(r)$. As is well-known, the scattering of two particles can be reduced to the scattering of one particle with a scattering potential, by going into the center-of-mass coordinate system. Here we consider only the scattering of distinguishable particles; in the case of identical particles quantum-mechanical symmetry requirements lead to some modifications, but we will not need to consider this.

Consider a collision, in the laboratory frame, of two particles with masses m_1, m_2 and velocities $\mathbf{v}_1$, $\mathbf{v}_2$ interacting by the potential $V(\mathbf{r}_1 - \mathbf{r}_2)$. Since the

interaction potential depends only on $\mathbf{r}_1 - \mathbf{r}_2$, the center-of-mass motion separates from the relative motion. In the center-of-mass frame of reference, this collision is described by the following equivalent process: a fictitious particle with

$$\text{position } \mathbf{r} = \mathbf{r}_1 - \mathbf{r}_2, \qquad \text{mass } m = \frac{m_1 m_2}{m_1 + m_2}, \tag{2.23}$$

$$\text{velocity } \mathbf{v} = \mathbf{v}_1 - \mathbf{v}_2, \qquad \text{momentum } \mathbf{p} = m\mathbf{v} \tag{2.24}$$

collides with a fixed scattering center with potential $V(\mathbf{r})$ located at the origin of coordinates. This can be used to calculate the quantities needed. For example, the total cross-section in the center-of-mass frame $\sigma(p)$ becomes $\sigma(|\mathbf{p}_1 - \mathbf{p}_2|)$ in the laboratory frame.

Consider a collision

$$A + B \to f \tag{2.25}$$

in the laboratory frame, where f is some final state. Let $\sigma(p)$ be the total cross-section for the equivalent process in the center-of-mass frame. From (2.19), the number of particles detected in state f is (N_α is the number of particles of type α and $n_\alpha = N_\alpha/\text{Vol}$):

$$N_f/\text{time} = \frac{N_A N_B}{\text{Vol}}\, v\sigma(\mathbf{p}), \qquad \text{or} \qquad n_f/\text{time} = n_A n_B\, v\sigma(\mathbf{p}) \tag{2.26}$$

with $v = |\mathbf{v}_1 - \mathbf{v}_2|$ and $\mathbf{p} = m(\mathbf{v}_1 - \mathbf{v}_2)$, m being the reduced mass.

2.4 Jost function

The scattering states and bound states of the *radial* Schrödinger equation can be studied using the formalism of Jost functions[3]. Two types of solutions of the radial equation, which obey certain boundary conditions at $r = 0$ and $r = \infty$, serve as a basis for the formalism. The main quantities are, however, not the wave functions themselves but a derived quantity $\mathcal{F}_\ell(k)$ called the Jost function, which depends only on the momentum k and the partial wave ℓ, and of course implicitly on the potential $V(r)$. The function $\mathcal{F}(k)$ is a complex function, and its argument k is, too, best viewed in the complex plane. The Jost function contains information on the scattering and on bound states; once the Jost function is known the scattering phase shift (and also the scattering amplitude) and the energies of the bound states are obtained in a simple way.

The formalism of Jost functions has originally been developed for three dimensions (see [63] for a detailed exposition), but with some changes it can be applied to the two-dimensional case. The two-dimensional formalism has been presented very clearly by Newton [64], the 2D Jost function also appears in [15, 33]. There is some freedom in the definitions, we will follow the conventions of Ref. [64].

[3]The formalism was developed by R. Jost and others, see [63, 24] for some historic remarks.

Summarizing, the Jost function formalism has the following advantages, some of which we will exploit:

- Scattering states and bound states can be studied in a unified way, see Sec. 2.7 and Sec. 2.9.
- Numerical methods can calculate the Jost function directly, see Sec. 2.5.
- For short-range potentials, the Jost function is analytic in the k-plane. But this gets more complicated in the two-dimensional case.
- The formalism is mathematically rigorous, and therefore allows general conclusions.

Solutions of the radial Schrödinger equation

The radial Schrödinger equation will be considered in two slightly different forms. The radial equation [Eq. (2.3)] for the angular momentum number $\ell = 0, 1, 2, \ldots$ is

$$\left(\frac{d^2}{dr^2} + \frac{1}{r}\frac{d}{dr} - \frac{\ell^2}{r^2} + k^2\right)\bar{\psi}(r) = V(r)\bar{\psi}(r). \tag{2.27}$$

The substitution

$$\bar{\psi}(r) = r^{-1/2}u(r) \tag{2.28}$$

results in the form

$$\left(\frac{d^2}{dr^2} + \left(\tfrac{1}{4} - \ell^2\right)\frac{1}{r^2} + k^2\right)u(r) = V(r)u(r). \tag{2.29}$$

For clarity, in this section solutions of the original radial Schrödinger equation (2.27) will be marked by a bar, and solutions of the substituted equation (2.29) will have no bar; the dependence on the partial wave ℓ will not be indicated explicitly. Ref. [64] employs only the substituted form of the Schrödinger equation.

There are two types of solutions of the radial Schrödinger equation which are used, they differ by their boundary conditions. The regular solution is defined by a boundary condition at $r = 0$, the irregular solution (also called Jost solution) by a boundary condition at $r \to \infty$. The definitions are summarized in the following table.

Name:		Boundary condition:		
		at point	for substituted Eq. (2.29)	for original Eq. (2.27)
$\varphi(r)$	regular solution	$r \to 0$	$r^{-\ell}r^{-1/2}\varphi(r) = 1$	$r^{-\ell}\bar{\varphi}(r) = 1$ (2.30)
$f(r)$	irregular solution	$r \to \infty$	$f(r) = e^{ikr}$	$\bar{f}(r) = \dfrac{e^{ikr}}{\sqrt{r}}$ (2.31)

Note that the scattering solution, i.e. the wave function which represents a scattering event (regular at $r = 0$ and behaving like Eq. (2.5) or equivalent for $r \to \infty$), is still a different solution. The relation between the regular solution and the scattering solution will be given later, in Eq. (2.44).

The regular solution satisfies the integral equation [64] : $(\bar{\varphi} = r^{-1/2}\varphi)$

$$\varphi(r) = \sqrt{r}\left(\frac{2}{k}\right)^{\ell} \ell!\, J_\ell(kr) - \int_0^r g(r,r')V(r')\varphi(r')\,dr' \tag{2.32}$$

$$\bar{\varphi}(r) = \left(\frac{2}{k}\right)^{\ell} \ell!\, J_\ell(kr) - \int_0^r \bar{g}(r,r')V(r')\bar{\varphi}(r')\,r'dr' \tag{2.33}$$

The irregular solution satisfies the equation: $(\bar{f} = r^{-1/2}f)$

$$f(r) = e^{i\pi\ell/2}\sqrt{\frac{i\pi kr}{2}}H_\ell(kr) + \int_r^\infty g(r,r')V(r')f(r')dr' \tag{2.34}$$

$$\bar{f}(r) = e^{i\pi\ell/2}\sqrt{\frac{i\pi k}{2}}H_\ell(kr) + \int_r^\infty \bar{g}(r,r')V(r')\bar{f}(r')\,r'dr' \tag{2.35}$$

with

$$g(r,r';k) = \sqrt{rr'}\,\frac{\pi}{2}[J_\ell(kr)Y_\ell(kr') - J_\ell(kr')Y_\ell(kr)] \tag{2.36}$$

and $\bar{g}(r,r') = g(r,r')/\sqrt{rr'}$.

The equations for the regular and the irregular solution are integral equations of Volterra type. This means that their solution is given by the series of iterations (Neumann series); this series is convergent for all values of the coupling constant, see e.g. [90]. We will use this fact in Sec. 2.7 and Sec. 2.9 to express the Jost function as a series.

Jost function properties

The Jost function $\mathcal{F}(k)$ is defined as the Wronskian of the two solutions $\varphi(r)$ and $f(r)$, see [64], but we shall work only with the integral representation of the Jost function.

The Jost function can be represented [64] in terms of the regular solution[4] as

$$\mathcal{F}_\ell(k) = 1 + \frac{1}{l!}\left(\frac{k}{2}\right)^\ell \frac{\pi}{2}\, e^{i\pi/2} \int_0^\infty V(r)\varphi(r;k)H_\ell(kr)\,\sqrt{r}dr \tag{2.37}$$

$$= 1 + \frac{1}{l!}\left(\frac{k}{2}\right)^\ell \frac{\pi}{2}\, e^{i\pi/2} \int_0^\infty V(r)\bar{\varphi}(r;k)H_\ell(kr)\,r dr, \tag{2.38}$$

and in terms of the irregular solution as

$$\mathcal{F}_\ell(k) = 1 + \sqrt{\frac{\pi}{2k}}\, e^{i\pi/4 - i\ell\pi/2} \int_0^\infty V(r)f(r;k)J_\ell(kr)\,\sqrt{r}dr \tag{2.39}$$

$$= 1 + \sqrt{\frac{\pi}{2k}}\, e^{i\pi/4 - i\ell\pi/2} \int_0^\infty V(r)\bar{f}(r;k)J_\ell(kr)\,r dr. \tag{2.40}$$

We have written the formulas for any ℓ, but in subsequent sections we will only need the case $\ell = 0$.

The Jost function is related to the scattering phase shift by

$$\tan\delta_\ell(k) = -\frac{\text{Im }\mathcal{F}_\ell(k)}{\text{Re }\mathcal{F}_\ell(k)}, \tag{2.41}$$

therefore

$$\mathcal{F}(k) = |\mathcal{F}(k)|\, e^{-i\delta(k)} \tag{2.42}$$

and the scattering amplitude is

$$f_\ell(k) = -\frac{\text{Im }\mathcal{F}_\ell(k)}{\mathcal{F}_\ell(k)}. \tag{2.43}$$

The Jost function also gives the relation between the scattering wave function ψ and the regular solution φ:

$$\psi(r) = i^\ell \frac{\varphi(r)}{\mathcal{F}(k)}. \tag{2.44}$$

Combining (2.44) and (2.4), we see that the regular solution has the asymptotic form

$$\bar{\varphi}(r) = \mathcal{F}(k)\big(J_\ell(kr) + i f_\ell(k)\, H_\ell(kr)\big). \tag{2.45}$$

The above equations refer to scattering states, so it is understood that $k > 0$. In order to apply the same formalism to bound states which have negative energy,

[4] In the first line of Eq. (3.8) in [64] the "−" should be "+".

we have to set $k = i\alpha$ with $\alpha > 0$. The integral representations for the Jost function remain valid for complex k.

A bound state at energy $\epsilon_b = -\alpha^2$ is characterized by the fact that the Schrödinger equation has a solution which is regular at the origin and falls off exponentially at infinity. Then it is easy to show that the energies of the bound states $\epsilon_b = -\alpha^2$ are the solutions of

$$\mathcal{F}(i\alpha) = 0, \tag{2.46}$$

in other words, the bound states are the zeros of the Jost function on the positive imaginary axis.

2.5 Numerical calculation of scattering parameters

Scattering parameters for $\ell = 0$ can be calculated numerically by solving the radial Schrödinger equation

$$\left(\frac{d^2}{dr^2} + \frac{1}{r}\frac{d}{dr} + k^2\right)\psi(r) = \frac{2m}{\hbar^2}U(r)\psi(r). \tag{2.47}$$

(In Sec. 2.4 this was called the original Schrödinger equation, and its solutions were marked with a bar.)

The regular solution is defined by its behavior at $r = 0$, therefore it can be found numerically by integrating the ordinary differential equation (2.47) with given initial conditions at $r = 0$. The boundary conditions for the regular solution are (cf. (2.30))

$$\begin{cases} \bar{\varphi}(r{=}0) = & 1 \\ \bar{\varphi}'(r{=}0) = & 0. \end{cases} \tag{2.48}$$

In the region of large r where the potential is not effective any more, any solution of (2.47) is a linear combination of Bessel functions J_0 and Y_0. Thus, in the asymptotic region we can write the regular solution in the form

$$\bar{\varphi}(r) = \mathcal{N}\big(J_0(kr) + if H_0(kr)\big) \tag{2.49}$$

with two complex constants $\mathcal{N}$, f (they are not independent). Comparing (2.49) with (2.45), we see that $f = f(k)$ is the partial scattering amplitude for $\ell = 0$ and that the "normalization constant" $\mathcal{N}$ is, in fact, the Jost function:

$$\mathcal{N} = \mathcal{F}(k). \tag{2.50}$$

Assuming that the regular solution has been found numerically, then one has fit this function for large r to the form (2.49) in order to determine $\mathcal{N}$ and f. This can be done using the method given in [10]: the right-hand side of Eq. (2.49) is fitted to the regular solution using the (known) zeros of the Bessel functions. One

may proceed as follows. The differential equation (2.47) is solved in dimensionless units; if r_0 is the unit of length, the dimensionless variables are $\tilde{r} = r/r_0$, $\tilde{k} = kr_0$. One has to fit the regular solution to the form

$$\bar{\varphi}(\tilde{r}) = \mathcal{N}\big(J_0(\tilde{k}\,\tilde{r}) + if H_0(\tilde{k}\,\tilde{r})\big) \tag{2.51}$$

in the asymptotic region. Let j, y be the zeros of the Bessel functions $J_0(x)$, $Y_0(x)$. Then, at the points $\tilde{r} = j/\tilde{k}$, $\tilde{r} = y/\tilde{k}$ we must have, from Eq. (2.51),

$$\bar{\varphi}\big(j/\tilde{k}\big) = -\mathcal{N}f\, Y_0(j) \tag{2.52}$$

$$\bar{\varphi}\big(y/\tilde{k}\big) = (\mathcal{N} + i\mathcal{N}f)\, J_0(y) \tag{2.53}$$

These are two equations for $\mathcal{N}$, f. Solving them, we get

$$\mathcal{N} = \mathcal{F}(k) = \frac{\bar{\varphi}\big(y/\tilde{k}\big)}{J_0(y)} + i\frac{\bar{\varphi}\big(j/\tilde{k}\big)}{Y_0(j)} \tag{2.54}$$

$$f^{-1} = -\frac{\bar{\varphi}\big(y/\tilde{k}\big)\, Y_0(j)}{\bar{\varphi}\big(j/\tilde{k}\big)\, J_0(y)} - i \tag{2.55}$$

The quantities $\mathcal{N} = \mathcal{F}$ and f are not independent, and these equations are in agreement with the various relations between $\mathcal{F}$ and f, Eqs. (2.12). The scattering phase shift is given by

$$\tan\delta = -\frac{\bar{\varphi}\big(j/\tilde{k}\big)\, J_0(y)}{\bar{\varphi}\big(y/\tilde{k}\big)\, Y_0(j)}. \tag{2.56}$$

Therefore in summary, the scattering parameters for a given k may be determined as follows:

1. Integrate equation (2.47), starting from $r = 0$ with initial conditions (2.48), to obtain the regular solution $\varphi(\tilde{r})$.

2. Let $\tilde{r} > \tilde{R}$ be the region where the potential is not effective anymore. Using Bessel function zeros chosen such that $j_n, y_m > \tilde{R}\tilde{k}$, determine the scattering parameters from any of the Eqs. (2.54), (2.55), (2.56). Repeat this for larger zeros until convergence is reached.

2.6 Simon's formula for weakly bound states

The bound states of the two-dimensional Schrödinger equation

$$\left(-\nabla^2 + gV(\mathbf{r})\right)\psi(\mathbf{r}) = \epsilon\,\psi(\mathbf{r}),$$

where $g > 0$ is a dimensionless coupling constant, were studied by B. Simon [86] for weak coupling. It was shown that as $g \to 0$, there is always a shallow bound state if $\int V(\mathbf{r})\,d^2r \le 0$, no matter how small g is. On the other hand, there is no bound state for $g \to 0$ if $\int V(\mathbf{r})\,d^2r > 0$. Furthermore, Simon [86] derived the binding energy ϵ_b of these weakly bound states ($|\epsilon_b| \ll 1$, $g \ll 1$), finding:

$$\epsilon_b \sim -\exp\Big(\frac{4\pi}{g\int V(\mathbf{r})d^2r}\Big) \qquad \text{if } \int V(\mathbf{r})\,d^2r < 0 \tag{2.57}$$

$$\epsilon_b \sim -\exp\Big(\frac{1}{g^2\,c}\Big) \qquad \text{if } \int V(\mathbf{r})\,d^2r = 0 \tag{2.58}$$

We are mostly interested in the second case[5], where $\int V(r)\,d^2r = 0$. The constant c is given by[6]

$$c = \frac{1}{8\pi^2}\int d^2r \int d^2r'\,V(\mathbf{r})\log|\mathbf{r}-\mathbf{r}'|V(\mathbf{r}'). \tag{2.59}$$

A different form is obtained (similarly to what was done for the one-dimensional case in [86]) writing

$$\log|\mathbf{r}-\mathbf{r}'| = -\lim_{\alpha\to 0}\left[K_0(\alpha|\mathbf{r}-\mathbf{r}'|) + \log\tfrac{e^\gamma}{2}\alpha\right] \tag{2.60}$$

and using the Fourier representation

$$K_0(\alpha|\mathbf{r}|) = \frac{1}{2\pi}\int \frac{e^{i\mathbf{k}\cdot\mathbf{r}}}{k^2+\alpha^2}d^2k. \tag{2.61}$$

Then one obtains, using $\int V(\mathbf{r})\,d^2r = 0$,

$$c = -\frac{1}{2}\frac{1}{2\pi}\int \frac{|V(\mathbf{k})|^2}{|\mathbf{k}|^2}\frac{d^2k}{(2\pi)^2} \tag{2.62}$$

which shows that the constant c is always negative.

If the potential is radially symmetric, $V = V(|\mathbf{r}|)$, then the angular integral in Eq. (2.59) can be carried out [72]. Using $\int V(r)rdr = 0$ this gives

$$c = \frac{1}{2}\int_0^\infty dr\,rV(r)\int_r^\infty dr'\,r'V(r')\log\frac{r'}{r}. \tag{2.63}$$

[5]The binding energy in the nonexceptional case, Eq. (2.57), is calculated in Ref. [48, §45] by a perturbative method.

[6]This expression follows from the calculations of Ref. [86]. It was given in [45], but unfortunately there is a misprint in Eq. (2) of [45]; there are also some misprints in Ref. [86].

The inter-layer dipole–dipole potential in dimensionless units is, cf. Sec. 1.5,

$$V_{\mathrm{dd}}(r) = U_0 \frac{r^2 - 2}{(r^2+1)^{5/2}}. \tag{2.64}$$

Here the dimensionless coupling constant is called U_0. It satisfies $\int V_{\mathrm{dd}}(r) d^2r = 0$ the expressions (2.63) or (2.62) (using $V_{\mathrm{dd}}(\mathbf{k}) = -2\pi|k|e^{-|k|}$) give $c = -1/8$, hence Simon's result (2.58) for the binding energy becomes:

$$\epsilon_b^{\mathrm{dd}} \sim -\exp\left[-\frac{8}{U_0^2}\right]. \tag{2.65}$$

A numerical calculation of the binding energy (see Fig. 2.1 on p. 33) shows that this result is not very accurate even when U_0 is very small.

2.7 Jost function: Weakly bound states

The leading-order expressions for the binding energy from the preceding Sec. 2.6, which were obtained in [86], are valid only for very small coupling g. Even in this regime the expression (2.65) is not very accurate when compared to numerics, at least for the dipole–dipole potential. This motivates us to extend Simon's result; we derive an analytic formula for the binding energy which is valid in a larger regime and is more accurate in comparison with the numerical result for the dipolar potential.

The Jost function for small momenta is obtained from the integral representations (2.38) or (2.40) by expanding in powers of k. Using $J_0(kr) = 1 + \dots$ and $Y_0(kr) = (2/\pi)\log(\frac{e^\gamma}{2}kr) + \dots$ we get:

$$\begin{aligned} \mathcal{F}(k) &= A\log k + B - i\frac{\pi}{2}A + O(k^2) \\ &= A\log(\tfrac{e^\gamma}{2}k) + B' - i\frac{\pi}{2}A + O(k^2) \end{aligned} \tag{2.66}$$

with $B = B' + A\log\frac{e^\gamma}{2}$; the factor $e^\gamma/2 = 0.89\cdots$ is not very important in practice. The constants A, B are given in terms of the regular solution by

$$A = -\int_0^\infty V(r)\bar{\varphi}(r, k{=}0)\, r dr \tag{2.67}$$

$$B' = 1 - \int_0^\infty \log r\, V(r)\bar{\varphi}(r, k{=}0)\, r dr \tag{2.68}$$

where the $\bar{\varphi}(k{=}0)$ satisfies

$$\bar{\varphi}(r; k{=}0) = 1 - \int_0^r \bar{g}(r, r'; k{=}0) V(r')\bar{\varphi}(r'; k{=}0)\, r' dr'. \tag{2.69}$$

In terms of the irregular solution, the constants are expressed by

$$A = -\int_0^\infty V(r) f_A(r)\, r dr \tag{2.70}$$

$$B' = 1 - \int_0^\infty V(r) f_B(r)\, r dr \tag{2.71}$$

where f_A, f_B satisfy

$$f_A(r) = 1 + \int_r^\infty \bar{g}(r, r'; k=0) V(r') f_A(r')\, r' dr' \tag{2.72}$$

$$f_B(r) = \log r + \int_r^\infty \bar{g}(r, r'; k=0) V(r') f_B(r')\, r' dr'. \tag{2.73}$$

The function $\bar{g}(r, r'; k)$, see Eq. (2.36) is, interestingly, an analytic function of k^2 and we have

$$\bar{g}(r, r'; k=0) \;=\; \log \frac{r'}{r}. \tag{2.74}$$

The constants A, B can be represented by infinite series by iterating the integral equations. We put

$$A = \sum_{n=1}^{\infty} A_n, \qquad B = 1 - \sum_{n=1}^{\infty} B_n, \tag{2.75}$$

and each A_n and B_n is proportional to g^n, the n-th power of the coupling constant. The first terms of these series, obtained from the irregular solution, Eqs. (2.70)–(2.73), are

$$A_1 = -\int_0^\infty dr_1 r_1 V(r_1) \tag{2.76}$$

$$A_2 = -\int_0^\infty dr_1 r_1 V(r_1) \int_{r_1}^\infty dr_2 r_2 V(r_2) \log\Big(\frac{r_2}{r_1}\Big) \tag{2.77}$$

$$A_3 = -\int_0^\infty dr_1 r_1 V(r_1) \int_{r_1}^\infty dr_2 r_2 V(r_2) \log\Big(\frac{r_2}{r_1}\Big) \int_{r_2}^\infty dr_3 r_3 V(r_3) \log\Big(\frac{r_3}{r_2}\Big) \tag{2.78}$$

$\ldots$

and

$$B_1' = \int_0^\infty dr_1 r_1 V(r_1) \log(r_1) \tag{2.79}$$

$$B_2' = \int_0^\infty dr_1 r_1 V(r_1) \int_{r_1}^\infty dr_2 r_2 V(r_2) \log\Big(\frac{r_2}{r_1}\Big) \log(r_2) \tag{2.80}$$

$\ldots$

To find the bound states, we look for the zeros of $\mathcal{F}(k)$ on the positive imaginary axis, cf. Eq. (2.46). Using the expansion of $\mathcal{F}$ for small k, Eq. (2.66), the equation $\mathcal{F}(i\alpha) = 0$ is solved and gives the binding energy

$$\epsilon_b = -\exp\left\{-2\frac{B}{A}\right\} = -\frac{4}{e^{2\gamma}} \exp\left\{-2\frac{B'}{A}\right\}. \tag{2.81}$$

This is an approximate expression which is valid only if $|\epsilon_b|$ is sufficiently small. We will see, however, that it gives sufficiently good results for the dipole–dipole

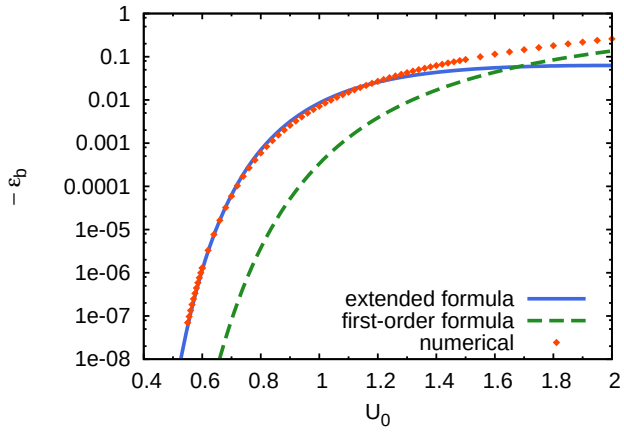

Figure 2.1: Binding energy as a function of the dipole strength U_0 for the dipole–dipole potential calculated numerically (dots) and from equation (2.84), compared to the first-order (Simon's) expression (2.65).

potential. Since $4/e^{2\gamma} = 1.261\cdots$, this factor is actually not important in practice because the exponential term is the dominant one for $|\epsilon_b| \ll 1$. The expression (2.81) reduces to the formulas of Sec. 2.6 in the limit $g \to 0$. The leading terms for small coupling g are: $A = A_1$, or if $A_1 = -\int V(r) r dr = 0$ then $A = A_2$, and $B = 1$.

2.8 Binding energy for the dipole–dipole potential

We consider the bound states of the dipole–dipole interaction of molecules in different layers, Eq. (1.16):

$$V_{\rm dd}(r) = U_0 \frac{r^2 - 2}{(r^2+1)^{5/2}}. \tag{2.82}$$

Here, the first few integrals A_n and B_n can be evaluated analytically. The results are given in Table 2.1.

Since $\int V_{\rm dd}(r) d^2 r = 0$, we have $A_1 = 0$ and the first non-vanishing term is A_2. Therefore, in the leading approximation $A \approx A_2$, $B \approx 1$ and the binding energy Eq. (2.81) then gives Simon's formula (2.65). A more precise formula is obtained by including higher terms:

$$\epsilon_b = -\exp\left\{-2\,\frac{1 - B_1 - B_2 - \ldots}{A_1 + A_2 + \ldots}\right\}. \tag{2.83}$$

Taking terms up to A_2 and B_2, we get

$$\epsilon_b^{\rm dd} = -\exp\left\{-\frac{8}{U_0^2}\left[1 - U_0 + U_0^2\left(\frac{5}{8} + \frac{1}{4}(\gamma - \ln 2)\right)\right]\right\}. \tag{2.84}$$

Table 2.1: Integrals for the dipole–dipole potential V_{dd}.

$A_1 = 0$	$B'_1 = 1$
$A_2 = 1/4$	$B'_2 = -5/8$
$A_3 = 1/60$	
$A_4 = -1/960$	

Each term A_n, B'_n carries an additional prefactor $(U_0)^n$.

Higher-order approximations can be obtained by including more terms from Table 2.1, the exponential will then contain a fraction[7], cf. Eq. (2.83).

Fig. 2.1 shows the comparison between the numerical result for ϵ_b^{dd} and the analytical expression of Eq. (2.84), showing that it provides a good approximation for ϵ_b^{dd} for $U_0 \lesssim 1.2$.

2.9 Jost function: Scattering

In this section we employ the Jost function formalism to study two-dimensional s-wave scattering.

An approximate expression of the Jost function $\mathcal{F}(k)$ for small coupling constant g is obtained by iterating twice the integral equation (2.35). Note that we keep all orders in k. The resulting scattering phase shift follows from the relation (2.41):

$$\tan\delta(k) = \frac{-\frac{\pi}{2} I_{JJ}(k) - \frac{\pi^2}{4}\left(I_{JJ,JY}(k) - I_{JY,JJ}(k)\right)}{1 - \frac{\pi}{2} I_{JY}(k) - \frac{\pi^2}{4}\left(I_{JJ,YY}(k) - \frac{1}{2} I_{JY}^2(k)\right)}, \tag{2.85}$$

where we have introduced the notation

$$I_{FG} = \int_0^\infty dr r V(r) F(r) G(r), \tag{2.86}$$

$$I_{FG,PQ} = \int_0^\infty dr r V(r) F(r) G(r) \int_r^\infty ds s V(s) P(s) Q(s), \tag{2.87}$$

and J, Y stand for $J_0(kr)$ and $Y_0(kr)$.

For small k it is possible to simplify Eq. (2.85). In leading order of k, the Jost function is logarithmic and we recover Eq. (2.66); the scattering phase shift is then, using (2.41),

$$\tan\delta(k) = \frac{\pi}{2} \frac{1}{\log k + B/A}, \tag{2.88}$$

[7] In Ref. [8] an expression for the bound-state energy was obtained using a different method. It agrees with our results if the expression inside the exponential is expanded in powers of U_0.

with constants A and B as defined in the previous section. Employing Eq. (2.81) to identify the binding energy ϵ_b, this gives the well-known logarithmic behavior

$$\tan\delta(k) = \left[\frac{1}{\pi}\log\frac{k^2}{|\epsilon_b|}\right]^{-1}, \tag{2.89}$$

which relates the phase shift and the binding energy of the weakly bound state. The logarithmic singularity at $k \to 0$ is characteristic of 2D s-wave scattering.

It is usually assumed (e.g. in [80]) that in two dimensions for low energies, the s-wave scattering phase shift is well-approximated by the logarithmic expression (2.89). Recall that the Jost function for small k is $\mathcal{F}(k) = A\log k + B + O(k^2)$. In the mathematical limit $k \to 0$, the logarithmic term is the dominant one. However, the logarithm is growing very slowly and it might happen that *extremely small* k are needed to "see" the logarithm; from Eq. (2.89) we see that in order to be in the logarithmic regime one needs

$$k^2/|\epsilon_b| \ll 1. \tag{2.90}$$

In the case $\int V(r)rdr = 0$, in particular, the binding energy $|\epsilon_b|$ can become very small, as was discussed before. Then, for reasonable k, the logarithm is not the leading term for low-energy scattering. This will be seen in the next section, where the dipole–dipole potential is discussed.

For large k, the logarithmic term is irrelevant. For large enough k and small g, the first integral $I_{JJ}(k)$ in Eq. (2.85) dominates and we recover the Born approximation, as expected for large energies. Furthermore, by expanding Eq. (2.85) in powers of g one obtains the terms of the Born series, which read to second order

$$\tan\delta(k) = -\frac{\pi}{2}I_{JJ} - \frac{\pi^2}{2}I_{JJ,JY}. \tag{2.91}$$

We note that the formula (2.85) interpolates smoothly between the correct low-energy and the correct high-energy behavior; this suggests that it may be valid, at least qualitatively, even for large g.

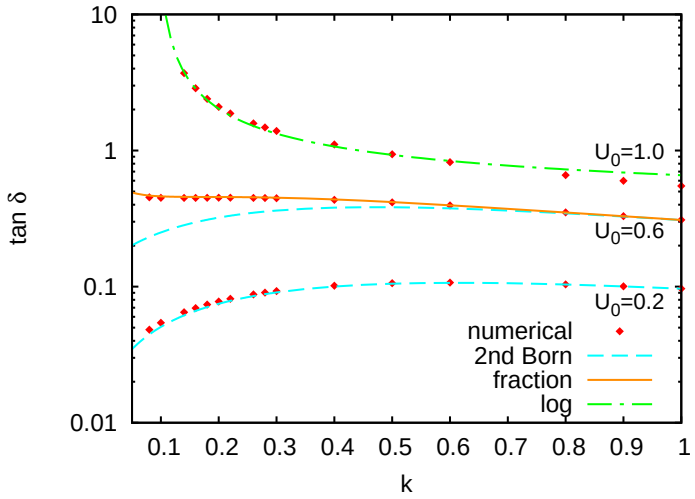

Figure 2.2: Scattering phase shift for $V_{\rm dd}$ as a function of k for different U_0 calculated numerically (dots) compared to the logarithmic behavior (2.66) for $U_0 = 1.0$, to the "fraction" formula (2.85) for $U_0 = 0.6$ and to the second Born approximation (2.91) for $U_0 = 0.6$ and $U_0 = 0.2$. The curves of the fraction, Eq. (2.85), for $U_0 = 1.0$ and $U_0 = 0.2$ are not drawn since they lie on top of the logarithmic and Born curves.

2.10 Scattering for the dipole–dipole potential

Now we discuss s-wave scattering for the case of the interlayer dipole–dipole potential $V_{\rm dd}$ of Eq. (2.82).

The scattering phase shift can be computed numerically, as described in Sec. 2.5. Comparing this to the approximate expression (2.85), we find that Eq. (2.85) provides the correct scattering phase shift with very good accuracy, at least in the range $0.03 \le k \le 5$ and $0.05 \le U_0 \le 2.0$. Hence Eq. (2.85) is a good approximation not only for $U_0 \ll 1$ (this is the condition used in the derivation above), but also for $U_0 \sim 1$. Clearly, if the interactions are too large ($U_0 \gg 1$), the contributions from higher iterations of the integral equation become more important and Eq. (2.85) looses its accuracy.

The first Born approximation for the potential $V_{\rm dd}$ can be evaluated analytically (see Sec. A3.1):

$$\tan\delta(k)_B = -\frac{\pi}{2}\int_0^\infty dr r V(r) J_0^2(kr) \tag{2.92}$$

$$= -\frac{\pi}{2}U_0\left[-\frac{4k}{\pi} - 2k\big(\mathbf{L}_1(2k) - I_1(2k)\big)\right], \tag{2.93}$$

where $\mathbf{L}_1$ is the modified Struve function.

Figure 2.2 compares the numerical results for the scattering phase shift for $V_{\rm dd}$ with the simple approximations of Eq. (2.89) (logarithmic behavior) and Eq. (2.91) (second Born approximation) as well as with the more elaborate formula Eq. (2.85). It is seen that for $U_0 \sim 1$, the scattering phase shift is best

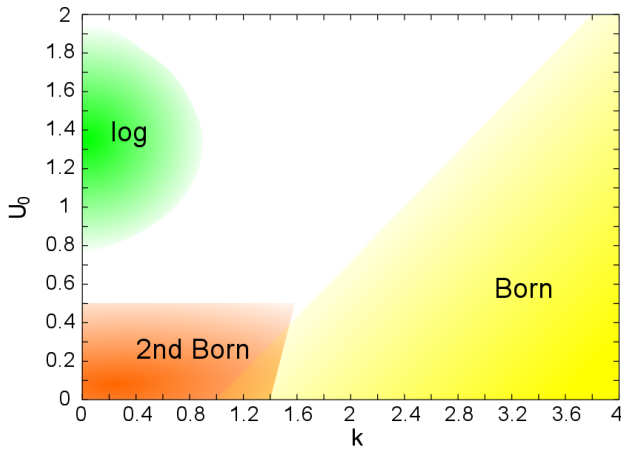

Figure 2.3: Qualitative sketch of the regimes of k and U_0 where the scattering phase shift for V_{dd} can be approximated by the logarithm Eq. (2.89) (green), the Born approximation Eq. (2.92) (yellow), and the second Born approximation Eq. (2.91) (orange).

approximated by the logarithmic expression (2.89), and for $U_0 \ll 1$ by the second Born approximation (2.91). For intermediate values of U_0 none of the limiting cases are accurate and the full expression (2.85) should be used. As mentioned, the full expression (2.85) contains the logarithmic and the second-Born behavior as limiting cases.

In Fig. 2.3 we sketch qualitatively the regimes of k and U_0, where the logarithm (2.89), the first Born approximation (2.92), and the second Born approximation (2.91) are good approximations, as compared with the numerical solution. Note that, excluding unreasonably small k, the logarithmic form (2.89) is just valid for $k \ll 1$ and the window $0.7 \lesssim U_0 \lesssim 2.0$.

CHAPTER 3

Interlayer superfluid and BCS–BEC crossover

Ultracold gases of dipolar particles attract great interest because the dipole–dipole interaction drastically changes the nature of quantum degenerate regimes compared to ordinary short-range interacting gases. Experiments which succeeded in creating polar molecules use confinement to two-dimensional geometries to suppress chemical losses, see Sec. 1.7. In these experiments, dipoles are confined to thin layers and the dipole moment of the molecules is oriented perpendicularly to the plane of motion.

Already in a geometry which consists of only two layers, the observation of new quantum phases is possible. The dipole–dipole interaction between the molecules in different layers may lead to a Cooper-like pairing of fermions, which gradually changes to a real-space pairing as the external electric field is increased.

Motivation & Summary

- Confining polar molecules in two-dimensional geometries reduces inelastic losses and therefore facilitates cooling towards quantum degeneracy.
- We consider fermionic polar molecules in a bilayer geometry, where the dipoles are oriented perpendicularly to the layers, in the quantum degenerate regime.
- It is shown that the interaction between dipoles of different layers may lead to the emergence of an *interlayer superfluid*, that is a superfluid 2D gas where Cooper pairs are formed by fermionic molecules of different layers.
- As the dipole–dipole coupling increases, the system undergoes a BCS–BEC crossover which presents some novel features compared to that for atomic fermions near a Feshbach resonance.

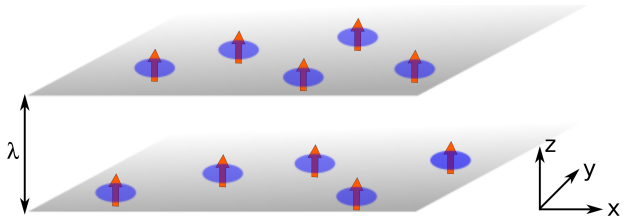

Figure 3.1: Bilayer dipolar system under consideration. The particles are confined to two thin parallel layers, the dipole is oriented in the z direction.

3.1 Introduction

We consider a degenerate gas of polar Fermi molecules, confined to two thin parallel layers, see Fig. 3.1. Such a confinement can be produced by a two-well optical potential along the z direction. The layer separation λ is sufficiently large such that inter-layer tunneling (hopping) can be neglected. An external electric field along z polarizes the molecules (orientational polarization), that the molecules acquire a electric dipole moment d in the laboratory frame.

First we will set up the Hamiltonian which describes this system. Using Bogoliubov's method, the pairing Hamiltonian is derived. It will be seen that the particles can form a Cooper pair where a particle in layer 1 and one in layer 2 form a pair. The gap equation and the number equation, which can be used to describe the crossover from the BCS regime to a condensate of dimers, are derived. The gap equation is transformed to a different form in order to obtain an expression for the critical temperature for the transition to the BCS state; the critical temperature will be shown to depend only on the two-body scattering properties. Here the results of Chapter 2 will be used to discuss and compare the analytical results with numerical calculations. Then, we discuss the solution of the equations which describe the BCS–BEC crossover. Finally, we determine the critical temperature for the superfluid transition across the whole crossover using Kosterlitz–Thouless theory.

It should be mentioned that the formation of Cooper pairs of fermions which move in different layers has been considered in semiconductor physics, see e.g. [56]. The model which describes the crossover from the BCS regime to a BEC of dimers, which we call the Eagles–Legget model, was first studied by Eagles [29] and later in much more detail by Leggett [51, 50]; see [53] for a historical overview.

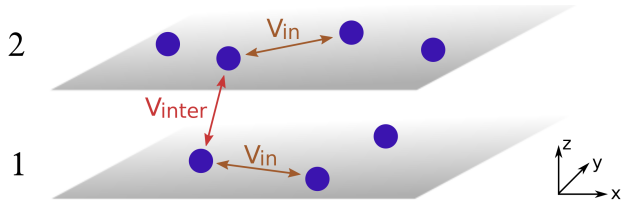

Figure 3.2: Schematic view of a bilayer system of interacting particles. The interaction is split into an in-layer part V_{in} and an inter-layer part V_{inter}.

3.2 Pairing Hamiltonian

The creation and annihilation operators for fermions in layer $\alpha = 1, 2$ are $\psi_\alpha^\dagger$ and ψ_α. Here and in the following, we omit the boldface letters for vectors. The general Hamiltonian for an interacting system of fermions (in position space) is

$$H = H_{\text{kin}} + \frac{1}{2}\sum_{\alpha,\beta}\int d^3r \int d^3r'\; V_{\alpha\beta}(r-r')\psi_\alpha^\dagger(r)\psi_\beta^\dagger(r')\psi_\beta(r')\psi_\alpha(r), \tag{3.1}$$

where H_{kin} is the kinetic energy part and $V_{\alpha\beta}$ is the interaction potential between a particle in layer α and a particle in layer β. We work in the grand canonical formalism (no particle number conservation), therefore we use the Hamiltonian $H - \mu N$, where μ is the chemical potential and N the number of particles. For a bilayer system, it is convenient to split the interaction Hamiltonian in two parts: interaction between particles within a layer (in-layer interaction V_{in}) and the interaction between particles in different layers (inter-layer interaction V_{inter}), see Fig. 3.2. Then

$$H = H_0 + H_{\text{in}} + H_{\text{inter}} \tag{3.2}$$

with

$$H_0 = \sum_{\alpha=1,2}\int d^3r\; \psi_\alpha^\dagger(r)(\mathcal{H}_{\text{kin}} - \mu)\psi_\alpha(r), \tag{3.3}$$

$$H_{\text{in}} = \frac{1}{2}\sum_{\alpha=1,2}\int d^3r \int d^3r'\; V_{\text{in}}(r-r')\,\psi_\alpha^\dagger(r)\psi_\alpha^\dagger(r')\psi_\alpha(r')\psi_\alpha(r), \tag{3.4}$$

$$H_{\text{inter}} = \int d^3r \int d^3r'\; V_{\text{inter}}(r-r')\,\psi_1^\dagger(r)\psi_2^\dagger(r')\psi_2(r')\psi_1(r). \tag{3.5}$$

Here $\mathcal{H}_{\text{kin}}$ is the kinetic energy operator; the interaction is symmetric with respect to $1 \leftrightarrow 2$, thus there is only one inter-layer term.

We consider two thin parallel layers, thus the system is quasi-two-dimensional. As described in Sec. A1.1, for low energies everything reduces to two-dimensional wave functions:

$$H_{\text{in}} = \frac{1}{2}\sum_{\alpha=1,2}\int d^2r \int d^2r'\; V_{\text{in}}^{\text{2d}}(r-r')\,\psi_\alpha^\dagger(r)\psi_\alpha^\dagger(r')\psi_\alpha(r')\psi_\alpha(r), \tag{3.6}$$

$$H_{\text{inter}} = \int d^2r \int d^2r'\; V_{\text{inter}}^{\text{2d}}(r-r')\,\psi_1^\dagger(r)\psi_2^\dagger(r')\psi_2(r')\psi_1(r), \tag{3.7}$$

where V^{2d} denotes the projected interaction (integrated over z direction, see Sec. A1.1) From now on r, r' denote two-dimensional vectors.

The mean-field approximation for four fermionic operators is (see [25])

$$c_1c_2c_3c_4 \overset{\text{MF}}{=} [\, c_1c_2; c_3c_4 \,] - [\, c_1c_3; c_2c_4 \,] + [\, c_1c_4; c_2c_3 \,], \tag{3.8}$$

where we have introduced the short-hand notation

$$[\, ab; cd \,] = \langle ab\rangle cd + \langle cd\rangle ab - \langle ab\rangle\langle cd\rangle. \tag{3.9}$$

The averages of operators give the following quantities. The density in layer $\alpha = 1, 2$ is given by the expectation value

$$n_\alpha(r) = \langle \psi_\alpha^\dagger(r)\psi_\alpha(r)\rangle. \tag{3.10}$$

A related quantity is the one-particle density matrix

$$\rho_\alpha(r, r') = \langle \psi_\alpha^\dagger(r)\psi_\alpha(r')\rangle, \qquad \rho_\alpha^*(r, r') = \langle \psi_\alpha^\dagger(r')\psi_\alpha(r)\rangle, \tag{3.11}$$

and the density is its diagonal element, $n(r) = \rho(r, r)$. To derive superfluid pairing, it is essential to introduce the quantity

$$F(r, r') = \langle \psi_2(r')\psi_1(r)\rangle, \qquad F^*(r, r') = \langle \psi_1^\dagger(r)\psi_2^\dagger(r')\rangle. \tag{3.12}$$

It describes pairing, more precisely F is the wave function of pairs [52]. The quantity F is also called anomalous average or Gorkov Green's function.

Now we apply the mean-field approximation using the operator averages defined above. For the inter-layer part, this gives

$$\begin{aligned}
\mathcal{H}_{\text{inter}} &= \psi_1^\dagger(r)\psi_2^\dagger(r')\psi_2(r')\psi_1(r) && && (3.13)\\
&\overset{\text{MF}}{=} +[\, \psi_1^\dagger(r)\psi_2^\dagger(r'); \psi_2(r')\psi_1(r) \,] && \text{pairing terms} && (3.14a)\\
&\quad -[\, \psi_1^\dagger(r)\psi_2(r'); \psi_2^\dagger(r')\psi_1(r) \,] && \text{tunneling terms} && (3.14b)\\
&\quad +[\, \psi_1^\dagger(r)\psi_1(r); \psi_2^\dagger(r')\psi_2(r') \,] && \text{density terms} && (3.14c)
\end{aligned}$$

Ignoring the tunneling terms which describe tunneling (hopping) between the layers, we get

$$\begin{aligned}
\mathcal{H}_{\text{inter}} \overset{\text{MF}}{=}\ & F^*(r, r')\psi_2(r')\psi_1(r) + F(r, r')\psi_1^\dagger(r)\psi_2^\dagger(r') - |F(r, r')|^2 \\
& + n_1(r)\psi_2^\dagger(r')\psi_2(r') + n_2(r')\psi_1^\dagger(r)\psi_1(r) - n_1(r)n_2(r')
\end{aligned} \tag{3.15}$$

For the in-layer part

$$\begin{aligned}
\mathcal{H}_{\text{in}} =& \psi_\alpha^\dagger(r)\psi_\alpha^\dagger(r')\psi_\alpha(r')\psi_\alpha(r) && && (3.16)\\
\overset{\text{MF}}{=}& + [\, \psi_\alpha^\dagger(r)\psi_\alpha^\dagger(r'); \psi_\alpha(r')\psi_\alpha(r) \,] && \text{pairing terms} && (3.17a)\\
& - [\, \psi_\alpha^\dagger(r)\psi_\alpha(r'); \psi_\alpha^\dagger(r')\psi_\alpha(r) \,] && \text{off-diagonal density matrix terms} && (3.17b)\\
& + [\, \psi_\alpha^\dagger(r)\psi_\alpha(r); \psi_\alpha^\dagger(r')\psi_\alpha(r') \,] && \text{density terms} && (3.17c)
\end{aligned}$$

Ignoring the paired terms, since there is no pairing inside one layer (the interaction if purely repulsive), and off-diagonal density matrix terms, we have

$$\mathcal{H}_{\text{in}} \overset{\text{MF}}{=} n(r)\psi_\alpha^\dagger(r')\psi_\alpha(r') + n(r')\psi_\alpha^\dagger(r)\psi_\alpha(r) - n(r)n(r'). \tag{3.18}$$

Terms in $\mathcal{H}_{\text{in}}$ and $\mathcal{H}_{\text{inter}}$ which involve the density n describe the energy change due to the interaction (Hartree terms). Those with $\psi^\dagger\psi$ renormalize the chemical potential $\mu \to \tilde{\mu}$. For clarity, we continue writing μ, which now stands for the renormalized chemical potential. The total energy of the system is changed by "vacuum terms" which involve n^2 and F^2. We abbreviate them by *V.T.* since they are not essential in our derivation. Collecting terms, the Hamiltonian is

$$\begin{aligned} H_{\text{MF}} = &\sum_\alpha \int d^2r\ \psi_\alpha^\dagger(r)(\mathcal{H}_0 - \mu)\psi_\alpha(r) \\ &+ \int d^2r \int d^2r'\ V_{\text{inter}}^{\text{2d}}(r-r') \left\{ F^*(r,r')\psi_2(r')\psi_1(r) + F(r,r')\psi_1^\dagger(r)\psi_2^\dagger(r')) \right\} + V.T. \end{aligned} \tag{3.19}$$

In the following, we consider a constant density

$$n(r) = n. \tag{3.20}$$

We assume that the pair wave function depends only on the relative distance

$$F(r,r') = F(r-r')$$

which means that the center-of-mass momentum of the pair is zero.

Now it is convenient to transform to Fourier space. The expression transform as given in App. (A2.2). We set

$$\Delta(k) = \int V_{\text{inter}}^{\text{2d}}(r) F(r) e^{ik\cdot r} d^2r, \tag{3.21}$$

where $r = r_1 - r_2$ is the relative distance. We will use the notation $\Delta(k)$ and Δ_k interchangeably. Then, recalling that the adjoint operators $\psi^\dagger$ transform with $-k$, the Hamiltonian (3.19) becomes in Fourier space

$$\begin{aligned} H_{\text{MF}} = &\int \frac{d^2k}{(2\pi)^2} \Big\{ \eta_k \Big(\psi_1^\dagger(k)\psi_1(k) + \psi_2^\dagger(k)\psi_2(k) \Big) + \Delta_k^*\, \psi_2(-k)\psi_1(k) + \Delta_k\, \psi_1^\dagger(-k)\psi_2^\dagger(k) \Big\} \\ &+ V.T. \end{aligned} \tag{3.22}$$

with the abbreviation

$$\eta_k = \epsilon_k - \mu. \tag{3.23}$$

The Hamiltonian (3.22) contains only products of two fermionic operators. It can be diagonalized using the Bogoliubov transformation, see Sec. A2.1. The

transformation introduces two new fermionic operators, $\varphi_+(k)$ and $\varphi_-(k)$. These fermions, the so-called Bogoliubov quasiparticles[1], are linear combinations of the original fermions ψ_1 and ψ_2. We take $\Delta(k) = \Delta(-k) = \Delta^*(k)$. Transforming the Hamiltonian (3.22) using Eqs. (A.13) in Sec. A2.1 gives, after some algebra,

$$\begin{aligned} H_{\mathrm{MF}} = \int \frac{d^2k}{(2\pi)^2} \Big\{ & \left[\eta_k(u_k^2 - v_k^2) + 2\Delta_k u_k v_k\right] \left(\varphi_+^\dagger(k)\varphi_-(k) + \varphi_-^\dagger(k)\varphi_-(k)\right) \\ & + \left[-2\eta_k u_k v_k + \Delta_k(u_k^2 - v_k^2)\right] \left(\varphi_+^\dagger(k)\varphi_-^\dagger(k) - \varphi_-(k)\varphi_-(k)\right) + 2\eta_k v_k^2 - 2\Delta_k u_k v_k \Big\} \\ & + V.T. \end{aligned} \tag{3.24}$$

The condition that the second bracket vanishes

$$-2\,\eta_k\, u_k v_k + \Delta_k(u_k^2 - v_k^2) = 0 \tag{3.25}$$

is solved writing $u = \cos\theta$ and $v = \sin\theta$, so $\sin 2\theta = 2u_k v_k$ and $\cos 2\theta = u_k^2 - v_k^2$. Then Eq. (3.25) gives $\tan 2\theta = \Delta_k/\eta_k$, therefore the expressions for the coefficients u_k, v_k are

$$\begin{aligned} 2u_k v_k &= \frac{\Delta_k}{E(k)}, & u_k^2 - v_k^2 &= \frac{\eta_k}{E(k)}, \\ u_k^2 &= \tfrac{1}{2}\Big(1 + \frac{\eta_k}{E(k)}\Big), & v_k^2 &= \tfrac{1}{2}\Big(1 - \frac{\eta_k}{E(k)}\Big), \end{aligned} \tag{3.26}$$

with

$$E(k) = \sqrt{(\epsilon_k - \mu)^2 + \Delta_k^2}. \tag{3.27}$$

Then the Hamiltonian finally becomes

$$H_B = \int \frac{d^2k}{(2\pi)^2} \Big\{ E(k) \left(\varphi_+^\dagger(k)\varphi_+(k) + \varphi_-^\dagger(k)\varphi_-(k)\right) + \epsilon_k - \mu - E(k) \Big\} + V.T. \tag{3.28}$$

The Hamiltonian (3.28) describes fermionic quasi-particles with the gapped energy dispersion $E(k)$.

3.3 Derivation of the gap and number equation

The self-consistent field method [25] may now be used to derive the so-called gap equation and number equation. One substitutes the original fields in terms of Bogoliubov-transformed quantities (quasiparticles) to obtain equations which must be satisfied for self-consistency. This method results in equations not only

[1] The physical meaning of the Bogoliubov quasiparticles is not easily visualized, since they are in fact combinations of particle and hole states. A discussion is given in [11, 81] and in [52, Sec. 5.5].

for zero temperature, but also for finite temperatures. To this end, expectation values of the quasiparticles φ_+, φ_- are assumed[2] to be

$$\begin{aligned}&\langle\varphi_+^\dagger(k)\varphi_+(k)\rangle = \langle\varphi_-^\dagger(k)\varphi_-(k)\rangle = f(k),\\ &\langle\varphi_+(k)\varphi_-(k')\rangle \text{ and all similar terms} = 0.\end{aligned} \tag{3.29}$$

where

$$f(k) = (e^{E_k/T}+1)^{-1} \tag{3.30}$$

is the Fermi distribution at temperature T with the gapped dispersion $E(k)$. The averages (3.29) mean that the quasiparticles are noninteracting fermions, and at zero temperature no quasiparticles are present.

The definition of F, Eq. (3.12), is written in Fourier space

$$F(k) = \langle\psi_2(-k)\psi_1(k)\rangle \tag{3.31}$$

where $F(k)$ is the Fourier transform of $F(r_1, r_2)$ with respect to the relative coordinate $r = r_1 - r_2$. Substituting the fields φ_+, φ_- and using the averages (3.29) gives

$$F(k) = -u_k v_k\,(1 - 2f(k)) \tag{3.32}$$

and the same is obtained for F^*. Note that

$$1 - 2f(k) = \tanh\frac{E_k}{2T} \tag{3.33}$$

and for $T = 0$ this factor is 1. Inserting the expressions for u_k and v_k from Eq. (3.26) into Eq. (3.32), we obtain

$$F(k) = -\frac{1}{2}\frac{\Delta_k}{\sqrt{(\epsilon_k-\mu)^2+\Delta_k^2}}\tanh\frac{E_k}{2T}. \tag{3.34}$$

Transforming back to position space this is

$$F(r) = -\frac{1}{2}\int\frac{d^2k}{(2\pi)^2}\,\frac{\Delta_k}{\sqrt{(\epsilon_k-\mu)^2+\Delta_k^2}}\tanh\frac{E_k}{2T}\,e^{-ik\cdot r}. \tag{3.35}$$

This equation can be brought into a more symmetric form by multiplying both sides by $V_{\text{inter}}^{2\text{d}}(r)e^{ikr}$ and integrating over r. Then, using the definition of Δ_k in (3.21) we get

$$\Delta(k) = -\frac{1}{2}\int\frac{d^2k'}{(2\pi)^2}\,\frac{V_{kk'}\Delta(k')}{\sqrt{(\epsilon_{k'}-\mu)^2+\Delta_{k'}^2}}\tanh\frac{E_{k'}}{2T} \tag{3.36}$$

[2]For a discussion the averages in Eqs. (3.29), see [11, Ch. VI.3].

with

$$V_{kk'} = \int V_{\text{inter}}^{\text{2d}}(r) e^{i(k-k')\cdot r}\, d^2 r. \tag{3.37}$$

Equation (3.36) is the BCS gap equation in standard form [52]; Eqs. (3.34) and (3.35) are different, but less common, forms of the same equation[3].

Now we derive the so-called number equation. The one-particle density matrix, Eq. (3.11), is written in Fourier space (with respect to the relative coordinate $r = r_1 - r_2$)

$$\rho(k) = \langle \psi_\alpha^\dagger(-k)\psi_\alpha(-k)\rangle \tag{3.38}$$

therefore the density is

$$n = \rho(r{=}0) = \int \frac{d^2k}{(2\pi)^2}\, \langle \psi_\alpha^\dagger(k)\psi_\alpha(k)\rangle. \tag{3.39}$$

The expressions for φ_+, φ_- with the quasiparticle averages (3.29) give

$$\langle \psi_\alpha^\dagger(k)\psi_\alpha(k)\rangle = (u_k^2 - v_k^2) f(k) + v_k^2\,. \tag{3.40}$$

Therefore, inserting the expressions for u_k, v_k from Eq. (3.26) we obtain

$$n = \frac{1}{2}\int \frac{d^2k}{(2\pi)^2} \left\{ 1 - \frac{\epsilon_k - \mu}{\sqrt{(\epsilon_k - \mu)^2 + \Delta_k^2}} \tanh \frac{E_k}{2T} \right\}. \tag{3.41}$$

3.4 BCS regime

The interaction potential between two dipoles belonging to different layers has the form, see Sec. 1.5:

$$V_{\text{dd}}(r) = D^2 \frac{r^2 - 2\lambda^2}{(r^2 + \lambda^2)^{5/2}}, \tag{3.42}$$

where r is the in-plane separation between these dipoles. The potential $V_{\text{dd}}(r)$ is attractive for $r < \sqrt{2}\lambda$ and repulsive at larger distances r. One expects that an attractive potential may lead to pairing, while there is usually no pairing in a repulsive potential. This intuitive picture is clearly insufficient in our case, since the potential changes sign. It has been shown [61, 80] (see also [79]) that the Cooper pairing at $T = 0$ occurs in a two-dimensional system exactly if the interaction produces a two-body bound state. In our case the inter-layer potential satisfies the relation

$$\int V_{\text{dd}}(r) d^2 r = 0, \tag{3.43}$$

[3] They are briefly mentioned in [52, pp. 189–190], his $F_k = u_k v_k$ being our $-F(k)$.

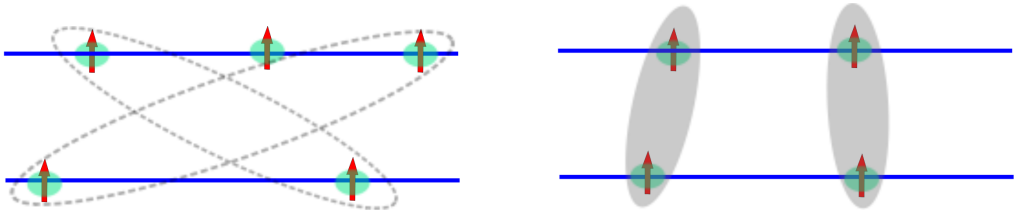

Figure 3.3: Evolution from small to large interactions. Left: weak attractive interactions, Cooper pairing. Right: strong attractive interactions, two-body bound state (dimer).

and, therefore, (see Chapter 2) this potential has a two-body bound state. Thus we can expect Cooper pairing in the system.

The Hamiltonian which describes the system at hand was derived in Sec. 3.2. It was shown that the fermions are described analogously to BCS theory. In BCS theory, Cooper pairs are formed from a spin-up and a spin-down electron. Here, a pair consists of a fermion in layer 1 and a fermion in layer 2.

The interaction potential is isotropic, $V = V(|\mathbf{r}|)$, and we consider an isotropic order parameter $\Delta = \Delta(|\mathbf{k}|)$. Then

$$V_{kk'} = 2\pi \int_0^\infty V(r) J_0(kr) J_0(k'r) r \, dr \tag{3.44}$$

The gap equation, as derived in Sec. 3.3, describes the effects of Cooper pairing in a simplified way. A more detailed calculation would include many-body effects beyond the gap equation: it is possible to include many-body corrections to the bare interaction potential and the contribution of mass renormalization due to interaction perturbatively (see e.g. [40, 8] for a discussion). These so-called Gorkov–Melik-Barkhudarov corrections change the results for the gap and the critical temperature by a numerical pre-exponential factor. A detailed calculation of these effects for the present system appears in Ref. [8]. It should be noted that these corrections, being of a perturbative nature, are only valid in the BCS regime. Since our aim here is to study the whole BCS–BEC crossover, we do not include them in our treatment.

3.5 BCS–BEC crossover

Let us consider the physics of inter-layer pairing as a function of the interaction strength. For very strong inter-layer interactions, particles in layer 1 and layer 2 form bound pairs. These bound states of two fermions of different layers in real space will be called dimers. The dimers are composite bosons, and for sufficiently low temperatures these bosons form a Bose-Einstein-Condensate (BEC). As the interaction gets weaker, the pairs become loosely bound, and their wave function broadens. If the interaction is weak, Cooper pairing occurs and the Cooper pairs condense in a superfluid state, provided the temperature is low enough. In this

regime the binding energy $|E_b|$ (recall that there is always a two-body bound state in the dipole–dipole potential, see Ch. 2) is much smaller than the Fermi energy ϵ_F, or equivalently the size of the interlayer two-body bound state greatly exceeds the intermolecular spacing in the plane. Therefore, as the interaction strength changes, we have a BEC of dimers on the one hand and a condensate of Cooper pairs (BCS state) on the other hand.

Remarkably, it was shown that there is a smooth crossover between the BCS and the BEC regime. This crossover can be described within a simple model, the so-called Eagles–Legett model. The main reason why the model works is that the BCS wave function, which describes a condensate of Cooper pairs, can be smoothly transformed into a wave function describing a BEC of dimers [51]. The model for the BCS–BEC crossover consists of two equations, the gap equation (3.36) and the number equation (3.41), which are solved simultaneously:

$$\Delta(k) = -\frac{1}{2}\int \frac{d^2k'}{(2\pi)^2}\,\frac{V_{kk'}\Delta(k')}{\sqrt{(\epsilon_{k'}-\mu)^2+\Delta_{k'}^2}}\tanh\frac{\sqrt{(\epsilon_{k'}-\mu)^2+\Delta_{k'}^2}}{2T} \tag{3.45a}$$

$$n = \frac{1}{2}\int \frac{d^2k}{(2\pi)^2}\left\{1-\frac{\epsilon_k-\mu}{\sqrt{(\epsilon_k-\mu)^2+\Delta_k^2}}\tanh\frac{\sqrt{(\epsilon_k-\mu)^2+\Delta_k^2}}{2T}\right\}. \tag{3.45b}$$

These equations are considered as equations for the unknowns $\Delta(k)$ and μ. The temperature T is fixed; at $T=0$ we have $\tanh\frac{E_k}{2T}=1$.

First we verify that the equations (3.45) give sensible results in the weak-coupling (BCS) and strong-coupling (BEC) regimes for $T=0$, respectively, following [51]. This will shed light on the physical meaning of these equations in these limiting cases. In the BCS regime, Δ is small and may be approximately neglected in the number equation (3.45b). Then the number equation gives

$$2\pi n\frac{\hbar^2}{m} = \mu, \tag{3.46}$$

and therefore μ is the Fermi energy (see A1.2). Then Eq. (3.45a) with $\mu=\epsilon_F$ is the usual BCS gap equation.

Now we consider the BEC limit. It is convenient to use instead of the gap equation (3.45a) the equivalent form Eq. (3.34), at $T=0$:

$$F(k) = -\frac{1}{2}\frac{\Delta_k}{\sqrt{(\epsilon_k-\mu)^2+\Delta_k^2}}, \tag{3.47}$$

where $\Delta_k = \int V(r)\psi(r)e^{ikr}d^2r$. In the denominator, we put $\sqrt{(\epsilon_k-\mu)^2+\Delta_k^2}\approx \epsilon_k-\mu$, since we expect μ to be negative and much larger than Δ and ϵ_F. Then the gap equation becomes identical to the Schrödinger equation, seen as follows. The Schrödinger equation for the bound state with energy E_b of two particles of mass m is

$$-\frac{\hbar^2}{m}\nabla^2\psi(r) - E_b\psi(r) = -V(r)\psi(r). \tag{3.48}$$

Table 3.1: Comparison of BCS–BEC crossover commonly considered and the case here.

usual BCS–BEC crossover	here
pair (spin $\uparrow$, spin $\downarrow$)	pair (layer 1, layer 2)
3D	2D
contact potential $\frac{4\pi\hbar^2 a}{m}\delta(r)$	inter-layer potential $U_0 V_{\mathrm{dd}}(r)$, long-range
gap equation & number equation	gap equation & number equation
crossover as function of $1/(k_F a)$	crossover as function of coupling strength U_0
critical temperature for superfluid transition by considering fluctuations	critical temperature for superfluid transition from Kosterlitz–Thouless theory

The binding energy is negative, we write for clarity $E_b = -|E_b|$. The equation becomes upon multiplication with e^{ikr} and integration over r:

$$\psi(k) = -\frac{1}{2}\frac{\int V(r)\psi(r)e^{ikr}d^2r}{\frac{\hbar^2k^2}{2m} + |E_b|/2}. \tag{3.49}$$

We see that the gap equation (3.47) in the extreme BEC limit becomes the Schrödinger equation for the two-body bound state, $F(r)$ is the wave function, and the chemical potential is negative and equals half the binding energy:

$$\mu = -|E_b|/2. \tag{3.50}$$

The gap and number equations thus give the correct behavior in the BCS (weak interaction, $\mu = \epsilon_F$) and BEC (strong attractive interaction) limits. The Eagles–Legget model gives a smooth crossover between these limits. It has been argued [80] that the point $\mu = 0$ may be regarded as the point of transition between the BCS and the BEC regime, but there is no precise criterion for where to place it.

Now we consider finite temperature. The gap equation at finite temperature behaves as follows: as we start at $T = 0$ and increase the temperature, the gap Δ becomes smaller until at a certain T_c the gap vanishes (see Fig. 3.6 on p. 56 for a plot of $\Delta(T)$). There is no solution for the gap equation for $T > T_c$, this T_c is called the critical temperature. In Sec. 3.7 we shall derive a relation between the gap at $T = 0$ and T_c.

The Eagles–Legget model provides the critical temperature throughout the whole BCS–BEC crossover. In the BCS regime T_c is the critical temperature for pair condensation, but in the BEC regime this critical temperature is the temperature of pair dissociation. To find the critical temperature for condensation, we employ Kosterlitz–Thouless theory. This is discussed further in Sec. 3.11.

The differences between the usual three-dimensional BCS–BEC crossover, which is observed across a Feshbach resonance and is decribed in Sec. 1.3, and the crossover in our system are summarized in Table 3.1.

3.6 Transformation of the gap equation

The gap equation can be transformed to an equivalent form where the Fourier components of the interaction potential $V_{kk'}$ are replaced by the off-shell scattering amplitude. Usually this is done [6, 80] if the interaction potential is not well-defined in Fourier space (e.g. if it has an infinitely hard core in real space); the resulting gap equation is then called a renormalized gap equation. In our case this problem does not arise, because the inter-layer dipole–dipole potential is regular everywhere. However the transformation is useful for the (approximate) analytical calculation of the gap and the critical temperature in Sec. 3.7.

The gap equation at finite temperature is

$$\Delta_k = -\int \frac{d^2k'}{(2\pi)^2}\, V_{kk'}\, \mathcal{K}(k')\Delta_{k'}, \tag{3.51}$$

where

$$\mathcal{K}(k) = \frac{1}{2E_k}\tanh\Big(\frac{E_k}{2T}\Big), \tag{3.52}$$

$$E_k = \sqrt{(\epsilon_k - \mu)^2 + \Delta_k^2}, \qquad \epsilon_k = \frac{(\hbar k)^2}{2m}. \tag{3.53}$$

This equation can be transformed into a form where the off-shell scattering amplitude appears instead of the potential. Let us switch for the moment the convention for the two-dimensional scattering amplitude to that used by Refs. [75, 77] which we denote by $\bar{f}$, the relation to the amplitude used in Sec. 2.2 being $f = -\bar{f}/4$. This off-shell scattering amplitude for the scattering of *two particles* of mass m (therefore $m \to m/2$ in Eq. (2.13)) is

$$\bar{f}(\mathbf{k}, \mathbf{k}') = \frac{m}{\hbar^2}\int e^{-i\mathbf{k}'\cdot\mathbf{r}}\, V(\mathbf{r})\Psi_k^+(\mathbf{r})\, d^2r. \tag{3.54}$$

It satisfies the integral equation [see Eq. (2.15)]

$$\bar{f}(k, k') = \frac{m}{\hbar^2}\, V_{kk'} + \frac{m}{\hbar^2}\int \frac{d^2q}{(2\pi)^2}\frac{V_{qk'}\bar{f}(k,q)}{k^2 - q^2 + i\eta}, \tag{3.55}$$

which we write in the form

$$\frac{\hbar^2}{m}\bar{f}(k, k') = \int \frac{d^2q}{(2\pi)^2}\, V_{qk'}\, \chi(k,q) + V_{kk'} \tag{3.56}$$

where

$$\chi(k,q) = \frac{\bar{f}(k,q)}{k^2 - q^2 + i\eta}. \tag{3.57}$$

Now multiply the gap equation (3.51) with $\chi(q,k)$ and integrate over k:

$$\int\frac{d^2k}{(2\pi)^2}\,\chi(q,k)\Delta_k = -\int\frac{d^2k'}{(2\pi)^2}\int\frac{d^2k}{(2\pi)^2}\,V_{kk'}\chi(q,k)\mathcal{K}(k')\Delta_{k'} \tag{3.58a}$$

$$= -\int\frac{d^2k'}{(2\pi)^2}\left(\frac{\hbar^2}{m}\bar{f}(q,k') - V_{qk'}\right)\mathcal{K}(k')\Delta_{k'} \qquad \text{using Eq. (3.56)} \tag{3.58b}$$

$$= -\int\frac{d^2k}{(2\pi)^2}\,\frac{\hbar^2}{m}\bar{f}(q,k)\mathcal{K}(k)\Delta_k - \Delta_q \qquad \text{using Eq. (3.51)} \tag{3.58c}$$

Inserting (3.57) into the left-hand side of (3.58), we obtain the transformed gap equation

$$\Delta_q = -\int\frac{d^2k}{(2\pi)^2}\,\bar{f}(q,k)\Delta_k\left(\frac{\hbar^2}{m}\mathcal{K}(k) - \frac{1}{-q^2+k^2-i\eta}\right) \tag{3.59}$$

$$= -\int\frac{d^2k}{(2\pi)^2}\,\frac{\hbar^2}{m}\bar{f}(q,k)\Delta_k\left(\mathcal{K}(k) - \frac{1}{2(-\epsilon_q+\epsilon_k)-i\eta}\right). \tag{3.60}$$

3.7 BCS regime: gap and critical temperature

It is possible to find an approximate explicit expression for gap at $T=0$ from the gap equation, and to relate it to the critical temperature.

The transformed gap equation (3.60) is

$$\Delta_{k'} = -\int\frac{d^2k}{(2\pi)^2}\,\frac{\hbar^2}{m}\bar{f}(k',k)\Delta_k\left(\mathcal{K}(k) - \frac{1}{2(-\epsilon_{k'}+\epsilon_k)-i\eta}\right). \tag{3.61}$$

We are looking for $\Delta(k_F)$, so we evaluate (3.61) at $k'=k_F$:

$$\Delta(k_F) = -\int\frac{d^2k}{(2\pi)^2}\,\frac{\hbar^2}{m}\bar{f}(k_F,k)\Delta_k\left(\mathcal{K}(k) - \frac{1}{2(\epsilon_k-\epsilon_F)-i\eta}\right). \tag{3.62}$$

The main contribution of the integral on the right-hand side of (3.62) comes from $k\approx k_F$, so taking $f(k_F,k)$ and $\Delta(k)$ to be slowly varying functions around k_F we approximate

$$\Delta(k_F) = -\frac{\hbar^2}{m}\bar{f}(k_F,k_F)\Delta(k_F)\int\frac{d^2k}{(2\pi)^2}\left(\mathcal{K}(k) - \frac{1}{2(\epsilon_k-\epsilon_F)-i\eta}\right) \tag{3.63}$$

and put $\Delta_k=\Delta$ inside the integral. This gives

$$1 = -\bar{f}(k_F,k_F)\frac{1}{2\pi}\int_0^\infty d\epsilon\left\{\frac{\tanh\left(\frac{1}{2T}\sqrt{(\epsilon-\epsilon_F)^2+\Delta^2}\right)}{2\sqrt{(\epsilon-\epsilon_F)^2+\Delta^2}} - \frac{1}{2(\epsilon-\epsilon_F)-i\eta}\right\}. \tag{3.64}$$

First, we calculate the gap at $T=0$. Equation (3.64) at $T=0$ reads

$$1 = -\frac{\bar{f}(k_F,k_F)}{2\pi}\int_0^\infty d\epsilon\left\{\frac{1}{2\sqrt{(\epsilon-\epsilon_F)^2+\Delta^2}} - \frac{1}{2(\epsilon-\epsilon_F)-i\eta}\right\}. \tag{3.65}$$

Expanding the term with the infinitesimal η using the Dirac identity and evaluating the principal-value integral for $\Delta \ll \epsilon_F$ (see Eq. (3.73)), we obtain

$$1 = -\frac{\bar{f}(k_F, k_F)}{2\pi}\left(\log\frac{2\epsilon_F}{\Delta} - \frac{i\pi}{2}\right). \tag{3.66}$$

Noting that $f(k,k)$ is the usual (on-shell) scattering amplitude $f(k)$, switching back to $f = -\bar{f}/4$, and using the relation between the amplitude and the scattering phase shift $f(k)^{-1} = \cot\delta(k) - i$ (see Eq. (2.12)), we get the result

$$\Delta = 2\epsilon_F \exp\left(-\frac{\pi}{2}\cot\delta(k_F)\right). \tag{3.67}$$

This expression is only valid if $\cot\delta(k_F)$ is large and positive (i.e. $\delta(k_F)$ is small and positive), since we have assumed that $\Delta \ll \epsilon_F$. In the limit of vanishing interaction, $\delta \to 0$ and $\Delta \to 0$ as expected. We remark that the expression (3.67) contains the scattering phase shift only at $k = k_F$. A better approximation in Eq. (3.63) would contain contributions from the scattering amplitude away from $k = k_F$. However, these "off-shell" contributions to the critical temperature are of the same order of magnitude as Gorkov–Melik-Barkhudarov corrections [8], thus we do not include them here.

Now we consider the critical temperature T_c. At the critical temperature the gap goes to zero, therefore

$$\left.\frac{\tanh\left(\frac{1}{2T}\sqrt{(\epsilon-\epsilon_F)^2+\Delta^2}\right)}{2\sqrt{(\epsilon-\epsilon_F)^2+\Delta^2}}\right|_{T=T_c,\,\Delta=0} = \frac{\tanh\left(\frac{\epsilon-\epsilon_F}{2T_c}\right)}{2(\epsilon-\epsilon_F)}. \tag{3.68}$$

Equation (3.64) becomes

$$1 = -\frac{\bar{f}(k_F, k_F)}{2\pi}\int_0^\infty d\epsilon\left\{\frac{\tanh\left(\frac{\epsilon-\epsilon_F}{2T_c}\right)}{2(\epsilon-\epsilon_F)} - \frac{1}{2(\epsilon-\epsilon_F)-i\eta}\right\} \tag{3.69}$$

Expanding the term with the infinitesimal η using the Dirac identity and evaluating the principal-value integral for $T_c \ll \epsilon_F$ (see Eq. (3.74)), we obtain

$$1 = -\frac{\bar{f}(k_F, k_F)}{2\pi}\left(\log\frac{2e^\gamma\epsilon_F}{\pi T_c} - \frac{i\pi}{2}\right) \tag{3.70}$$

and comparing with (3.66), we get

$$T_c = \frac{2e^\gamma}{\pi}\epsilon_F \exp\left(-\frac{\pi}{2}\cot\delta(k_F)\right). \tag{3.71}$$

and the relation between the gap and the critical temperature is

$$T_c = (e^\gamma/\pi)\Delta = 0.567\,\Delta. \tag{3.72}$$

Equations (3.67) and (3.71) express the gap and the critical temperature in the BCS regime in terms of the scattering phase shift at $k = k_F$. Remarkably, the relation between the gap at $T = 0$ and the critical temperature, Eq. (3.72), is independent of the interaction potential. It is interesting to note that the relation (3.72), first derived in [61], is the same as in the usual three-dimensional BCS theory [81].

Approximation of integrals The following principal-value integrals, where $\mu > 0$, are approximated:

$$I_1 = \int_0^\infty \left\{ \frac{1}{2\sqrt{(\epsilon-\mu)^2+\Delta^2}} - \frac{1}{2(\epsilon-\mu)} \right\} d\epsilon = \log\frac{2\mu}{\Delta} \qquad \text{for } \Delta \ll \mu \tag{3.73}$$

$$I_2 = \int_0^\infty \frac{1}{2(\epsilon-\mu)} \left\{ \tanh\left(\frac{\epsilon-\mu}{2T}\right) - 1 \right\} d\epsilon = \log\frac{2e^\gamma\mu}{\pi T} \qquad \text{for } T \ll \mu \tag{3.74}$$

3.8 Solution for the crossover in the logarithmic regime

The Eagles–Leggett model in two dimensions at $T = 0$ can be solved exactly under certain assumptions [80]. With the help of a transformed gap equation, similarly to what was done in Sec. 3.6, it was shown by Randeria et al. [80] that *in the logarithmic regime*, the gap and number equations give

$$\Delta = \sqrt{2\epsilon_F|E_b|} \tag{3.75a}$$

$$\mu = \epsilon_F - |E_b|/2. \tag{3.75b}$$

In particular, in this regime $\Delta(k) = \Delta$ is a constant.

We compare this to our results for the gap in the BCS regime, Sec. 3.7. The low-energy scattering phase shift is expressed in the logarithmic regime through the binding energy E_b, as discussed in Sec. 2.9. Note that the unit of energy was $E_0 = \hbar^2/m\lambda^2$ and the unit of length was λ, so the phase shift is given by (see (2.89))

$$\cot\delta(k) = \frac{2}{\pi}\log\left(\frac{\lambda k_F}{\sqrt{|E_b|/E_0}}\right) \tag{3.76}$$

Inserting this into the formula for the gap (3.67) gives

$$\Delta = \sqrt{2\epsilon_F\,|E_b|}, \tag{3.77}$$

thus recovering Eq. (3.75a). The formula for the gap presented in Sec. 3.7 is more general than (3.75a) since it is valid also outside the logarithmic regime of scattering. However, Randeria's solution (3.75) is more general since it describes the whole BCS–BEC crossover.

3.9 Numerical solution of the crossover equations

We express energies in units of the Fermi energy ϵ_F, momenta in units of the Fermi momentum k_F, and lengths in units of λ. Then the gap and number equations (3.45) read

$$\frac{\Delta(k)}{\epsilon_F} = -U_0 \int_0^\infty \frac{d\left(\frac{k'}{k_F}\right)\frac{k'}{k_F}\tilde{V}_{kk'}\frac{\Delta(k')}{\epsilon_F}}{E(k')/\epsilon_F} \tanh\frac{E(k')/\epsilon_F}{2T/\epsilon_F} \tag{3.78a}$$

$$1 = \int_0^\infty d\left(\frac{k}{k_F}\right)\frac{k}{k_F}\left\{1 - \frac{(k/k_F)^2 - \mu/\epsilon_F}{E(k)/\epsilon_F}\tanh\frac{E(k)/\epsilon_F}{2T/\epsilon_F}\right\} \tag{3.78b}$$

with $U_0 = mD^2/(\hbar^2\lambda)$,

$$E(k)/\epsilon_F = \sqrt{((k/k_F)^2 - \mu/\epsilon_F)^2 + (\Delta(k)/\epsilon_F)^2}, \tag{3.79}$$

and (see (3.44))

$$\tilde{V}_{kk'} = \frac{1}{2\pi}\frac{m}{\hbar^2}V_{kk'} = \int_0^\infty \frac{(r/\lambda)^2 - 2}{((r/\lambda)^2+1)^{5/2}} J_0\left(\lambda k_F \tfrac{k}{k_F}\tfrac{r}{\lambda}\right) J_0\left(\lambda k_F \tfrac{k'}{k_F}\tfrac{r}{\lambda}\right) \tfrac{r}{\lambda} d\left(\tfrac{r}{\lambda}\right). \tag{3.80}$$

The Eqs. (3.78) are now in a form where they can be solved numerically. The parameters are the dimensionless potential strength U_0 and the dimensionless quantity λk_F. Since k_F is related to the density by $k_F^2 = 4\pi n$ (see Sec. (A1.2)), the parameter $(\lambda k_F)^2$ is proportional to the density and $1/(\lambda k_F)$ is proportional to the mean interparticle distance, for fixed λ.

It is convenient to split off the value of $\Delta(k)$ at $k = k_F$, writing

$$\Delta(k) = \Delta_0\,\tilde{\Delta}(k), \tag{3.81}$$

where $\Delta_0 = \Delta(k_F)$ and the function $\tilde{\Delta}$ is normalized $\tilde{\Delta}(k{=}k_F) = 1$. Then Δ_0 is the energy gap[4], and the function $\tilde{\Delta}(k)$ gives the variation of the gap with respect to the momentum. We regard the gap and number equations as equations for the unknowns Δ_0, μ, and $\tilde{\Delta}(k)$.

Equations (3.78a) and (3.78b) are a system of nonlinear integral equations. We solve them by iteration as follows:

Start with an initial guess for Δ_0, μ, $\tilde{\Delta}(k)$.

Repeat:

1. Put Δ_0, μ, $\tilde{\Delta}(k)$ into the equations and solve for new Δ_0 and μ while keeping $\tilde{\Delta}(k)$ fixed.
2. Set $\tilde{\Delta}(k)$ to the right-hand side of the gap equation.

From a numerical point of view, there are two difficulties in the procedure: the evaluation of the integral on the right-hand side of the gap equation (3.78a)

[4]It is only true in the BCS regime that $\Delta(k_F)$ is the gap, but we call Δ_0 gap for brevity.

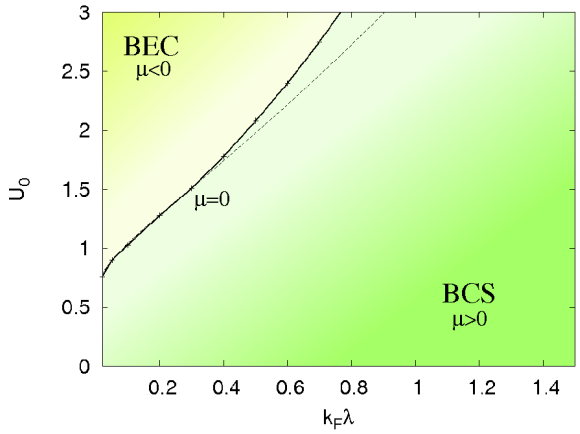

Figure 3.4: BCS–BEC crossover: The chemical potential is indicated as a function of the dipole strength U_0 and the Fermi momentum $k_F\lambda$. The line $\mu = 0$ as calculated numerically (solid line) and compared to the exact solution in the logarithmic regime, from Eq. (3.75b) (dashed).

for very small Δ and the evaluation of the oscillating integral in equation (3.80). The integral in the gap equation is easier to evaluate numerically for small Δ if the substitution $y = \xi/\Delta_0$ is made, $\xi = \epsilon_k - \mu$. The matrix elements of the potential, $V_{kk'}$, are numerically conveniently calculated using the representation in Eq. (A.18) given in App. A3.1, its advantage being that no Bessel function appear.

3.10 Results for the BCS–BEC crossover

Here we present some results from the numerical solution of the gap and number equations, mostly at $T = 0$.

Fig. 3.5 shows the gap at the Fermi momentum $\Delta_0 = \Delta(k_F)$ as a function of $k_F\lambda$ for different values of U_0. Note that Δ_0 develops a maximum for small U_0. The maximum vanishes for $U_0 \gtrsim 0.7$, which is the regime where the scattering amplitude is logarithmic, see the discussion in Sec. 2.10. In the regime of logarithmic scattering amplitude, Eq. (3.75a) gives in our units

$$\Delta_0/\epsilon_F = 2\frac{\sqrt{|E_b|/E_0}}{k_F\lambda} \tag{3.82}$$

and indeed for sufficiently large U_0 we observe a monotonic $1/k_F\lambda$ decay.

Fig. 3.6 shows the temperature dependence of the gap $\Delta_0(T)$ in the BCS regime ($\mu \approx \epsilon_F$). The critical temperature T_c agrees, within numerical accuracy, with the relation $T_c = 0.567\,\Delta_0(T=0)$ as in usual BCS theory.

In Fig. 3.7 we show the normalized gap function $\tilde{\Delta}_k = \Delta_k/\Delta_0$ obtained from a numerical solution of the gap equation. Even though the important quantity is

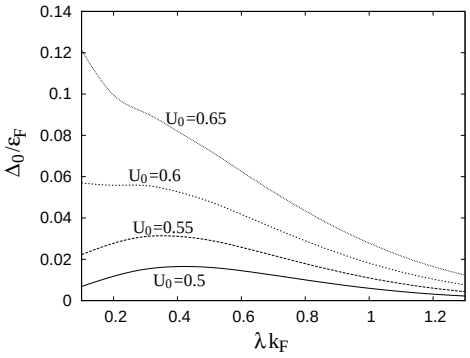

Figure 3.5: Gap at the Fermi momentum as a function of $k_F\lambda$, for different values of U_0.

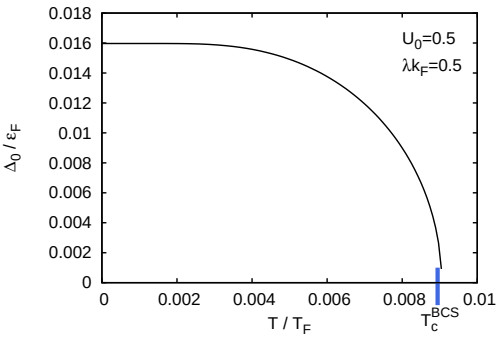

Figure 3.6: Gap at the Fermi momentum as a function of temperature. The critical temperature is at $T_c^{\mathrm{BCS}} = 0.567\,\Delta_0(T=0)$ within numerical accuracy.

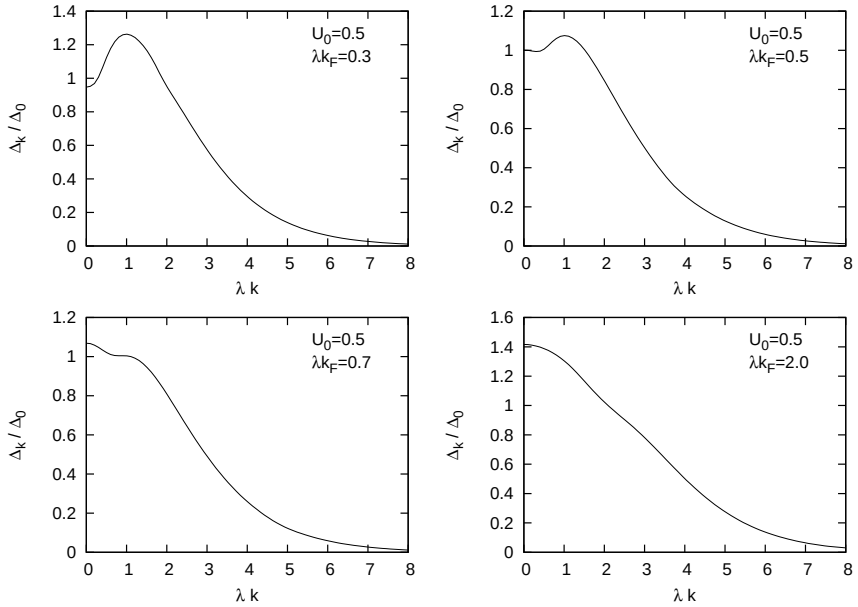

Figure 3.7: Normalized gap function $\tilde{\Delta}_k = \Delta_k/\Delta_0$ as a function of momentum $k\lambda$, for different values of $k_F\lambda$.

Δ_0 and not $\tilde{\Delta}_k$, we show the gap function since it has some non-trivial behavior and needs to be calculated for a complete solution of the equations.

Fig. 3.4 illustrates the transition from the BCS regime ($\mu > 0$) to the BEC regime ($\mu < 0$) and the border line $\mu = 0$. In this figure the numerical results for the line $\mu = 0$ are compared with those expected from the Eq. (3.75b) in the logarithmic regime. Note that the agreement is very good for small $k_F\lambda$.

3.11 Critical temperature for superfluid transition

In two dimensions the transition from the normal to superfluid state is known to be of Kosterlitz–Thouless type. It was realized by Miyake [61] that it is possible to employ Kosterlitz–Thouless theory in conjunction with the Eagles–Leggett model to describe the transition between the normal state (Fermi gas) and the superfluid state (BCS superfluid or BEC of dimers, depending on the interaction strength). In the BCS limit, the Kosterlitz–Thouless transition temperature T_{KT} is very close to the critical temperature T_c from the BCS gap equation [61]. Therefore, as long as the interaction is weak ($\mu \approx \epsilon_F$), no recourse to Kosterlitz–Thouless theory is needed, and the BCS gap equation can be used to calculate the superfluid transition temperature. This is what we have done so far.

For strong interactions, the critical temperature T_c calculated from the gap and number equations, i.e. the temperature where the gap vanishes, cannot be interpreted as the critical temperature for the onset of superfluidity in the BEC regime. Instead, it corresponds to the temperature of pair dissociation due to thermal energy [83]. Hence at the crossover ($\mu = 0$) this T_c is of the order of the Fermi energy and in the BEC regime it is comparable to the binding energy E_b. To determine the critical temperature for the superfluid transition across the crossover and in the BEC regime, we use the relation between the transition temperature and superfluid density from Kosterlitz–Thouless theory.

The temperature of the Kosterlitz–Thouless transition T_{KT}, below which the system is superfluid, satisfies the equation [62]

$$T_{KT} = \frac{1}{2}\pi\hbar^2\frac{\rho_s(T_{KT})}{M^2}, \tag{3.83}$$

where $M = 2m$ is the dimer (Cooper-pair) mass, and ρ_s is the superfluid mass density just below T_{KT}. This relation can also be written in a more appealing way as [91]

$$n_s\Lambda_{\mathrm{T}}^2 = 4, \tag{3.84}$$

where $n_s = \rho_s/M$ is the superfluid number density and $\Lambda_{\mathrm{T}} = h/\sqrt{2\pi MT}$ is the thermal de Broglie wavelength.

Recall that n is the number density in *one* layer, m is the mass of a particle in one layer, therefore the mass density in *both* layers is $\rho_{\mathrm{tot}} = 2mn$. The superfluid

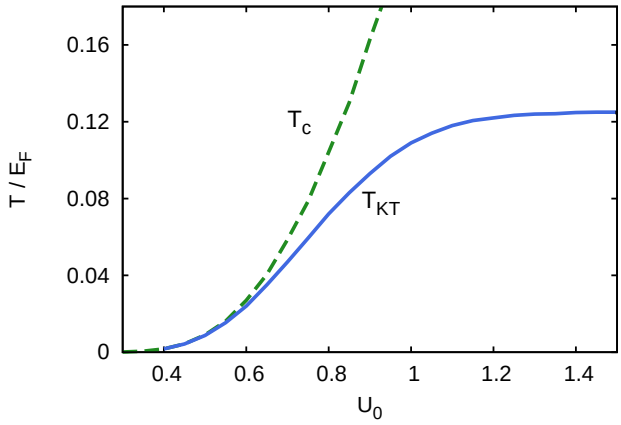

Figure 3.8: Kosterlitz–Thouless critical temperature T_{KT} and the critical temperature from the Eagles–Leggett model T_c as a function of the dipole strength U_0, for $k_F\lambda = 0.5$.

density can be calculated using the Landau formula, assuming that the elementary excitations interact weakly (see [57] for a more detailed discussion of the validity). The total mass density $\rho_{tot} = \rho_s + \rho_n$ consists of the normal density ρ_n and the superfluid density ρ_s. The normal mass density is, adapting the Landau argument from [54] to two dimensions, given by

$$\rho_n = \int_0^\infty \frac{-\partial f(E_k)}{\partial E_k} (\hbar k)^2 \frac{k dk}{2\pi}, \tag{3.85}$$

where as before $E_k = \sqrt{(\epsilon_k - \mu(T))^2 + \Delta_k(T)^2}$ is the dispersion relation of fermionic excitations and $f(E) = (1 + e^{E/T})^{-1}$ is the Fermi distribution.

Combining Eqs. (3.83) and (3.85), the equation for the Kosterlitz–Thouless temperature reads in dimensionless form

$$\frac{T_{KT}}{\epsilon_F} = \frac{1}{8}\left\{1 - 2\int_0^\infty \frac{-\partial f(\tilde{E})}{\partial \tilde{E}}\bigg|_{T_{KT}} \tilde{k}^3 d\tilde{k}\right\}, \tag{3.86}$$

with $\tilde{k} = k/k_F$ and $\tilde{E} = E_k/\epsilon_F$.

In the extreme limit of vanishing gap ($\Delta \to 0$) and $\mu = \epsilon_F \ll T$, we can put $-\partial f/\partial E = \delta(E)$. Thus Eq. (3.85) gives $\rho_n = \rho_{\text{tot}}$; the integral on the right-hand side of (3.86) goes to 1/2 and hence there is no superfluidity ($T_{KT} \to 0$). In the opposite extreme BEC limit[5], $\rho_s = \rho_{\text{tot}}$ so from (3.83) we get

$$T_{KT} = \frac{1}{8}\epsilon_F. \tag{3.87}$$

This result was given in [16].

[5] According to our model, the normal density ρ_n in the deep BEC regime is zero. Actually, it is known that $\rho_n > 0$ in the BEC regime due to the contribution of collective bosonic excitations to the normal density, therefore T_{KT} should be somewhat lower than in our calculations [84].

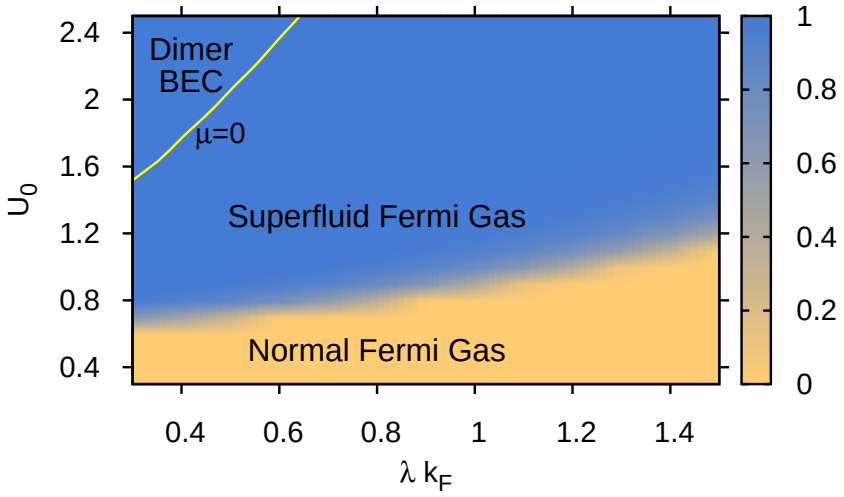

Figure 3.9: BCS–BEC transition: phase diagram for $T = 0.05\,\epsilon_F$. The color scale shows the superfluid density ρ_s/ρ_{tot}. The line $\mu = 0$ is drawn.

Fig. 3.8 shows T_{KT} and T_c as a function of U_0 for $k_F\lambda = 0.5$, obtained by numerical solution of the gap and number equations in conjunction with Eq. (3.86). Note that T_{KT} is always smaller than T_c. In the BCS regime ($\mu = \epsilon_F \ll T$) we have $T_{KT} \approx T_c$, while in the opposite limit where $\Delta_0 \sim \epsilon_F$ we obtain $T_{KT} = 0.125\,\epsilon_F$, as in Eq. (3.87). For intermediate regimes T_{KT} interpolates smoothly between these limiting cases.

For a given temperature $0 < T < T_{KT}$, a "phase diagram" can be obtained by displaying the superfluid density as a function of the coupling strength U_0 and interparticle distance λk_F, since regions of zero superfluid density correspond to the normal Fermi gas while a superfluid density of ~ 1 corresponds to a superfluid state (either BCS state of Cooper pairs or BEC of dimers). One such diagram, for $T = 0.05\,\epsilon_F$, is shown in Fig. 3.9. Here the phase diagram splits in three distinct regions: a normal gas of unpaired polarized fermions at each layer, an interlayer superfluid induced by Cooper-like pairing of fermions in different layers, and a dimer BEC formed by tightly-bound molecules on top of each other.

CHAPTER 4

State-changing collisions

The observation of effects of dipolar interaction in gases of polar molecules typically demands the polarization of the molecules in an external electric field. The reason is that although a polar molecule may have a large dipole moment in the molecular frame, in the absence of an external electric field the dipole moment in the laboratory frame averages to zero, see Sec. 1.4. For example, the KRb molecule in its singlet ground state has a permanent dipole moment of 0.56 Debye in the molecular frame, but rather large fields of several kV/cm must be employed to reach effective dipoles of ~ 0.2 Debye in the laboratory frame [67].

Dipolar interactions may play a significant role even for weak external electric fields, if the molecules are prepared in different rotational states (cf. e.g. [9]). In that case, the interaction between molecules in different rotational states can exchange a quantum of angular momentum, thus swapping the rotational state.

Motivation & Summary

- Observation of effects of dipole–dipole interaction usually requires high electric fields.
- We show that dipole–dipole interaction significantly affects *non-equilibrium* dynamics in a bilayer geometry.
- This effect is observable for chemically reactive molecules even for temperatures far above the Fermi temperature.

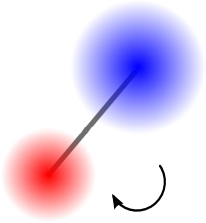

Figure 4.1: Model view of a diatomic heteronuclear molecule. The arrow indicates that the molecule is rotating about its center of mass.

4.1 Diatomic molecules

Diatomic heteronuclear molecules are made up of two atoms of different chemical elements. Figure 4.1 shows a model view of a diatomic molecule. Three energy scales (aside from translational motion) enter the description of such a molecule:

A) motion of electrons

B) vibrations of the atoms (here: change of internuclear distance)

C) rotation of the molecule as a whole about its center of mass

These energy scales are usually well-separated [48]:

A. electronic motion $\gg$ B. vibration $\gg$ C. rotation

The electronic states do not concern us here very much, but for orientation we give some basic notation (following [48, 55]) for the electronic states of diatomic molecules:

- The projection Λ of the orbital angular momentum on the axis of a diatomic molecule is a conserved quantity. States with $\Lambda = 0, 1, 2 \ldots$ are denoted by $\Sigma, \Pi, \Delta \ldots$. The phenomenon of Λ-doubling occurs for $\Lambda \neq 0$.
- The total spin of all electrons is denoted by S. The multiplicity of the state, $2S + 1$, is written as a superscript before the letter. States with $S = 0$ are referred to as singlet states, states with $S \geq 1$ are the multiplet states. In multiplet states, spin-orbit interaction plays a role, leading to the four Hund's coupling schemes.

Furthermore:

- The function of the $^1\Sigma$ can be either symmetric or antisymmetric with respect to reflections in any plane passing through the axis, this is denoted by $^1\Sigma^+$ or $^1\Sigma^-$. Usually $^1\Sigma^+$ is the ground state.
- The symbols $X, a, b \ldots$ precede a state to indicate that the state is the ground state, 1st excited state, 2nd excited state, etc. Most of diatomic molecules have $^1\Sigma$ as the ground state [55].

Table 4.1: Data for the KRb molecule.

$^{40}K^{87}Rb$, singlet state $X^1\Sigma$		
electric dipole moment d_0	0.57 Debye	[65]
rotational constant B	1.114 GHz	[66]
equilibrium radius r_e	$4.07 \cdot 10^{-10}$ m	[71]
vibrational constant ω_e	$2.7 \cdot 10^{12}$ Hz	[65, 82]
dissociation energy	$0.52\,\text{eV} = 6.0 \cdot 10^3$ K	[66, 71]
reduced mass	27.40 amu	

For a diatomic molecule, there is only one type of vibration, namely the change of internuclear distance. The vibrational states can be taken as harmonic oscillator states in the first approximation, with energy $\hbar\omega_e(v + 1/2)$.

Rotational motion is the motion of the nuclei about the center of mass of the molecule. The rotation of the diatomic molecule for the electronic singlet states can be described as the rotation of the symmetrical top. The states of the symmetric top are described by *three* quantum numbers: the total angular momentum J or K, its projection on the z-axis M, and the projection of the total angular momentum[1] on the internuclear axis Λ. In the case $\Lambda = 0$ (Σ state), the states reduce [48] to ordinary spherical harmonics with quantum numbers J and M :

$$|J, M\rangle = Y_{J,M}(\theta, \varphi). \tag{4.1}$$

They are eigenstates of $H_{\text{rot}} = B\mathbf{J}^2$, with energy $BJ(J+1)$, where the rotational constant is

$$B = \frac{\hbar^2}{2M_r r_e^2}, \tag{4.2}$$

with $M_r = m_1 m_2/(m_1 + m_2)$ the reduced mass of the molecule consisting of atoms with masses m_1, m_2, r_e is the equilibrium internuclear radius, and the moment of inertia of the molecule is Mr_e^2.

4.2 Dipole moments in an external electric field

The distribution of charge in a heteronuclear molecule (see. Fig. 4.1) has a dipole moment pointing in the direction of the molecular axis, a so-called permanent dipole moment in the molecular frame[2]. Since the molecule is rotating, however, in the laboratory frame this dipole moment averages to zero. If an external

[1] We use the same letter Λ for the total and the orbital angular momentum, since both are equal for the spin singlet state.

[2] Symmetry prohibits a permanent dipole moment in a *homonuclear* diatomic molecule.

electrical field is applied, a dipole moment in the laboratory frame can be induced. What is discussed here is the quantum-mechanical orientational polarization; the classical orientational polarization of an ensemble of molecules was considered in Sec. 1.4.

The effect of the external electric field on the rotational states is the strongest. In a classical picture, the molecule becomes more oriented along the direction of the electric field, but is still rotating. Quantum mechanically, the rotational states of the molecule are replaced by the rotational eigenstates in the presence of the electric field (Stark states); the dipole moment in the laboratory frame is the expectation value of the dipole operator in the rotational state of the molecule. This appearance of the dipole moment in the laboratory frame is referred to as orientational polarization.

It should be noted that an external electric field polarizes the charge distribution (i.e. it changes the electronic states) of the molecule, therefore leading to an induced dipole moment. This works for any distribution of charges, independent of a permanent dipole moment. However, the electric fields required to significantly polarize the electrons are extremely large, and at usual laboratory electric fields of the order of kV/cm this effect can be neglected.

In the following, we consider a polar diatomic molecule in an electronic singlet, $\Lambda = 0$ state ($^1\Sigma$) and vibrational ground state. The Hamiltonian for the rotational levels of the molecule in an external electric field E in the z direction is

$$\begin{aligned} H_{\mathrm{mol}} &= H_{\mathrm{rot}} + H_S && (4.3)\\ &= B\mathbf{J}^2 - d_0 E\cos\theta && (4.4) \end{aligned}$$

where d_0 is the permanent dipole moment in the frame of reference of the rotating molecule. It is assumed that the electric field is not strong enough to cause any polarization, i.e. the electronic states are unchanged. The dipole moment operator is $\mathbf{d} = d_0(\sin\theta\cos\varphi, \sin\theta\sin\varphi, \cos\theta)$, and $H_S = -\mathbf{d}\cdot\mathbf{E}$.

The eigenstates of H_{rot} are the angular momentum eigenstates $\mid J, M\rangle$, see Eq. (4.1). The matrix elements for $H_S \sim \cos\theta$ are

$$\begin{aligned} \langle J, M \mid \cos\theta \mid J+1, M\rangle &= \sqrt{\frac{(J+1)^2 - M^2}{(2J+1)(2J+3)}},\\ \langle J, M \mid \cos\theta \mid J-1, M\rangle &= \sqrt{\frac{J^2 - M^2}{(2J-1)(2J+1)}} \end{aligned} \qquad (4.5)$$

and all other matrix elements are zero. The eigenstates $\varphi_{J,M}$ for H_{mol} can be found using perturbation theory for a weak electric field, such that

$$\beta = \frac{d_0 E}{B} \ll 1, \qquad (4.6)$$

so $H_S = -d_0 E\cos\theta$ is a small perturbation and the eigenstates are still well described by the quantum numbers J and M. The eigenstates for H_{mol} are, to

Table 4.2: Stark-shifted states with $J = 0, 1$.

State			Energy
$\varphi_{0,0}$	=	$\mid 0,0\rangle + \beta\frac{1}{2\sqrt{3}} \mid 1,0\rangle$	$-\frac{B\beta^2}{6}$
$\varphi_{1,-1}$	=	$\mid 1,-1\rangle + \beta\frac{1}{4\sqrt{5}} \mid 2,-1\rangle$	$2B - \frac{B\beta^2}{20}$
$\varphi_{1,1}$	=	$\mid 1,1\rangle + \beta\frac{1}{4\sqrt{5}} \mid 2,1\rangle$	$2B - \frac{B\beta^2}{20}$
$\varphi_{1,0}$	=	$\mid 1,0\rangle + \beta\frac{1}{2\sqrt{15}} \mid 2,0\rangle - \beta\frac{1}{2\sqrt{3}} \mid 0,0\rangle$	$2B + \frac{B\beta^2}{10}$

lowest order in β, [89, 41, 60]:

$$\varphi_{J,M} = \mid J,M\rangle + \beta\, C_+ \mid J+1,M\rangle + \beta\, C_- \mid J-1,M\rangle \tag{4.7}$$

The perturbation mixes each $\mid J,M\rangle$ with the states with $J+1$ and $J-1$ and the same M, as seen from the matrix elements (4.5) or since $H_S = -d_0 E\cos\theta \sim Y_{10}$. The coefficients are

$$\begin{aligned} C_+ &= \frac{1}{2(J+1)}\sqrt{\frac{(1+J)^2 - M^2}{(2J+1)(2J+3)}}, \\ C_- &= -\frac{1}{2J}\sqrt{\frac{J^2-M^2}{4J^2-1}} \qquad (J \neq 0), \qquad C_-(J=0, M=0) = 0. \end{aligned} \tag{4.8}$$

The energy of $\varphi_{J,M}$ is

$$\begin{aligned} E_{J,M} &= BJ(J+1) + B\beta^2 \frac{J(J+1) - 3M^2}{2J(J+1)(2J-1)(3+2J)} \qquad (J \neq 0), \\ E_{0,0} &= -B\beta^2/6. \end{aligned} \tag{4.9}$$

Table 4.2 lists the wave functions and energies for the states $\varphi_{J,M}$ for $J = 0, 1$. The electric field lifts the degeneracy of the three $J = 1$ states, they become separated by the energy

$$\Delta E = E_{1,0} - E_{1,\pm 1} = \frac{3}{20}\beta^2 B. \tag{4.10}$$

An external field produces a dipole moment in the laboratory frame, which is the expectation value of the dipole operator in the rotational state of the molecule: $d_{\text{eff}} = \langle d_z\rangle = -d_0\langle\cos\theta\rangle$. This can be written [47], using the Hellman-Feynman theorem,

$$d_{\text{eff}} = -d_0 \left\langle \frac{\partial H_{\text{mol}}}{\partial E} \right\rangle = -d_0 \frac{\partial}{\partial E}\langle H_{\text{mol}}\rangle \tag{4.11}$$

Therefore, for a molecule in its ground state, the induced dipole moment can be calculated as the derivative of the ground-state energy with respect to the electric field E. For small electric fields, to be more precise to first nonvanishing

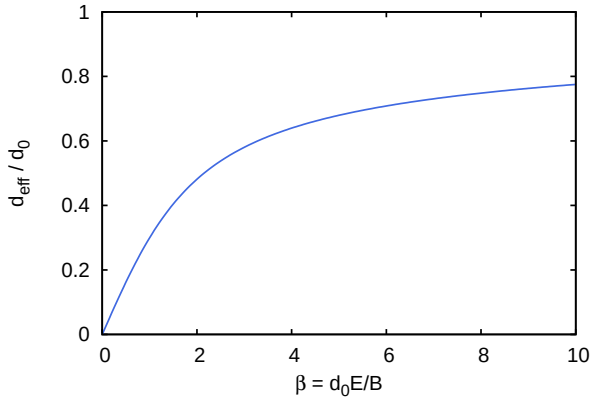

Figure 4.2: Effective dipole moment in the laboratory frame as a function of applied field.

order in β, the ground-state energy is (see Table 4.2) $E_0 = -B\beta^2/6$, therefore by Eq. (4.11) we have

$$d_{\text{eff}} = \frac{d_0 B\beta}{3} = \frac{d_0^2 E}{3B} \tag{4.12}$$

For the KRb molecule in the electronic singlet ground state, the current experiments [67] are at fields of the order of kV/cm, which is in this linear regime. They reach up to $d_{\text{eff}} = 0.2\,\text{D}$ at $E = 5\,\text{kV/cm}$, which is the highest field available in this experiment [65].

For high electric fields the perturbative first-order result (4.11) is, of course, insufficient since β is no longer small. Then, d_{eff} can be found by diagonalizing H_{mol} numerically in the basis of the $|J, M\rangle$ states. From (4.5), we have

$$\langle J, M |\, H_{\text{mol}} \,| J', M' \rangle = \delta_{MM'}[BJ(J{+}1)\delta_{JJ'} - d_0 E\{a(M, J)\delta_{J',J-1} + a(M{+}1, J)\delta_{J',J+1}\}] \tag{4.13}$$

with

$$a(M, J) = \sqrt{\frac{J^2 - M^2}{(2J-1)(2J+1)}}. \tag{4.14}$$

Figure 4.2 shows the result[3] for the effective dipole as a function of β. As is seen, for strong fields d_{eff} approaches d_0, but quite slowly.

[3] When diagonalizing (4.13) numerically, the matrix has to be truncated, such that only states with $J \le J_{\max}$ are taken. The convergence is very fast, however, and for the values of β shown in Fig. 4.2, $J_{\max} = 2$ or 3 is sufficient. Note also that this is not the same as going to higher orders in β in the perturbation series.

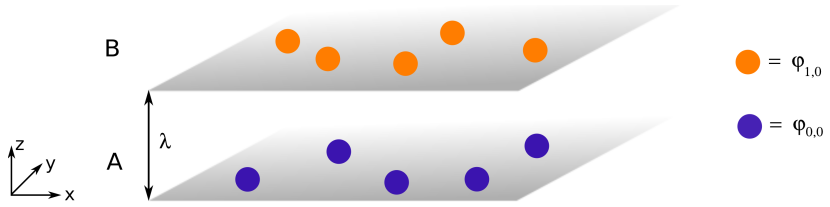

Figure 4.3: Schematic set-up of the considered experiment. Layer A contains molecules in state $\varphi_{0,0}$, layer B contains molecules in state $\varphi_{1,0}$.

4.3 Non-equilibrium collisions of dipolar molecules

We consider fermionic polar molecules confined in two thin parallel layers, A and B, separated by a distance λ. A weak external field along the z-direction is applied, such that the molecules have well-defined rotational states, as described above. We suppose that, initially, the molecules in layer A are prepared to be in the rotational ground state $\varphi_{0,0}$, while the molecules in layer B are prepared in the rotational state $\varphi_{1,0}$ (see Fig. 4.3).

The dipole–dipole interaction between two molecules with center-of-mass positions $\mathbf{r_1}$ and $\mathbf{r_2}$ is given by

$$H_{\mathrm{DDI}} = \frac{1}{4\pi\epsilon_0}\left[\frac{\mathbf{d}_1\cdot\mathbf{d}_2}{|\mathbf{r}|^3} - \frac{3(\mathbf{d}_1\cdot\mathbf{r})(\mathbf{d}_2\cdot\mathbf{r})}{|\mathbf{r}|^5}\right] \tag{4.15}$$

with $\mathbf{r} = \mathbf{r_1} - \mathbf{r_2}$. Here $\mathbf{d}_1$, $\mathbf{d}_2$ is the dipole moment operator of molecule 1, 2.

We are interested in two-particle scattering, where a particle in layer A in state α scatters with a particle in layer B in a state β. The dipole–dipole interaction may lead to a change of the rotational states of the particles involved due to the anisotropic character of H_{DDI}, schematically:

$$A\alpha + B\beta \to A\alpha' + B\beta' \tag{4.16}$$

Note that the particles never come closer than the distance λ, since they are confined to different layers. Still a collision takes place since the molecules are interacting by the long-range dipole–dipole interaction. In this way, the collision and the subsequent possible exchange of rotational state can be considered *non-local*.

Initially the particles are in the internal states $\varphi_{0,0}$ and $\varphi_{1,0}$. The only energy-preserving (elastic) collisions starting from these states are:

	$A\alpha$	$B\beta$	$\to$	$A\alpha'$	$B\beta'$
I:	$\varphi_{0,0}$	$\varphi_{1,0}$	$\to$	$\varphi_{0,0}$	$\varphi_{1,0}$
II:	$\varphi_{0,0}$	$\varphi_{1,0}$	$\to$	$\varphi_{1,0}$	$\varphi_{0,0}$
III:	$\varphi_{1,0}$	$\varphi_{0,0}$	$\to$	$\varphi_{0,0}$	$\varphi_{1,0}$
IV:	$\varphi_{1,0}$	$\varphi_{0,0}$	$\to$	$\varphi_{1,0}$	$\varphi_{0,0}$

All other collisions are inelastic. Inelastic collisions to final states not listed above

involve an energy change of at least (using the fact that $\beta \ll 1$)

$$\Delta E = \frac{3}{20} B\beta^2 \tag{4.17}$$

This is much larger than other energy scales in the system, such as the dipolar energy $E_D = d^2/(4\pi\epsilon_0\lambda^3)$. For KRb, $\Delta E = 80\,\mu$K for $\beta = 0.1$, while $E_D = 15\,$nK.

We may introduce a pseudospin notation for the internal states of the particles, since we will be only dealing with the two states $\varphi_{0,0}$ and $\varphi_{1,0}$:

$$\varphi_{0,0} \equiv|\uparrow\rangle, \qquad \varphi_{1,0} \equiv|\downarrow\rangle$$

Two-particle states, where a particle in layer A is in state α and a particle in layer B in state β will written $|\,\alpha\beta\rangle$.

The interaction potential $H_{\rm DDI}$ is symmetric with respect to the interchange of layers A, B. Therefore, processes I, IV and II, III have the same amplitude, up to a sign. The investigation is reduced to two types of collisions:

$$\begin{array}{lll} \text{I.} & \text{state-preserving collisions} & \varphi^A_{1,0}\,\varphi^B_{0,0} \;\to\; \varphi^A_{1,0}\,\varphi^B_{0,0} \quad |\uparrow\downarrow\rangle \;\to |\uparrow\downarrow\rangle \\ \text{II.} & \text{state-changing collisions} & \varphi^A_{1,0}\,\varphi^B_{0,0} \;\to\; \varphi^A_{0,0}\,\varphi^B_{1,0} \quad |\uparrow\downarrow\rangle \;\to |\downarrow\uparrow\rangle \end{array} \tag{4.18}$$

The matrix elements of the dipole–dipole interaction of interest to us are: (up to β^2)

$$\langle\uparrow\downarrow|\, H_{\rm DDI}\, |\uparrow\downarrow\rangle = \langle\downarrow\uparrow|\, H_{\rm DDI}\, |\downarrow\uparrow\rangle \;=\; -d^2\frac{\beta^2}{15}\left[\frac{1}{r^3} - \frac{3z^2}{r^5}\right] \tag{4.19}$$

$$\langle\uparrow\downarrow|\, H_{\rm DDI}\, |\downarrow\uparrow\rangle = \langle\downarrow\uparrow|\, H_{\rm DDI}\, |\uparrow\downarrow\rangle \;=\; d^2\left(\frac{1}{3} - \frac{\beta^2}{30}\right)\left[\frac{1}{r^3} - \frac{3z^2}{r^5}\right] \tag{4.20}$$

$$\langle\uparrow\downarrow|\, H_{\rm DDI}\, |\uparrow\downarrow\rangle = \langle\downarrow\uparrow|\, H_{\rm DDI}\, |\downarrow\uparrow\rangle \;=\; 0 \tag{4.21}$$

Changing the basis to the two-particle singlet and triplet states[4]

$$\begin{array}{l} |\,S\rangle = (|\uparrow\downarrow\rangle - |\downarrow\uparrow\rangle)/\sqrt{2}, \\ |\,T_0\rangle = (|\uparrow\downarrow\rangle + |\downarrow\uparrow\rangle)/\sqrt{2}, \qquad |\,T_{-1}\rangle = |\downarrow\downarrow\rangle, \qquad |\,T_1\rangle = |\uparrow\uparrow\rangle \end{array} \tag{4.22}$$

the interaction between $|\,S\rangle$ and $|\,T_0\rangle$ becomes diagonal:

$$\begin{array}{l} \langle S|\, H_{DDI}\, |\,S\rangle = -d^2\left(\frac{1}{3} + \frac{\beta^2}{30}\right)\left[\frac{1}{r^3} - \frac{3z^2}{r^5}\right], \\ \langle T_0|\, H_{DDI}\, |\,T_0\rangle = d^2\left(\frac{1}{3} - \frac{3\beta^2}{30}\right)\left[\frac{1}{r^3} - \frac{3z^2}{r^5}\right], \\ \langle S|\, H_{DDI}\, |\,T_0\rangle = 0. \end{array} \tag{4.23}$$

We will ignore terms $O(\beta^2)$ in (4.23). Then it is seen that

$$\begin{array}{llll} \text{states} & |\,T_0\rangle & \text{interact by} & V_{dd}(r) \;\; = \frac{d_0^2}{3}\left[\frac{1}{r^3} - \frac{3z^2}{r^5}\right], \\ \text{states} & |\,S\rangle & \text{interact by} & -V_{dd}(r) \; = -\frac{d_0^2}{3}\left[\frac{1}{r^3} - \frac{3z^2}{r^5}\right], \end{array} \tag{4.24}$$

[4]The states T_{-1} and T_1 are listed for completeness, they are not involved in elastic collisions.

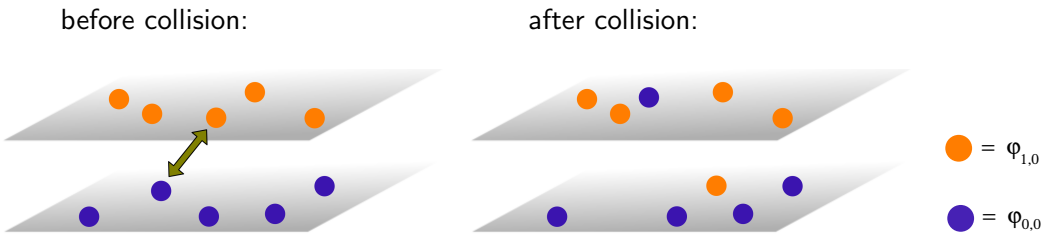

Figure 4.4: A state-changing collision $\varphi^A_{0,0}\varphi^B_{1,0} \to \varphi^A_{1,0}\varphi^B_{0,0}$. Left: initial state, right: final state.

and there is no interaction between $|S\rangle$ and $|T_0\rangle$.

As mentioned before, since we are dealing only with two internal states, the system can be described as a (pseudo)-spin 1/2 system. It this way, the state-changing collisions are analogous to spin exchange collisions between atoms, see, for example [35]. Then, another way to write the interaction between two molecules is

$$V = V_{dd}(r)P_{T_0} - V_{dd}(r)P_S \tag{4.25}$$

where

$$P_S = \frac{1}{4}(1 - \vec{\sigma}_1 \cdot \vec{\sigma}_2), \tag{4.26}$$

$$P_{T_0} = \frac{1}{4}(1 + \sigma_1^x\sigma_2^x + \sigma_1^y\sigma_2^y - \sigma_1^z\sigma_2^z) \tag{4.27}$$

are the projection operators for states $|S\rangle$, $|T_0\rangle$, and σ_α are the Pauli matrices acting on state $\alpha = 1, 2$.

Generally, in quantum-mechanical scattering, the scattering amplitude for scattering from ψ_i to ψ_f is given by the matrix element of the $\mathcal{T}$-operator, $\langle\psi_f|\mathcal{T}|\psi_i\rangle$. We consider two-particle scattering, so, ψ_i and ψ_f are two-particle states. Let f_+ be the scattering amplitude for two particles interacting with potential $V_{dd}(r)$, and f_- be the scattering amplitude for two particles interacting with $-V_{dd}(r)$:

$$\begin{aligned} &\langle S|\mathcal{T}|S\rangle = f_-, \qquad \langle T_0|\mathcal{T}|T_0\rangle = f_+, \\ &\langle S|\mathcal{T}|T_0\rangle = 0. \end{aligned} \tag{4.28}$$

Expressing the two-particle product states for the processes in Eq. (4.18) as linear combinations in terms of $|S\rangle$ and $|T_0\rangle$, we get for the scattering amplitudes:

$$\begin{aligned} &\text{I.} \quad \text{spin-preserving collisions} \quad f_{\text{sp}} = (f_+ + f_-)/2 \\ &\text{II.} \quad \text{spin-changing collisions} \quad f_{\text{sc}} = (f_+ - f_-)/2 \end{aligned} \tag{4.29}$$

4.4 Scattering amplitude for spin-changing collisions

The scattering amplitude for spin-changing collisions between a particle in layer A and a particle in layer B is

$$f_{\rm sc} = \frac{1}{2}(f_+ - f_-) \tag{4.30}$$

where $f_\pm$ is the scattering amplitude for *two-dimensional* scattering with interaction $\pm V_{\rm dd}(r)$,

$$V_{\rm dd}(r) = \frac{D^2}{3}\,\frac{r^2 - 2\lambda^2}{(r^2+\lambda^2)^{5/2}} \tag{4.31}$$

where $D^2 = D_0^2/(4\pi\epsilon_0)$ and λ is the interlayer separation. Two-particle scattering amplitudes are usually calculated in the center-of-mass frame, using the quantities m and k. The relation to the scattering of two particles with masses m_1, m_2 and velocities v_1, v_2 is

$$m = \frac{m_1 m_2}{m_1 + m_2}, \qquad k = m|\mathbf{v}_1 - \mathbf{v}_2| \tag{4.32}$$

We have studied the s-wave scattering of $+V_{\rm dd}$ analytically and numerically in Ch. 2, as a function of the dimensionless coupling strength[5]

$$U_0 = \frac{1}{3}\frac{m d_0^2}{\hbar^2 \lambda} \tag{4.33}$$

and dimensionless momentum $q = k\lambda$. The formulas for scattering by $-V_{dd}$ are obtained by putting $U_0 \to -U_0$. It was found in Sec. 2.9 for a large range of values, the scattering can be calculated in the 2nd Born approximation. Writing the scattering phase shift $\tan_+\delta(k)$ as a series in U_0,

$$\tan\delta_+(k) = U_0\,\tan\delta_+^{(1)}(k) + U_0^2\,\tan\delta_+^{(2)}(k) + \ldots \tag{4.34}$$

we obtain (using the relation between f and $\tan\delta$ from Eq. (2.12)) for the scattering amplitude of spin-changing collisions

$$|f_{sc}|^2 = |(f_+ - f_-)/2|^2 = U_0^2\,[\tan\delta_+^{(1)}(k)]^2 \;+\; O(U_0^4) \tag{4.35}$$

and the Born approximation for $\tan\delta_+$ is [45]

$$\tan\delta_+^{(1)}(q) = -\frac{\pi}{2}\left[-\frac{4q}{\pi} - 2q(\mathbf{L}_1(2q) - I_1(2q))\right], \qquad q = \lambda k \tag{4.36}$$

For large q, this expression behaves like

$$\tan\delta_+^{(1)}(q) = \frac{1}{2q} + \frac{3}{8q^3} + \ldots \tag{4.37}$$

The validity of Eq. (4.35) can be checked numerically by comparing it with the result from the numerical solution of the Schrödinger equation. Figure 4.5 shows that the Born approximation is good for a large range of values.

[5] To use the plots and results in Ch. 2 and [45] directly, we have now defined U_0 with a factor 1/3.

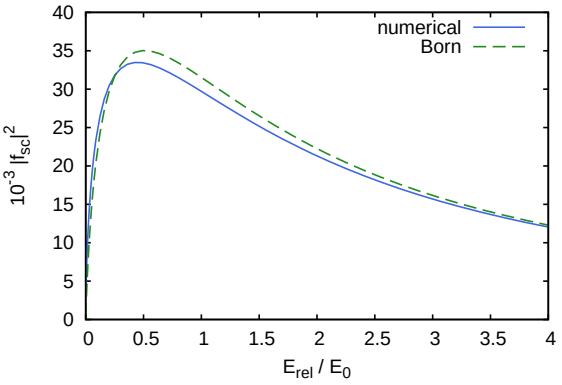

Figure 4.5: Scattering amplitude for state-changing collisions calculated numerically, compared with the Born expression Eq. (4.36).

For state-preserving collisions, the scattering amplitude is much smaller

$$|f_{sp}|^2 = |(f_+ + f_-)/2|^2 = O(U_0^4).$$

This can be also seen from the fact that the matrix element for the state-preserving collision vanishes, Eq. (4.21), therefore the process is of higher order. We will thus neglect these state-preserving collisions.

Only s-wave scattering will be considered. If f_0 is the s-wave scattering amplitude, then the total 2D s-wave scattering cross-section is given by

$$\sigma = \frac{4}{k}|f_0|^2 \tag{4.38}$$

It has dimensions 1/length. We will need the quantity

$$v\sigma(k) = \frac{p}{m}\sigma(k) = 4\frac{\hbar}{m}|f_0(k)|^2$$

with dimensions $(\text{length})^2/\text{time}$.

4.5 Averaged collision rates

Consider a collision of the type $A + B \to f$ in the laboratory frame, where f is some final state. Let $\sigma(p)$ be the total cross-section for the equivalent process in the center-of-mass frame. The number of particles detected in state f is ($n_\alpha = N_\alpha/\text{Vol}$):

$$N_f/\text{time} = \frac{N_A N_B}{\text{Vol}}\, v\sigma(\mathbf{p}), \qquad \text{or} \qquad n_f/\text{time} = n_A n_B\, v\sigma(\mathbf{p}) \tag{4.39}$$

with $v = |\mathbf{v}_A - \mathbf{v}_B|$ and $\mathbf{p} = m(\mathbf{v}_A - \mathbf{v}_B)$, m being the reduced mass. This is valid in both 3D and 2D: in 3D σ has dimensions $1/\text{length}^2$, in 2D σ has dimension 1/length. For continuous times, this gives the rate equation

$$\frac{dn_f}{dt} = \mathcal{K}\, n_A n_B \tag{4.40}$$

with $\mathcal{K} = v\sigma$.

The relevant quantity for experiments is the two-particle collision rate *averaged* over the distribution of velocities in the system [85]. If velocities of particles of type A, B are distributed according to the distributions $\bar{f}_A$, $\bar{f}_B$, the averaged collision rate, having dimension (length)^2/time, is [85]

$$K = \langle v\sigma \rangle = \iint v\sigma(p) \bar{f}_A(v_A) \bar{f}_B(v_B)\, d^2v_A d^2v_B \tag{4.41}$$

This expression does not include effects of quantum-mechanical statistics. It applies to scattering of identical Fermions if the Pauli principle can be neglected, i.e. if the final state is empty.

To keep things general, we consider particles A and B with masses m_A, m_B. We assume that the velocity distributions depend only on the energy of the particles

$$E_A = \frac{1}{2} m_A v_A^2, \qquad E_B = \frac{1}{2} m_B v_B^2. \tag{4.42}$$

The integral (4.41) can be transformed to relative and center-of-mass velocities

$$\begin{aligned} &\mathbf{v} = \mathbf{v}_A - \mathbf{v}_B, \qquad (m_A + m_B)\mathbf{V} = m_A \mathbf{v}_A + m_B \mathbf{v}_B, \\ &m = \frac{m_A m_B}{m_A + m_B}, \qquad \gamma = \angle(\mathbf{v}, \mathbf{V}), \end{aligned} \tag{4.43}$$

and the related energies

$$E_{\mathrm{cm}} = \frac{1}{2}(m_A + m_B)V^2, \quad E_{\mathrm{rel}} = \frac{1}{2} m v^2, \tag{4.44}$$

the Jacobian of the transformation is

$$\frac{\partial(\mathbf{v}_A, \mathbf{v}_B)}{\partial(\mathbf{v}, \mathbf{V})} = 1. \tag{4.45}$$

The velocity distribution functions $\bar{f}$ are normalized to $\int \bar{f}(v) d^2v = 1$, the energy distribution functions f are normalized to $\int_0^\infty dE f(E) = 1$, so $f_{A,B} = (2\pi/m_{A,B})\bar{f}$. Then we obtain

$$K = \int_0^\infty \frac{p}{m} \sigma(p)\, F(E_{\mathrm{rel}})\, dE_{\mathrm{rel}} \tag{4.46}$$

with

$$F(E_{\mathrm{rel}}) = \int_0^{2\pi} \frac{d\gamma}{2\pi} \int_0^\infty f_A(E_A) f_B(E_B)\, dE_{\mathrm{cm}} \tag{4.47}$$

Here $f_{A,B}(E)$ are the energy distribution functions.

The distribution of relative energies $F(E_{\mathrm{rel}})$, Eq. (4.47), can be evaluated analytically for limiting cases.

A) $T \to \infty$, Boltzmann: If both distributions are Boltzmann distributions with possibly different temperatures

$$f_A(E) = \frac{1}{T_A}\, e^{-E/T_A}, \qquad f_B(E) = \frac{1}{T_B}\, e^{-E/T_B} \tag{4.48}$$

then F is a Boltzmann distribution in the relative energy

$$F(E_{\rm rel}) = \frac{1}{T_*} e^{-E_{\rm rel}/T_*}, \tag{4.49}$$

with the effective temperature

$$T_* = \frac{m_A T_B + m_B T_A}{m_A + m_B}. \tag{4.50}$$

This result has the same form as in 3D [85].

B) $T = 0$, Fermions: Let the particles be distributed according to Fermi distributions for $T = 0$, possibly with different chemical potentials:

$$f_A(E) = \frac{1}{\mu_A}\theta(\mu_A - E), \qquad f_B(E) = \frac{1}{\mu_B}\theta(\mu_B - E), \tag{4.51}$$

and we allow the particles to have different masses m_A, m_B. It is convenient to write

$$\nu_A = \frac{2m_B}{m_A + m_B}\mu_A, \qquad \nu_B = \frac{2m_A}{m_A + m_B}\mu_B. \tag{4.52}$$

For equal masses we have $\nu_{A,B} = \mu_{A,B}$. The calculation (see App. A3.2) shows that F is given by

$$F(E_{\rm rel}) = g_1(E_{\rm rel}) + g_2(E_{\rm rel}) \tag{4.53}$$

with

$$g_1(E) = \begin{cases} \dfrac{2}{\nu_A \nu_B} \min(\nu_A, \nu_B) & \text{for} \quad E < \dfrac{|\nu_A - \nu_B|}{2} \\ 0 & \text{otherwise} \end{cases} \tag{4.54}$$

$$g_2(E) = \begin{cases} \bar{g}_2(E) & \text{for} \quad \dfrac{\nu_a + \nu_b}{2} - \sqrt{\nu_a \nu_b} < E < \dfrac{\nu_a + \nu_b}{2} + \sqrt{\nu_a \nu_b} \\ 0 & \text{otherwise} \end{cases} \tag{4.55}$$

and

$$\bar{g}_2(E) = -\frac{1}{\pi}\frac{2}{\nu_A \nu_B}\sqrt{X} + \frac{2}{\pi \nu_B} \arctan \frac{\sqrt{X}}{\frac{1}{2}(2E + \nu_A - \nu_B)} + \frac{2}{\pi \nu_A} \arctan \frac{\sqrt{X}}{\frac{1}{2}(2E + \nu_B - \nu_A)},$$

$$\text{with} \quad X = -E^2 - \tfrac{1}{4}(\nu_A - \nu_B)^2 + E(\nu_A + \nu_B). \tag{4.56}$$

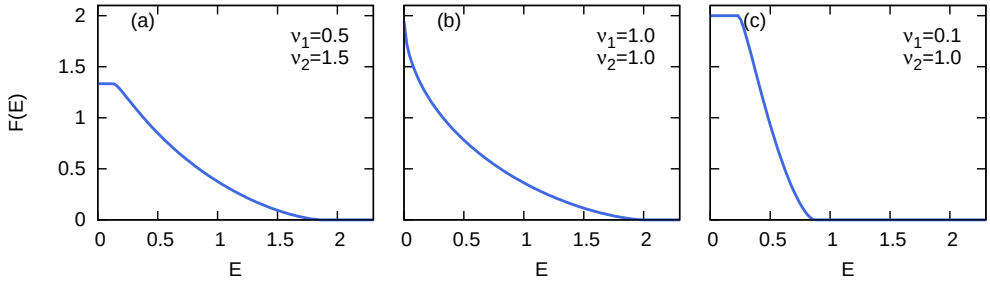

Figure 4.6: Distribution function of relative energies $F(E_{\text{rel}})$ for Fermions at $T = 0$ for different ν_1, ν_2; from Eq. (4.53). The panel (a) shows the generic case, (b) shows $\nu_A = \nu_B$, (c) shows $\nu_A \ll \nu_B$.

A plot of this function is shown in Fig. 4.6. The generic case is shown in Fig. 4.6a, further special cases are:
Fig. 4.6b: In case $\mu = \nu_A = \nu_B$, this expression simplifies considerably:

$$F(E_{\text{rel}}) = \begin{cases} -\dfrac{2}{\pi\mu^2}\sqrt{2\mu E_{\text{rel}} - E_{\text{rel}}^2} + \dfrac{4}{\pi\mu}\arctan\sqrt{2\mu/E_{\text{rel}} - 1} & \text{for} \quad 0 < E_{\text{rel}} < 2\mu \\ 0 & \text{otherwise} \end{cases} \tag{4.57}$$

Fig. 4.6c: For $\mu_A \ll \mu_B$, it can be seen that $F(E)$ becomes a broadened step function:

$$F(E_{\text{rel}}) \simeq \text{Step function } \frac{2}{\mu_B}\theta\left(\frac{\mu_B}{2} - E_{\text{rel}}\right), \text{ FWHM broadening } 2\sqrt{\mu_A\mu_B} \tag{4.58}$$

C) Fermions, $T > 0$. For a finite T, the function $F(T)$ has to be calculated from (4.47) numerically.

Figure 4.7 shows some results for fermions, where the functions $f_{A,B}$ are Fermi distributions

$$f(E) = \mathcal{N}^{-1}\,\frac{1}{e^{(E-\mu)/T} + 1} \tag{4.59}$$

(the normalization constant is $\mathcal{N} = T\log(1 + e^{\mu/T})$ such that $\int_0^\infty f(E)dE = 1$), and compares them with the limits $T = 0$ and $T \to \infty$ (Boltzmann).

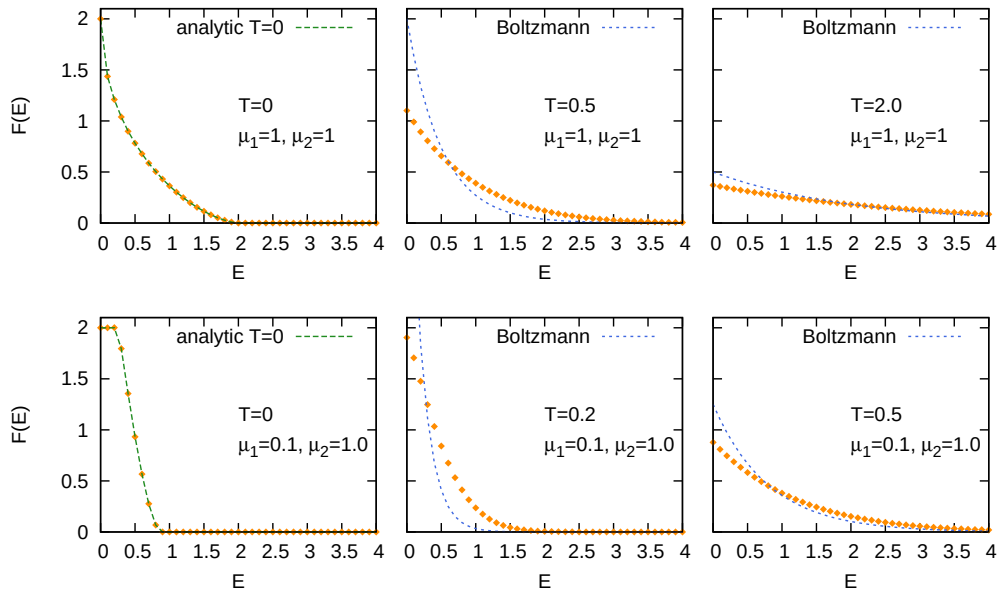

Figure 4.7: Distribution function of relative energies $F(E_{\text{rel}})$ for different temperatures T for Fermions, calculated numerically and compared with the exact expressions for $T = 0$ and $T \to \infty$ (Boltzmann). In the upper row $\mu_A = \mu_B = 1$, in the lower row $\mu_A \ll \mu_B$.

4.6 Results for KRb

We consider the rate of state-exchange collisions for the set-up described above, as a function of temperature T and density of particles $n_{A,B}$ in layer A, B. It is convenient to use the unit of energy

$$E_0 = \frac{\hbar^2}{\lambda^2 m_0}$$

where m_0 is the mass of a molecule (this notation avoids confusion, since m was used as the reduced mass). The results are presented for the molecule KRb (see Table 4.1 on p. 63) and an interlayer spacing $\lambda = 532$nm.

We take the chemical potential $\mu(T)$ as a function of temperature from the ideal Fermi gas (see Sec. A1.2), i.e. the solution of

$$\log(1 + e^{\mu/T}) = E_F/T \tag{4.60}$$

for a given temperature T and Fermi energy $E_F = 2\pi n\hbar^2/m_0$, here n is the 2D density of molecules in one layer.

The collision rate in dimensionless units ($q = \lambda k$) is given by, see (4.46),

$$K = 8\frac{\hbar}{m_0}\int_0^\infty |f_{\text{sc}}(x = q^2)|^2 \; E_0 F(x = E_{\text{rel}}/E_0)\, dx. \tag{4.61}$$

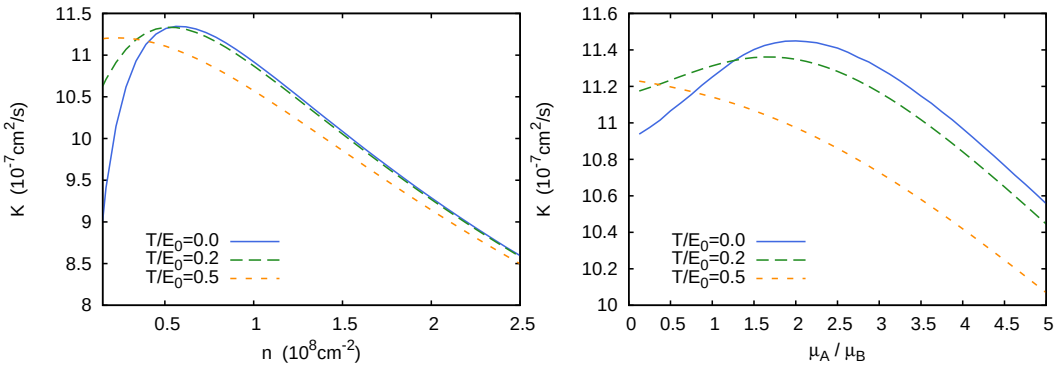

Figure 4.8: Rate of state-changing collisions K, for different temperatures (for KRb). a) as a function of the density $n = n_A = n_B$, b) as a function of the population imbalance $\mu_A/\mu_B = n_A/n_B$.

The rate K is the overlap integral between $F(E)$ and $|f_{\rm sc}|^2$. The qualitative dependence of the collision rate on the density, interlayer spacing λ, and temperature can therefore be obtained from the behavior of $|f_{\rm sc}|^2$ and $F(E)$. The scattering amplitude has a maximum close to $E_{\rm rel}/E_0 = (\lambda k_{\rm rel})^2 = 0.5$ [see Fig. 4.5 on p. 71], so at $T = 0$ the maximal rate occurs for Fermi momenta $k_F\lambda \sim 1$. The distribution function of relative energies $F(E)$ becomes broader at larger temperatures, therefore the effects of this maximum of $f_{\rm sc}$ are smeared at larger temperatures. Figure 4.8a shows the rate of state exchange collisions as a function of the density of molecules n in one layer, at different temperatures, calculated from Eq. (4.61) for KRb.

It is interesting to consider the case where the particle densities in layer A and B are different. For strong population imbalance, $n_A \ll n_B$ (or equivalently $\mu_A \ll \mu_B$), the distribution function of relative energies F is a broadened step function, see Eq. (4.58). Then, the collision rate K shows a maximum as a function of the imbalance $\mu_A/\mu_B = n_A/n_B$, as shown in Fig. 4.8b. At $T > 0$ this maximum persists, but is smeared at higher temperatures.

The previous results suggest interesting effects for temperatures close to the Fermi energy E_F. However, typical experimental values for E_0 and E_F are in the range of 10 nK, while the temperature in current experiments is in the range of several 100 nK. Therefore, we discuss a consequence of state-changing collisions for high temperatures. In the following we use a density $n = 5.6 \times 10^7\,\mathrm{cm}^{-2}$ for KRb, which gives $E_F/E_0 = 1.0$. Figure 4.9 shows the temperature dependence of the rate of state-changing collisions.

An analytical approximation to the curve in Fig. 4.9 can be derived as follows. For large T, the distribution of relative energies is a Boltzmann distribution. The main contribution to K comes from large momenta. Approximating the scattering amplitude by the first term in Eq. (4.37) and choosing a cut-off Λ,

$$K \approx \frac{8\hbar}{m_0} U_0^2 \int_\Lambda^\infty \frac{1}{4x}\frac{1}{T} e^{x/T} dx = \frac{8\hbar}{m_0} U_0^2 \frac{\log T}{4T} + \ldots \tag{4.62}$$

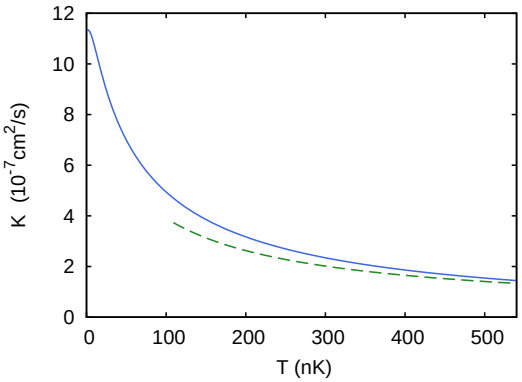

Figure 4.9: Rate of state-changing collision as a function of temperature, for $E_F/E_0 = 1.0$. The dashed line is from Eq. (4.62).

where a large-T expansion has been taken.

4.7 Observation for reactive molecules

KRb molecules are chemically highly reactive. It has been observed [26] that they undergo the exothermic chemical reaction

$$\mathrm{KRb} + \mathrm{KRb} \to \mathrm{K_2} + \mathrm{Rb_2}. \tag{4.63}$$

In the experiment, where the KRb molecules are confined in an optical trap, this means that the products K_2 and Rb_2 leave the trap. The losses are usually a disadvantage for experimental observation. Remarkably, in the case of the set-up considered here, the reactivity can be turned into an advantage, and it will help to observe the effect of state-changing collisions.

The molecules KRb are fermions, and the Pauli principle inhibits collisions of identical molecules in the same quantum state. More precisely, identical fermions do not scatter in the s-wave channel, while non-identical fermions scatter s-wave. The temperatures are so low in the experiments that this quantum-mechanical effect has been observed [26, 67] for the reaction (4.63). The orders of magnitude of the collision rates are:

s-wave (non-identical fermions):	10^{-5} cm^2/s	(at T=800 nK, see [26])
p-wave (identical fermions):	10^{-7} cm^2/s	(at T=800 nK, see [26])
state-changing collisions:	10^{-6}...10^{-7} cm^2/s	(see Fig. 4.9)

In the set-up considered here, initially all particles in layer A are in state $\varphi_{0,0}$ and all particles in layer B are in state $\varphi_{1,0}$ (see Fig. 4.10). In each layer the particles are identical, thus the chemical reaction proceeds in the p-wave channel. The reaction is slow and the losses are small. A state-changing collision exchanges the internal states, thus creating a "defect molecule" in layer A in state $\varphi_{1,0}$ and in layer B in state $\varphi_{0,0}$, see Fig. 4.10. This defect molecule now reacts with a majority molecule in the fast s-wave channel. Since the s-wave reaction rate is

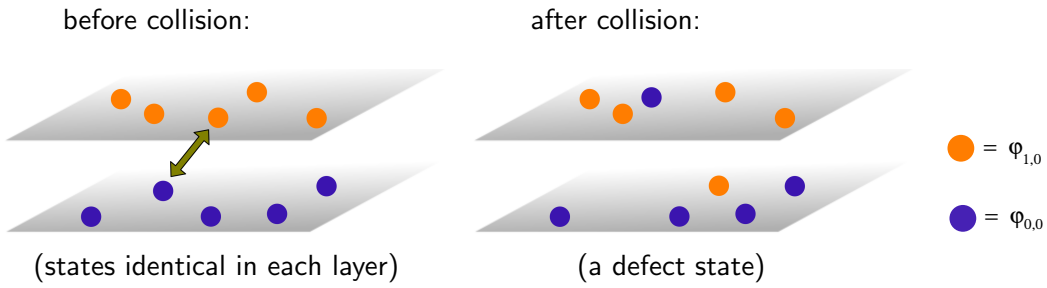

Figure 4.10: A state-changing collision $\varphi^A_{0,0}\varphi^B_{1,0} \rightarrow \varphi^A_{1,0}\varphi^B_{0,0}$. Left: initial state, right: final state.

much larger than the rate of state-exchange collisions, the defect molecules are quickly lost, and their number is always small. The rate of losses due to reactions between a defect and a majority state is therefore approximately the same as the rate of state-changing collisions.

The temperature dependence of the rate of losses from the trap gives evidence for state-changing collisions. At high temperatures, losses are due to chemical reactions between molecules colliding in the p-wave channel. As the temperature decreases, the rate of p-wave collisions decreases (Wigner threshold law). On the other hand, the rate of state-changing collisions is weakly dependent on temperature for high temperatures. Therefore, at some temperature T_c (we estimate $T_c \sim 500$ nK) the losses due to the defect states become comparable to the p-wave rate, and for lower temperatures the dominant loss mechanism is due to state-changing collisions. This clear deviation from the Wigner threshold law below T_c should be observable in the experiment.

Conclusions & Outlook

In conclusion, we have investigated two-body states, many-body regimes, and nonequilibrium properties of fermionic polar molecules in bilayer geometries.

It was shown that bilayer systems of fermionic polar molecules may allow the observation of interesting regimes of interlayer superfluidity. These regimes range from fermionic BCS-like superfluidity where Cooper pairs are formed by molecules of different layers, to a BEC of interlayer dimers. The system exhibits a peculiar BCS-BEC crossover. The transition temperature to the superfluid regime was calculated.

We have studied in detail the weakly bound states and the scattering properties at low energies for the two-dimensional Schrödinger equation. Approximate analytical expressions for the bound-state energy and for the scattering phase shift were given and compared with exact numerical calculations. Some special features of the dipole–dipole interaction were pointed out.

It was shown that effects of the dipole–dipole interaction can be observable in nonequilibrium situations. In a weak electric field, the dipole–dipole interaction leads to collisions which exchange the rotational state of the particles. These state-changing collisions can be used to observe an effect of interactions at temperatures far above the Fermi temperature, particularly for chemically reactive molecules such as KRb.

The investigations of this thesis motivate further research in the following directions.

We have investigated the BCS–BEC crossover in a bilayer geomtery with equal particle densities in both layers. New phenomena arise if an imbalanced system is considered, i.e. one where the particle densities in the layers are different. Here new types of paired states can arise, both spatially homogeneous and inhomogeneous, since some particles cannot be paired. The properties of this system, such

as the transition temperature, then depend on the population imbalance.

In the present study of the BCS–BEC crossover we have paid attention mostly to the limiting regimes: BCS superfluid and BEC of dimers. The intermediate regime merits a separate investigation, since recent experiments [32] have explored this regime. The observations indicate that as the temperature is lowered, first pairs form and then they condense to a superfluid. Thus there is a temperature region where non-condensed pairs exist, the so-called pre-formed pair phase or pseudogap phase. It is worthwhile to study this regime in the present setting.

We have considered bound states and scattering of the two-dimensional Schrödinger equation for radially symmetric potentials. Much less is known about the two-dimensional Schrödinger equation with a potential which is not radially symmetric. Such an interaction potential is encountered, for example, if two dipoles interact whose axis is not perpendicular to the plane of motion. However, the formalism used here (Jost functions) is specific for the radially symmetric case; therefore, presumably a somewhat different approach is needed for the non-symmetric case.

Appendix

A1 Two-dimensional systems

A1.1 Reduction of 3D quantities to 2D

A system which is confined to a thin layer is often referred to as *quasi-two-dimensional*. It depends very much on the physical situation whether one has to use a three-dimensional (in other words, a quasi-two-dimensional) description where the thickness of the layer is important, or a purely two-dimensional description where the thickness of the layer is irrelevant.

A thin layer can be viewed as a three-dimensional system which is confined to a thin layer in the x-y plane by a confining potential $V_c(z)$. The confining potential can be assumed a harmonic potential with a frequency ω_c, and we can take the the thickness of the layer ℓ_z as the oscillator length: $\ell_z = \sqrt{\hbar/m\omega_c}$. For energies which are much smaller than ω_c, we can write all wave functions in the layer in the form

$$\Psi(x, y, z) = \psi(x, y)\varphi(z) \tag{A.1}$$

where

$$\varphi(z) = \frac{1}{(\sqrt{\pi}\ell_z)^{1/2}} e^{-z^2/2\ell_z^2} \tag{A.2}$$

is the ground-state wave function of the harmonic oscillator, $\int \varphi^2(z)dz = 1$. In this way all terms involving three-dimensional wave functions can be transformed to two-dimensional wave functions. Sometimes ℓ_z will disappear from the formulas, sometimes it will not, and physical reasoning should confirm this.

A1.2 Ideal Fermi gas in 2D

Consider N particles in an area (=2D Volume) Vol, each has mass m and spin factor (number of internal states) g. From

$$\sum_k \frac{1}{e^{(E_k-\mu)/T}+1} = N \tag{A.3}$$

where $E_k = \frac{\hbar^2 k^2}{2m}$, use

$$\sum_k \to g \text{ Vol} \int \frac{d^2k}{(2\pi)^2} \tag{A.4}$$

so

$$g \int \frac{d^2k}{(2\pi)^2} \frac{1}{e^{(E_k-\mu)/T}+1} = n \tag{A.5}$$

with $n = N/\text{Vol}$ the two-dimensional number density. At $T = 0$ all states are filled up to the Fermi momentum k_F [or in energy space up to the Fermi energy $E_F = \frac{\hbar^2 k_F^2}{2m} = \mu(T=0)$], so from (A.5) we get

$$n = g \frac{k_F^2}{4\pi}, \tag{A.6}$$

$$E_F = 2\pi \frac{n}{g} \frac{\hbar^2}{m}. \tag{A.7}$$

The integral (A.5) for $T > 0$ can be evaluated to give an elementary function , in contrast to the three-dimensional case. Change to integration over E and write $y = E/T$, then (A.5) becomes

$$E_F = T \int_0^\infty (e^y e^{-\mu/T} + 1)^{-1} dy = T \log(1 + e^{\mu/T}). \tag{A.8}$$

Therefore the equation for $\mu(T)$ is

$$\log(1 + e^{\mu/T}) = E_F/T, \tag{A.9}$$

which has to be solved numerically to find μ, for given E_F and T.

A2 Transformations

A2.1 Bogoliubov transformation

The fermionic anticommutation relations are

$$\{\psi_\alpha^\dagger, \psi_\beta\} = \delta_{\alpha\beta}, \qquad \{\psi_\alpha, \psi_\beta\} = 0, \qquad \{\psi_\alpha^\dagger, \psi_\beta^\dagger\} = 0. \tag{A.10}$$

Here we consider two types of fermionic field operators, $\psi_1(k)$ and $\psi_2(k)$. The anticommutation relations are, written out more explicitly,

$$\begin{aligned}
\psi_1(k)\psi_2(k') + \psi_2(k')\psi_1(k) &= 0 && \text{(A.11a)}\\
\psi_1^\dagger(k)\psi_2^\dagger(k') + \psi_2^\dagger(k')\psi_1^\dagger(k) &= 0 && \text{(A.11b)}\\
\psi_1^\dagger(k)\psi_1(k') + \psi_1(k')\psi_1^\dagger(k) &= \delta_{kk'} && \text{(A.11c)}\\
\psi_2^\dagger(k)\psi_2(k') + \psi_2(k')\psi_2^\dagger(k) &= \delta_{kk'} && \text{(A.11d)}
\end{aligned}$$

The Bogoliubov transformation defines two new operators φ_+ and φ_- as follows:

$$\begin{aligned}
\varphi_+(k) &= u_k\,\psi_1(k) + v_k\,\psi_2^\dagger(-k) && \text{(A.12a)}\\
\varphi_-(k) &= u_k\,\psi_2(k) - v_k\,\psi_1^\dagger(-k) && \text{(A.12b)}
\end{aligned}$$

where u_k, v_k are real,

$$u_k = u_{-k}, \qquad v_k = v_{-k}, \qquad u_k^2 + v_k^2 = 1. \tag{A.12c}$$

The reverse transformation is

$$\begin{aligned}
\psi_1(k) &= u_k\,\varphi_+(k) - v_k\,\varphi_-^\dagger(-k) && \text{(A.13a)}\\
\psi_2(k) &= u_k\,\varphi_-(k) + v_k\,\varphi_+^\dagger(-k) && \text{(A.13b)}
\end{aligned}$$

The new operators $\varphi_+(k)$ and $\varphi_-(k)$ satisfy the fermionic anticommutation relations, as in Eqs. (A.11).

A more general transformation is possible than what was given here.

A2.2 Fourier transforms

The convention for Fourier transforms is

$$f(k) = \int f(x) e^{ikx}\, dx, \qquad f(x) = \int \frac{dk}{2\pi}\, f(k) e^{-ikx}.$$

Then some expressions transform as

position space	Fourier space
$\int f(x)g(x)\, dx$	$\int \frac{dk}{2\pi}\, f(-k)g(k) = \int \frac{dk}{2\pi}\, f(k)g(-k)$
transforms with respect to the variable $x - x'$:	
$\int dx \int dx'\, V(x-x') f(x) g(x')$	$\int \frac{dk}{2\pi}\, V(k) f(-k) g(k)$
$F(x-x') = \langle f(x) g(x') \rangle$	$F(k) = \langle f(k) g(-k) \rangle$

The formulas hold in any number of dimensions n, with the obvious replacements $dx \to d^n x$, $dk/2\pi \to d^n k/(2\pi)^n$, and $kx \to \vec{k} \cdot \vec{x}$.

A3 Evaluation of integrals

A3.1 Matrix elements for the dipole–dipole potential

Here we consider the integral

$$\tilde{V}_{kk'} = \int_0^\infty dr r \frac{r^2-2}{(r^2+1)^{5/2}} J_0^2(kr) J_0^2(k'r). \tag{A.14}$$

Using an integral representation for the products of Bessel functions [30]

$$J_0(ar)J_0(br) = \frac{1}{\pi}\int_0^\pi d\theta J_0\left(r\sqrt{a^2+b^2-2ab\cos\theta}\right), \tag{A.15}$$

we write the original integral as

$$\int_0^\infty dr r \frac{r^2-2}{(r^2+1)^{5/2}} J_0(ar)J_0(br) = \frac{1}{\pi}\int_0^\pi d\theta \left\{\int_0^\infty dr r \frac{r^2-2}{(r^2+1)^{5/2}} J_0(r\omega)\right\} \tag{A.16}$$

with $\omega = \sqrt{a^2+b^2-2ab\cos\theta}$. The inner integral can be carried out:

$$\int_0^\infty dr r \frac{r^2-2}{(r^2+1)^{5/2}} J_0(r\omega) = \frac{\sqrt{\omega}}{\sqrt{2}\Gamma(3/2)} K_{1/2}(\omega) - \frac{3\omega^{3/2}}{2^{3/2}\Gamma(5/2)} K_{3/2}(\omega) = -\omega e^{-\omega}. \tag{A.17}$$

Therefore we obtain the representation

$$\tilde{V}_{kk'} = \int_0^\infty dr r \frac{r^2-2}{(r^2+1)^{5/2}} J_0(kr)J_0(k'r) = \frac{1}{\pi}\int_0^\pi (-\omega e^{-\omega})\, d\theta. \tag{A.18}$$

For $k = k'$ the integral can be evaluated in terms of special functions. Then we have $\omega = 2k\sin(\theta/2)$ and the integral on the right-hand side of Eq. (A.18) gives:

$$\begin{aligned} \tilde{V}_{kk} &= -\frac{1}{\pi}\int_0^\pi \left(2k\sin\tfrac{\theta}{2}\right)\exp\left(-2k\sin\tfrac{\theta}{2}\right) d\theta = -\frac{4k}{\pi}\int_0^1 \frac{z e^{-2kz}}{\sqrt{1-z^2}}\, dz \\ &= -2k\left(\mathbf{L}_1(2k) - I_1(2k)\right) - \frac{4k}{\pi}, \end{aligned} \tag{A.19}$$

where $\mathbf{L}_1$ is the modified Struve function and I_1 the modified Bessel function of the first kind, see [1].

A3.2 Distribution function of relative velocities at $T = 0$

The distribution function of relative energies is given by the double integral

$$F(E_{\rm rel}) = \int_0^{2\pi} \frac{d\gamma}{2\pi} \int_0^{\infty} f_A(E_A) f_B(E_B) dE_{\rm cm} \tag{A.20}$$

with

$$E_A = \frac{m_A}{m_B + m_B} E_{\rm cm} + \frac{m}{m_A} E_{\rm rel} + \sqrt{2mE_{\rm rel}} \sqrt{\frac{2E_{\rm cm}}{m_A + m_B}} \cos\gamma \tag{A.21}$$

$$E_B = \frac{m_A}{m_B + m_B} E_{\rm cm} + \frac{m}{m_A} E_{\rm rel} - \sqrt{2mE_{\rm rel}} \sqrt{\frac{2E_{\rm cm}}{m_A + m_B}} \cos\gamma \tag{A.22}$$

and $m = m_A m_B/(m_A + m_B)$ the reduced mass.

It is possible to evaluate F for the case where the functions f_A, f_B are Fermi distributions with possibly different chemical potentials μ_A, μ_B:

$$f_A = \frac{1}{\mu_A} \theta(\mu_A - E_A), \qquad f_B = \frac{1}{\mu_B} \theta(\mu_A - E_B). \tag{A.23}$$

Here θ is the step function; the normalization factors here are chosen such that $\int f(E) dE = 1$.

The method of calculation of the double integral used here requires tedious algebraic manipulations; presumably shorter and more elegant methods exist. Therefore, we just give an outline of the approach. One has to evaluate

$$F(E_{\rm rel}) = \frac{1}{\mu_A \mu_B} \int_0^{\infty} dE_{\rm cm} \int_0^{2\pi} \frac{d\gamma}{2\pi} \, \theta(\mu_A - E_A) \theta(\mu_B - E_B). \tag{A.24}$$

First, the inner angular integral

$$I = \int_0^{2\pi} \frac{d\gamma}{2\pi} \, \theta(\mu_A - E_A) \theta(\mu_B - E_B) \tag{A.25}$$

is calculated. It can be determined, by some geometric reasoning, to be

$$I = \begin{cases} \frac{1}{\pi}(\operatorname{Arcsin} b - \operatorname{Arcsin} a) & \text{for } a < b \\ 0 & \text{for } a > b \end{cases} \tag{A.26}$$

where we used the abbreviations

$$a = \frac{-\mu_B - \frac{m_B}{m_A + m_B} E_{\rm cm} - \frac{m}{m_B} E_{\rm rel}}{\sqrt{2mE_{\rm rel}} \sqrt{\frac{2E_{\rm cm}}{m_A + m_B}}}, \qquad b = \frac{\mu_A - \frac{m_A}{m_A + m_B} E_{\rm cm} - \frac{m}{m_A} E_{\rm rel}}{\sqrt{2mE_{\rm rel}} \sqrt{\frac{2E_{\rm cm}}{m_A + m_B}}} \tag{A.27}$$

and we have introduced the continuous extension of the arcsin function

$$\operatorname{Arcsin} x = \begin{cases} \pi/2 & \text{for } x > 1 \\ \arcsin x & \text{for } -1 < x < 1 \\ -\pi/2 & \text{for } x < -1 \end{cases} \tag{A.28}$$

Next, we have

$$F(E_{\rm rel}) = \frac{1}{\mu_A \mu_B} \int_0^\infty I(a,b)\, dE_{\rm cm} \tag{A.29}$$

$$= \frac{1}{\mu_A \mu_B} \int_0^{E^*} I(a,b)\, dE_{\rm cm} \tag{A.30}$$

with

$$E^* = \mu_A + \mu_B - E_{\rm rel}. \tag{A.31}$$

To calculate this, we use the following indefinite integral (here $E > 0$)

$$\int \arcsin \frac{E + P^2 Q}{2P\sqrt{E}}\, dE = E \arcsin \frac{QP + E/P}{2\sqrt{E}} \pm \sqrt{P^2 E - (P^2 Q + E)^2/4} \pm (1-Q)P^2 \arctan \frac{P^2 - (P^2 Q + E)/2}{\sqrt{P^2 E - (P^2 Q + E)^2/4}} + C \tag{A.32}$$

(sign depending on $P > 0$, $P < 0$)

The integral only makes sense, of course, only if the argument of the arcsin is between -1 and 1 and if the expression under the square root is positive. This two conditions are equivalent, in fact.

Using (A.32), the definite integral in Eq. (A.30) is evaluated. After some lengthy algebraic manipulations, we obtain the following result. Put

$$\nu_A = \frac{2m_B}{m_A + m_B}\mu_A, \qquad \nu_B = \frac{2m_A}{m_A + m_B}\mu_B \tag{A.33}$$

Then

$$F(E_{\rm rel}) = g_1(E_{\rm rel}) + g_2(E_{\rm rel}) \tag{A.34}$$

where

$$\begin{aligned} g_1(E) &= -\frac{1}{\pi}\frac{2}{\nu_A \nu_B}\sqrt{-E^2 - (\nu_A - \nu_B)^2/4 + E(\nu_A + \nu_B)} \\ &\quad + \left[\frac{1}{\pi}\frac{2}{\nu_B} \arctan \frac{\sqrt{-E^2 - (\nu_A - \nu_B)^2/4 + E(\nu_A + \nu_B)}}{\frac{1}{2}(2E + \nu_A - \nu_B)} + (A \leftrightarrow B)\right] \\ &\qquad \text{for } \frac{\nu_A + \nu_B}{2} - \sqrt{\nu_A \nu_B} < E < \frac{\nu_A + \nu_B}{2} + \sqrt{\nu_A \nu_B}, \\ &= 0 \quad \text{otherwise} \end{aligned} \tag{A.35}$$

and

$$g_2(E) = \begin{cases} \frac{2}{\nu_A \nu_B} \min(\nu_A, \nu_B) & \text{for } E < \frac{|\nu_A - \nu_B|}{2} \\ 0 & \text{otherwise} \end{cases} \tag{A.36}$$

Acknowledgements

I would like to thank my thesis advisor, Prof. Luis Santos, for the help and guidance throughout the PhD work. He intorducted me to the interesting research field and was always supportive during the project work. I was happy to be part of Luis Santos' research group, which had interesting people and conveyed a positive atmosphere. I thank Luis Santos not only for discussions and advice concerning the projects he had in mind, but also for giving me the freedom to explore questions that I find interesting.

I thank Prof. G. V. Shlyapnokov for the fruitful collaboration, for his patience in answering simple questions, and for his hospitality during my visit in Orsay. The work on the BCS–BEC crossover greatly benefitted from his knowledge and experience. I would like to thank, too, Dr. A. Recati for the collaboration and helpful discussions, and for his hospitality in Trento.

The productive collaboration with M. Klawunn, for which I am greateful, deserves special mentioning. Most topics in this thesis were discussed with him, and I have always profited from these conversations.

I enjoyed being member of the Institute for Theoretical Physics, with its welcoming atmosphere, friendly staff, cozy kitchen, and its nice library.

I would like to thank my friends from the university, in particular A. del Campo, A. Argüelles, M. Colomé, M. Jona-Lasinio, H. Kelkar, K. Rodriguez, and T. Vekua for all the things we did together.

This work was made possible by a PhD fellowship of the Centre for Space-Time Research and Quantum Engeneering (QUEST), an Excellence Cluster funded by the D.F.G. I was happy to receive this scholarship and to be able to come to Hannover for a PhD. I thank the QUEST steering comitee, and in particular its speaker Prof. W. Ertmer, for awarding the fellowship and for providing an excellent working environment. I would like to thank the administrative staff of QUEST, most notably B. Ohlendorf and also B. Thiele-Bode, as well as its coordinators S. Pfalz and P. Barthold, for the friendly support in all matters.

I thank H. Kelkar and D. Noe for reading parts of the thesis.

Finally, I want to thank my family for constant support.

List of Publications

1. Two-dimensional scattering and bound states of polar molecules in bilayers
   Michael Klawunn, Alexander Pikovski, Luis Santos
   Physical Review A ***82***, 044701 (2010).

2. Interlayer superfluidity in bilayer systems of fermionic polar molecules
   A. Pikovski, M. Klawunn, G.V. Shlyapnikov, L. Santos
   Physical Review Letters ***105***, 215302 (2010).

3. Nonlocal state swapping of polar molecules in bilayers
   A. Pikovski, M. Klawunn, A. Recati, L. Santos
   Physical Review A ***84***, 061605(R) (2011).

Bibliography

[1] Abramowitz, M., and Stegun., I. A., Eds. *Handbook of mathematical functions*. 10th printing. U.S. Government Printing Office, Washington, D.C., 1972.

[2] Abrikosov, A. A., Gorkov, L. P., and Dzyaloshinki, I. E. *Methods of Quantum Field Theory in Statistical Physics*. Dover, New York, 1974.

[3] Adhikari, S. K. Quantum scattering in two dimensions. *American Journal of Physics* ***54*** (1986), 362.

[4] Aikawa, K., Frisch, A., Mark, M., Baier, S., Rietzler, A., Grimm, R., and Ferlaino, F. Bose-Einstein Condensation of Erbium. *Physical Review Letters* ***108*** (2012).

[5] Anderson, M. H., Ensher, J. R., Matthews, M. R., Wieman, C. E., and Cornell, E. A. Observation of bose-einstein condensation in a dilute atomic vapor. *Science* ***269*** (1995), 198.

[6] Anderson, P. W., and Morel, P. Generalized Bardeen-Cooper-Schrieffer States and the Proposed Low-Temperature Phase of Liquid He^3. *Physical Review* ***123*** (1961), 1911.

[7] Baranov, M. Theoretical progress in many-body physics with ultracold dipolar gases. *Physics Reports* ***464*** (2008), 71.

[8] Baranov, M., Micheli, A., Ronen, S., and Zoller, P. Bilayer superfluidity of fermionic polar molecules: Many-body effects. *Physical Review A* ***83*** (2011), 043602.

[9] Barnett, R., Petrov, D., Lukin, M., and Demler, E. Quantum Magnetism with Multicomponent Dipolar Molecules in an Optical Lattice. *Physical Review Letters* ***96*** (2006), 190401.

[10] Bernstein, R. B. Quantum Mechanical (Phase Shift) Analysis of Differential Elastic Scattering of Molecular Beams. *The Journal of Chemical Physics* ***33*** (1960), 795.

[11] Blatt, J. M. *Theory of Superconductivity.* Academic Press, New York, 1964.

[12] Bloch, I. Ultracold quantum gases in optical lattices. *Nature Physics* ***1*** (2005), 23.

[13] Bloch, I., Dalibard, J., and Zwerger, W. Many-body physics with ultracold gases. *Reviews of Modern Physics* ***80*** (2008), 885.

[14] Bollé, D., and Gesztesy, F. Low-Energy Parametrization of Scattering Observables in n-Dimensional Quantum Systems. *Physical Review Letters* ***52*** (1984), 1469.

[15] Bollé, D., and Gesztesy, F. Scattering observables in arbitrary dimension $n \geq 2$. *Physical Review A* ***30*** (1984), 1279.

[16] Botelho, S., and Sá de Melo, C. Vortex-Antivortex Lattice in Ultracold Fermionic Gases. *Physical Review Letters* ***96*** (2006), 040404.

[17] Carr, L. D., DeMille, D., Krems, R. V., and Ye, J. Cold and ultracold molecules: science, technology and applications. *New Journal of Physics* ***11*** (2009), 055049.

[18] Chadan, K., Martin, A., and Wu, T. T. Universality of low-energy scattering in 2+1 dimensions. *Physical Review D* ***58*** (1998), 025014.

[19] Chen, Q., Stajic, J., Tan, S., and Levin, K. BCS–BEC crossover: From high temperature superconductors to ultracold superfluids. *Physics Reports* ***412*** (2005), 1.

[20] Chin, C., Julienne, P., and Tiesinga, E. Feshbach resonances in ultracold gases. *Reviews of Modern Physics* ***82*** (2010), 1225–1286.

[21] Dalfovo, F., Giorgini, S., and Stringari, S. Theory of Bose-Einstein condensation in trapped gases. *Reviews of Modern Physics* ***71*** (1999), 463.

[22] Danzl, J. G., Mark, M. J., Haller, E., Gustavsson, M., Hart, R., Aldegunde, J., Hutson, J. M., and Nägerl, H.-C. An ultracold high-density sample of rovibronic ground-state molecules in an optical lattice. *Nature Physics* ***6*** (2010), 265.

[23] Davis, K., Mewes, M., Andrews, M., van Druten, N., Durfee, D., Kurn, D., and Ketterle, W. Bose-Einstein Condensation in a Gas of Sodium Atoms. *Physical Review Letters* ***75*** (1995), 3969.

[24] de Alfaro, V., and Regge, T. *Potential scattering.* North-Holland, Amsterdam, 1965.

[25] de Gennes, P.-G. *Superconductivity of Metals and Alloys*, 3rd ed. Perseus Books, 1999.

[26] de Miranda, M. H. G., Chotia, A., Neyenhuis, B., Wang, D., Quéméner, G., Ospelkaus, S., Bohn, J. L., Ye, J., and Jin, D. S. Controlling the quantum stereodynamics of ultracold bimolecular reactions. *Nature Physics* ***7*** (2011), 502.

[27] Deiglmayr, J., Grochola, A., Repp, M., Mörtlbauer, K., Glück, C., Lange, J., Dulieu, O., Wester, R., and Weidemüller, M. Formation of Ultracold Polar Molecules in the Rovibrational Ground State. *Physical Review Letters* ***101*** (2008), 133004.

[28] DeMarco, B., and Jin, D. S. Onset of Fermi Degeneracy in a Trapped Atomic Gas. *Science* ***285*** (1999), 1703.

[29] Eagles, D. Possible Pairing without Superconductivity at Low Carrier Concentrations in Bulk and Thin-Film Superconducting Semiconductors. *Physical Review* ***186*** (1969), 456.

[30] Eason, G., Noble, B., and Sneddon, I. N. On Certain Integrals of Lipschitz-Hankel Type Involving Products of Bessel Functions. *Philosophical Transactions of the Royal Society A: Mathematical, Physical and Engineering Sciences* ***247*** (1955), 529.

[31] Fattori, M., Roati, G., Deissler, B., D'Errico, C., Zaccanti, M., Jona-Lasinio, M., Santos, L., Inguscio, M., and Modugno, G. Magnetic Dipolar Interaction in a Bose-Einstein Condensate Atomic Interferometer. *Physical Review Letters* ***101*** (2008).

[32] Gaebler, J. P., Stewart, J. T., Drake, T. E., Jin, D. S., Perali, A., Pieri, P., and Strinati, G. C. Observation of pseudogap behaviour in a strongly interacting Fermi gas. *Nature Physics* ***6*** (2010), 569.

[33] Gibson, W. Two-dimensional scattering: Low-energy behaviour of the Jost function and Levinson's theorem. *Physics Letters A* ***117*** (1986), 107.

[34] Giorgini, S., and Stringari, S. Theory of ultracold atomic Fermi gases. *Reviews of Modern Physics* ***80*** (2008), 1215.

[35] Glassgold, A. Spin Exchange in Collisions between Atoms. *Physical Review* ***132*** (1963), 2144.

[36] Goldberger, M. L., and Watson, K. M. *Collision theory.* Wiley, New York, 1964.

[37] Greiner, M., Mandel, O., Esslinger, T., Hänsch, T. W., and Bloch, I. Quantum phase transition from a superfluid to a Mott insulator in a gas of ultracold atoms. *Nature* ***415*** (2002), 39.

[38] Grimm, R., Weidemüller, M., and Ovchinnikov, Y. B. Optical dipole traps for neutral atoms. *Advances in Atomic, Molecular and Optical Physics* ***42*** (1999), 95. Also at arXiv:physics/9902072.

[39] Hadzibabic, Z., and Dalibard, J. Two-dimensional Bose fluids: An atomic physics perspective. *Rivista del Nuovo Cimento* ***34*** (2011). Also at arXiv:0912.1490.

[40] Heiselberg, H., Pethick, C., Smith, H., and Viverit, L. Influence of Induced Interactions on the Superfluid Transition in Dilute Fermi Gases. *Physical Review Letters* ***85*** (2000), 2418.

[41] Herzberg, G. *Molecular spectra and molecular structure*, 2nd ed. Van Nostrand, Princeton, 1953.

[42] Jackson, J. D. *Classical electrodynamics*, 3rd ed. Wiley, 1999.

[43] Khuri, N. N., Martin, A., Richard, J.-M., and Wu, T. T. Low-energy potential scattering in two and three dimensions. *Journal of Mathematical Physics* ***50*** (2009), 072105.

[44] Kinoshita, T., Wenger, T., and Weiss, D. S. Observation of a one-dimensional Tonks-Girardeau gas. *Science* ***305*** (2004), 1125.

[45] Klawunn, M., Pikovski, A., and Santos, L. Two-dimensional scattering and bound states of polar molecules in bilayers. *Physical Review A* ***82*** (2010), 044701.

[46] Lahaye, T., Koch, T., Fröhlich, B., Fattori, M., Metz, J., Griesmaier, A., Giovanazzi, S., and Pfau, T. Strong dipolar effects in a quantum ferrofluid. *Nature* ***448*** (2007), 672.

[47] Lahaye, T., Menotti, C., Santos, L., Lewenstein, M., and Pfau, T. The physics of dipolar bosonic quantum gases. *Reports on Progress in Physics* ***72*** (2009), 126401.

[48] Landau, L. D., and Lifshitz, E. M. *Quantum Mechanics*, 3rd ed. Pergamon Press, 1977.

[49] Lang, F., Winkler, K., Strauss, C., Grimm, R., and Denschlag, J. Ultracold Triplet Molecules in the Rovibrational Ground State. *Physical Review Letters* ***101*** (2008).

[50] Leggett, A. J. Cooper pairing in spin-polarized Fermi systems. *Le Journal de Physique Colloques* ***41*** (1980), C7–19.

[51] Leggett, A. J. Diatomic Molecules and Cooper Pairs. In *Modern Trends in the Theory of Condensed Matter (Proceedings of the XVI Karpacz Winter School of Theoretical Physics).*, Lecture Notes in Physics Vol 115. Springer, New York, 1980.

[52] Leggett, A. J. *Quantum Liquids.* Oxford University Press, Oxford, 2006.

[53] Leggett, A. J., and Zhang, S. The BEC-BCS Crossover: Some History and Some General Observations. In *The BCS-BEC Crossover and the Unitary Fermi Gas. Lecture Notes in Physics 836*, W. Zwerger, Ed. Springer, 2012.

[54] Lifshitz, M. E., and Pitaevskii, L. P. *Statistical Physics, Part 2.* Pergamon Press, Oxford, 1980.

[55] Lovas, F. J., and Tiemann, E. Microwave Spectral Tables I. Diatomic Molecules. *Journal of Physical and Chemical Reference Data* ***3*** (1974), 609.

[56] Lozovik, Y., and Yudson, V. A new mechanism for superconductivity: pairing between spatially separated electrons and holes. *Sov. Phys. JETP* ***44*** (1976), 389.

[57] Lozovik, Y. E., Kurbakov, I. L., Astrakharchik, G. E., and Willander, M. Bose condensation of two-dimensional dipolar excitons: Simulation by the quantum Monte Carlo method. *Journal of Experimental and Theoretical Physics* ***106*** (2008), 296.

[58] Lu, M., Burdick, N., and Lev, B. Quantum Degenerate Dipolar Fermi Gas. *Physical Review Letters* ***108*** (2012).

[59] Lu, M., Burdick, N., Youn, S., and Lev, B. Strongly Dipolar Bose-Einstein Condensate of Dysprosium. *Physical Review Letters* ***107*** (2011).

[60] Micheli, A., Pupillo, G., Büchler, H. P., and Zoller, P. Cold polar molecules in two-dimensional traps: Tailoring interactions with external fields for novel quantum phases. *Physical Review A* ***76*** (2007), 043604.

[61] Miyake, K. Fermi Liquid Theory of Dilute Submonolayer ^{3}He on Thin ^{4}He II Film. *Progress of Theoretical Physics* ***69*** (1983), 1794.

[62] Nelson, D. R. Universal Jump in the Superfluid Density of Two-Dimensional Superfluids. *Physical Review Letters* ***39*** (1977), 1201.

[63] Newton, R. G. *Scattering Theory of Waves and Partilces*, 2nd ed. Springer, New York, 1982.

[64] Newton, R. G. Low-energy scattering for medium-range potentials. *Journal of Mathematical Physics* ***27*** (1986), 2720.

[65] Ni, K.-K. *A Quantum Gas of Polar Molecules.* PhD thesis, University of Colorado, 2009.

[66] Ni, K.-K., Ospelkaus, S., de Miranda, M. H. G., Pe'er, A., Neyenhuis, B., Zirbel, J. J., Kotochigova, S., Julienne, P. S., Jin, D. S., and Ye, J. A high phase-space-density gas of polar molecules. *Science* ***322*** (2008), 231.

[67] Ni, K.-K., Ospelkaus, S., Wang, D., Quéméner, G., Neyenhuis, B., de Miranda, M. H. G., Bohn, J. L., Ye, J., and Jin, D. S. Dipolar collisions of polar molecules in the quantum regime. *Nature* ***464*** (2010), 1324.

[68] Ospelkaus, C., Ospelkaus, S., Ernst, P., Wille, O., Succo, M., Humbert, L., Sengstock, K., and Bongs, K. Fermi-Bose Mixtures in Three-Dimensional Optical Lattices. *AIP Conference Proceedings* ***869*** (2006), 219.

[69] Ospelkaus, S., Ni, K.-K., Wang, D., de Miranda, M. H. G., Neyenhuis, B., Quéméner, G., Julienne, P. S., Bohn, J. L., Jin, D. S., and Ye, J. Quantum-state controlled chemical reactions of ultracold potassium-rubidium molecules. *Science* ***327*** (2010), 853.

[70] Paredes, B., Widera, A., Murg, V., Mandel, O., Fölling, S., Cirac, I., Shlyapnikov, G. V., Hänsch, T. W., and Bloch, I. Tonks-Girardeau gas of ultracold atoms in an optical lattice. *Nature* ***429*** (2004), 277.

[71] Pashov, A., Knöckel, H., and Tiemann, E. Coupling of the $X^1\Sigma^+$ and $a^3\Sigma^+$ states of KRb. *Physical Review A* ***76*** (2007), 022511.

[72] Patil, S. Ground-state energy of two-dimensional weakly coupled Hamiltonians. *Physical Review A* ***22*** (1980), 2400.

[73] Patil, S. Wave functions for weakly coupled bound states. *Physical Review A* ***25*** (1982), 2467.

[74] Petrov, D., Baranov, M., and Shlyapnikov, G. Superfluid transition in quasi-two-dimensional Fermi gases. *Physical Review A* ***67*** (2003), 031601.

[75] Petrov, D., and Shlyapnikov, G. V. Interatomic collisions in a tightly confined Bose gas. *Physical Review A* ***64*** (2001), 012706.

[76] Pikovski, A., Klawunn, M., Recati, A., and Santos, L. Nonlocal state swapping of polar molecules in bilayers. *Physical Review A* ***84*** (2011), 061605.

[77] Pikovski, A., Klawunn, M., Shlyapnikov, G., and Santos, L. Interlayer Superfluidity in Bilayer Systems of Fermionic Polar Molecules. *Physical Review Letters* ***105*** (2010), 215302.

[78] Pollack, S. E., Dries, D., Junker, M., Chen, Y. P., Corcovilos, T. A., and Hulet, R. G. Extreme Tunability of Interactions in a ^{7}Li Bose-Einstein Condensate. *Physical Review Letters* ***102*** (2009).

[79] Randeria, M. Crossover from BCS Theory to Bose-Einstein Condensation. In *Bose-Einstein Condensation*, A. Griffin, Ed. Cambridge University Press, 1995, p. 355.

[80] Randeria, M., Duan, J.-M., and Shieh, L.-Y. Superconductivity in a two-dimensional Fermi gas: Evolution from Cooper pairing to Bose condensation. *Physical Review B* ***41*** (1990), 327.

[81] Rickayzen, G. *Theory of superconductivity.* Interscience, New York, 1965.

[82] Ross, A. J., Effantin, C., Crozet, P., and Boursey, E. The ground state of KRb from laser-induced fluorescence. *Journal of Physics B: Atomic, Molecular and Optical Physics* ***23*** (1990), L247.

[83] Sá de Melo, C., Randeria, M., and Engelbrecht, J. Crossover from BCS to Bose superconductivity: Transition temperature and time-dependent Ginzburg-Landau theory. *Physical Review Letters* ***71*** (1993), 3202.

[84] Shlyapnikov, G. V. Private communication.

[85] Shuler, K. E. Reaction Cross Sections, Rate Coefficients and Nonequilibrium Kinetics. In *Chemische Elementarprozesse*, H. Hartmann, Ed. Springer, Berlin, 1968.

[86] Simon, B. The bound state of weakly coupled Schrödinger operators in one and two dimensions. *Annals of Physics* ***97*** (1976), 279.

[87] Stenger, J., Inouye, S., Stamper-Kurn, D. M., Miesner, H.-J., Chikkatur, A. P., and Ketterle, W. Spin domains in ground-state Bose-Einstein condensates. *Nature* ***396*** (1998), 345.

[88] Timmermans, E., Tommasinib, P., Hussein, M., and Kermand, A. Feshbach resonances in atomic Bose-Einstein condensates. *Physics Reports* ***315*** (1999), 199.

[89] Townes, C., and Schawlow, A. L. *Microwave spectroscopy.* McGraw-Hill, New York, 1955.

[90] Tricomi, F. G. *Integral equations.* Interscience, New York, 1957.

[91] Ueda, M. *Fundamentals and New Frontiers of Bose-Einstein Condensation.* World Scientific, 2010.

[92] van Vleck, J. H. *The theory of electric and magnetic susceptibilities.* Clarendon Press, Oxford, 1932.

[93] Vengalattore, M., Leslie, S. R., Guzman, J., and Stamper-Kurn, D. M. Spontaneously Modulated Spin Textures in a Dipolar Spinor Bose-Einstein Condensate. *Physical Review Letters* ***100*** (2008).

[94] Weiner, J., and Julienne, P. S. Experiments and theory in cold and ultracold collisions. *Reviews of Modern Physics* ***71*** (1999), 1.

[95] Zwerger, W., Ed. *The BCS–BEC Crossover and the Unitary Fermi gas.* Lecture Notes in Physics Vol. 836. Springer, Berlin/Heidelberg, 2012.